A First-Principles Alternative to Empirical Solvent Parameters

Kasimir P. Gregory,[1,2,3] Erica J. Wanless,[1] Grant B. Webber,[4] Vince S. J. Craig,[2] Alister J. Page[1]*

[1] *Discipline of Chemistry, College of Engineering, Science & Environment, University of Newcastle, Callaghan 2308 Australia*

[2] *Research School of Materials Physics, Australian National University, 0200, Australia*

[3] *Division of Biomedical Science and Biochemistry, Research School of Biology, The Australian National University, Canberra, ACT 0200, Australia*

[4] *Discipline of Chemical Engineering, College of Engineering, Science & Environment, University of Newcastle, Callaghan 2308 Australia*

Supporting Information – Table of contents

S1. First-Principles Solvent Parameters

Table S1: Solvent's positive and negative radial charge densities values (þ$^{\pm}_{\text{solvent}}$), charges ($q^{\pm}$), cubed root of the r-cubed moment ($\sqrt[3]{\langle \mathbf{r}^{\pm 3} \rangle}$), polarisabilities ($\alpha$) and C_6 dispersion coefficients calculated with MP2/aug-cc-pVTZ. Ordered from largest to smallest by the sum of the magnitudes of þ$^{-}_{\text{solvent}}$ and þ$^{+}_{\text{solvent}}$.

Solvent (full name)	**þ$^{-}_{\text{solvent}}$** ($\times 10^{-10}$ C·m^{-1})	**þ$^{+}_{\text{solvent}}$** ($\times 10^{-10}$ C·m^{-1})	**q^{-}** (a.u.)	**q^{+}** (a.u.)	$\sqrt[3]{\langle r^{-3} \rangle}$ (Å)	$\sqrt[3]{\langle \mathbf{r}^{+3} \rangle}$ (Å)	**α_{avg}** (Å^3)	**C_6** (a.u.)
water (water)	-7.82	8.55	-0.79	0.39	1.61	0.74	1.25	44.84
NH_3 (ammonia)	-8.46	6.31	-0.92	0.31	1.74	0.78	1.91	81.95
Glycerol(glycerol)	-5.68	8.18	-0.56	0.36	1.59	0.71	7.31	1549.86
PhOH (phenol)	-5.19	8.45	-0.50	0.37	1.56	0.71	10.67	2362.47
tBuOH (tert-butanol)	-5.83	7.59	-0.58	0.35	1.59	0.74	7.90	1527.38
TFE (trifluoroethanol)	-4.91	8.45	-0.48	0.37	1.56	0.69	4.62	798.63
2PrOH (2-propanol)	-5.72	7.51	-0.56	0.35	1.58	0.74	6.25	947.72
PhMeOH (benzyl alcohol)	-5.29	7.93	-0.52	0.35	1.57	0.71	12.46	3294.55
PrOH (1-propanol)	-5.48	7.64	-0.54	0.35	1.58	0.73	6.28	964.73
EtOH (ethanol)	-5.50	7.62	-0.54	0.35	1.58	0.73	4.61	520.90
BuOH (1-butanol)	-5.45	7.65	-0.54	0.35	1.58	0.73	7.99	1556.00
sEG (ethylene glycol)	-5.29	7.57	-0.52	0.35	1.57	0.73	5.15	721.86
MeOH (methanol)	-5.07	7.56	-0.49	0.34	1.56	0.73	2.92	213.62
$PhNH_2$ (aniline)	-6.37	6.23	-0.67	0.29	1.69	0.75	11.50	2664.17
FA (formamide)	-5.00	7.42	-0.49	0.32	1.59	0.74	3.71	369.94
$SeOCl_2$ (selenium oxychloride)	-4.91	7.18	-0.50	0.99	1.62	2.20	8.98	1393.94
NMA (*N*-methylacetamide)	-5.52	5.50	-0.55	0.26	1.60	0.76	6.98	1252.71
NMF (*N*-methylformamide)	-4.90	5.51	-0.48	0.26	1.58	0.76	5.35	741.26
TMP (trimethylphosphate)	-7.67	2.24	-0.79	0.11	1.65	0.79	9.95	3058.75
$SOCl_2$ (thionyl chloride)	-3.89	5.77	-0.38	0.74	1.55	2.05	8.22	1214.78
HMPT* (hexamethyl phosphoric triamide)	-7.19	2.28	-0.74	0.12	1.66	0.84	17.33	8145.01
DMSO (dimethyl sulfoxide)	-5.98	3.40	-0.61	0.17	1.64	0.79	7.30	1128.78
TMS (tetramethylene sulfone)	-6.05	2.93	-0.61	0.15	1.61	0.80	9.82	2500.50
$C_5H_{11}N$ (Piperidine)	-4.05	4.71	-0.42	0.23	1.67	0.77	9.49	2186.59
DMA (*N*,*N*-dimethylacetamide)	-5.51	3.14	-0.55	0.16	1.59	0.81	8.67	1879.83
PC (propylene carbonate)	-4.42^	2.89	-0.53	0.14	1.57	0.79	7.82	1785.41
NMPy (*N*-methyl pyrrolidinone)	-5.42	2.52	-0.54	0.13	1.60	0.82	9.65	2400.50
ACE (acetone)	-4.81	3.04	-0.47	0.15	1.57	0.81	5.78	795.18
GBL (γ-butyrolactone)	-5.04	2.66	-0.50	0.13	1.58	0.80	7.25	1433.01
DMF (*N*,*N*-dimethyl formamide)	-4.89	2.61	-0.48	0.13	1.59	0.82	7.08	1257.11
MeCN (acetonitrile)	-4.10	3.23	-0.43	0.16	1.68	0.79	4.25	436.38
$MeNO_2$ (nitromethane)	-3.71	3.30	-0.36	0.16	1.55	0.78	4.55	517.29
$POCl_3$ (phosphorus oxychloride)	-5.95	-	-0.59	-	1.60	-	9.25	1992.04
$PhNO_2$ (nitrobenzene)	-3.46	2.46	-0.33	0.13	1.54	0.82	12.46	3209.58
PhCN (benzonitrile)	-3.53	2.31	-0.37	0.12	1.66	0.81	12.56	3160.53
DEE (diethylether)	-3.04	2.36	-0.29	0.12	1.54	0.82	8.09	1615.04
THF (tetrahydrofuran)	-3.20	1.73	-0.31	0.09	1.54	0.82	7.18	1293.14
Py (pyridine)	-2.84	2.07	-0.30	0.11	1.66	0.82	9.23	1756.35
SO_2Cl_2 (sulfuryl chloride)	-4.67	-	-0.45	-	1.56	-	7.98	1449.39
$C_4H_8O_2$ (1,4-dioxane)	-2.94	1.55	-0.28	0.08	1.54	0.82	7.72	1647.29
11DCE (1,1-dichloroethane)	-0.70	3.67	-0.09	0.18	2.14	0.79	7.79	1233.25
TEA* (triethylamine)	-2.07	1.98	-0.21	0.10	1.63	0.85	13.10	3607.82
TOL (toluene)	-1.15	2.41	-0.16	0.12	1.68	0.82	11.89	2804.57
CHCl3 (chloroform)	-0.80	1.98	-0.11	0.10	2.14	0.82	4.18	1403.48
EDC (1,2-dichloroethane)	-1.17	2.12	-0.16	0.11	2.15	0.83	7.86	1336.99
THT (tetrahydrothiophene)	-0.98	1.93	-0.14	0.10	2.24	0.82	9.52	1889.37
benzene (benzene)	-0.91	1.81	-0.09	0.09	1.67	0.83	10.09	1960.57
hexane (hexane)	-	2.01	-	0.10	-	0.82	10.79	2655.79

*These solvents had their properties calculated with MP2/aug-cc-pVDZ.

^This is a mixed value, based on the fact that PC interacts via multiple oxygens at once (Figure S40)

S2. Proposed Relationship between LSER and the þ Parameter

The linear solvation energy relationship (LSER) discussed by Kamlet *et al.*[1] (which are based on at least 46 articles[2]) takes a generalised form of:

$$XYZ \approx XYZ_0 + s(\pi^* + d\delta) + a\alpha + b\beta + h\delta_H + e\xi \tag{S1}$$

where XYZ_0 is a system dependent "y-intercept", π^* is an index of solvent dipolarity/polarisability, δ is a polarisability correction term, α and β are hydrogen bond acceptor and donor scales respectively, δ_H is the Hildebrand solubility parameter and ξ is a coordinate covalency parameter. The *s*, *a*, *b*, *h* and *e* coefficients measure the relative influence of each respective solvent property on *XYZ*. A somewhat similar approach is that of Abraham and Platts,[3] who suggested that hydrogen bonding between various functional groups and a solvent could be described generally via an association constant (K),

$$\log K = c_1 \alpha_2^H \beta_2^H + c_2 \tag{S2}$$

where, c_1 and c_2 are solvent-dependent constants and α_2^H and β_2^H are the hydrogen bond donor and acceptor properties of the interacting functional groups, respectively.

Empirical relationships such as the Kamlet-Taft LSER may be reduced to more specific correlations of one, two or three-parameters for particular solvents, reactants or indicators. For example, free energies of proton transfer to the aqueous bases from aqueous NH_4^+, $\Delta G_f(aq\ BH^+)$, are functional group dependent (i.e., distinct correlations exist for different H-bond acceptor sites) when correlating solely with β (Figure S1(a)). This can be made functional group independent (Figure S1(b)) if a coordinate covalency parameter, ξ, is incorporated, i.e.,

$$\Delta G_f(aq\ BH^+) = 26.4 - 17.4\beta - 15.7\xi. \tag{S3}$$

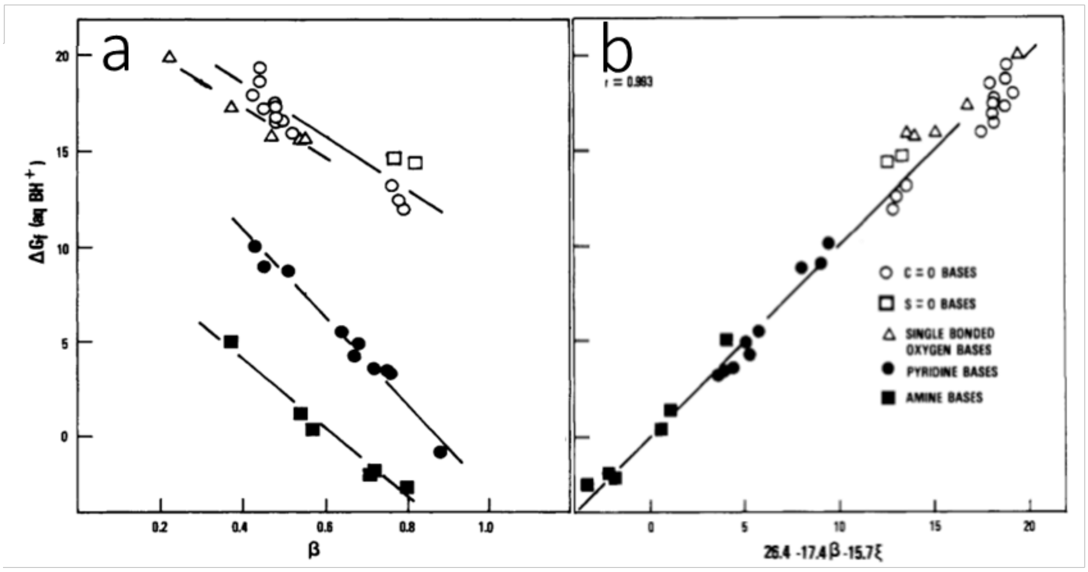

Figure S1. The free energy of transfer of protons between NH_4^+ and BH^+ (a) has a relationship with β, that is dependent on the available functional groups of the base B, however (b) a direct linear relationship that is family independent may be observed if the coordinate covalency parameter, ξ, is accounted for. Figures reprinted with permission from Ref. [1] with permission from J. Org. Chem.

The empirical nature of these correlations is highlighted by the values of ξ, which are −0.2 for P=O bases, 0.0 for C=O bases, S=O and N=O bases, 0.2 for single bonded oxygen bases, 0.6 for pyridine bases and 1.0 for sp^3-hybridised amine bases.[1]

The system-dependent coefficients s, a, b, h and e from Eq. S1, in some cases relate to assigned general solute properties. For instance, recent work[4] demonstrated the link between fundamental properties of relatively simple solutes (ions) and by using a reduced form of Kamlet-Taft LSER,[1] *i.e.*,

$$XYZ \approx XYZ_0 + a\alpha \qquad \text{(S4)}$$

for XYZ measures such as Gibbs energies of transfer or S_N2 reaction rates, where a is approximated by the radial charge density of the anions ($þ^{-}_{\text{anion}}$) and α by the Lewis acidity of the solvent (AN).

Given each of the parameters in the general form of the LSER (Eq. S1) are representative of fundamental properties of the solvents themselves and correlate with similarly classified solvent properties (Figure S2), it is conceivable that macroscopic LSER can be reformulated using molecular-level quantum chemical descriptions more generally, independent of probe molecules. This would overcome the empiricism of Eq. S1-3, thereby increasing the utility and transferability of the LSER as a predictive model. Therefore, in a simple LSER we might be able to use $þ^{-}_{\text{anion}}\cdot þ^{+}_{\text{solvent}}$ in place of $a\alpha$.

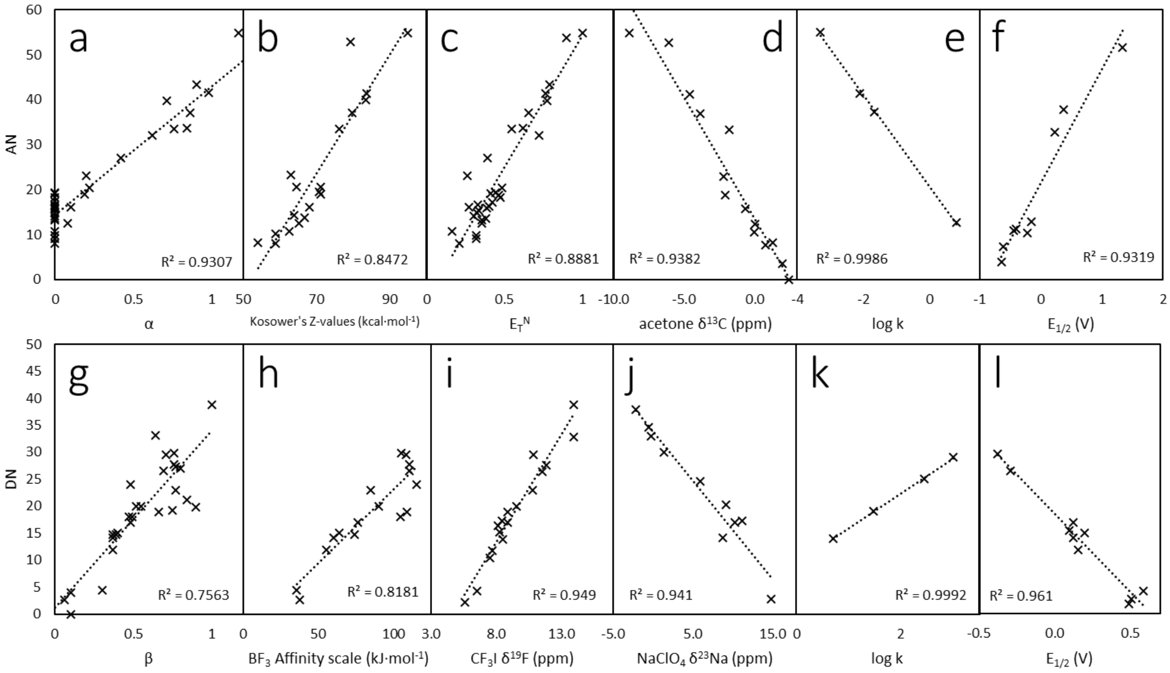

Figure S2. Correlations between the solvents' empirical parameters (Table 1) and various solvent properties. There is a general correlation between the Gutmann acceptor number (AN) and the (a) Kamlet-Taft α values of Lewis acidity, (b) Kosower's Z-values, (c) Dimroth Reichardt's normalised E_T values, (d) the ^{13}C chemical shift of acetone (e) the 2nd order rate constants of the reaction between CH_3I and labelled I^- and (f) the polorgraphic half-wave potential of Zn^{2+}. Similar relationships can be found for the Gutmann donor number (DN) and (g) the Kamlet-Taft β values of Lewis basicity, (h) the BF_3 affinity scale, the chemical shift of (i) ^{19}F for CF_3I and (j) ^{23}Na for $NaClO_4$, (k) the rate of solvent (S) substitution of trifluoroacetate (TFA^-) in $[NiS_5\ TFA]^+$ to have $[NiS_6]^{2+}$ and TFA^-. Data collated from Ref 5.

S3. Solvent intermolecular interaction energy analyses

The intermolecular interactions between solvents and ions, or themselves, was investigated in three parts according to Figure S3, viz. a pairwise SAPT2+3 interaction analysis, a cluster GKS-EDA pairwise analysis and a GKS-EDA "cluster" analysis. The interaction energy of the three models are denoted by ΔE[solvent(gas phase)--M^+/X^-], ΔE[solvent(specific)--M^+/X^-] and ΔE[solvent(cluster)--M^+/X^-] respectively in many of the Figures.

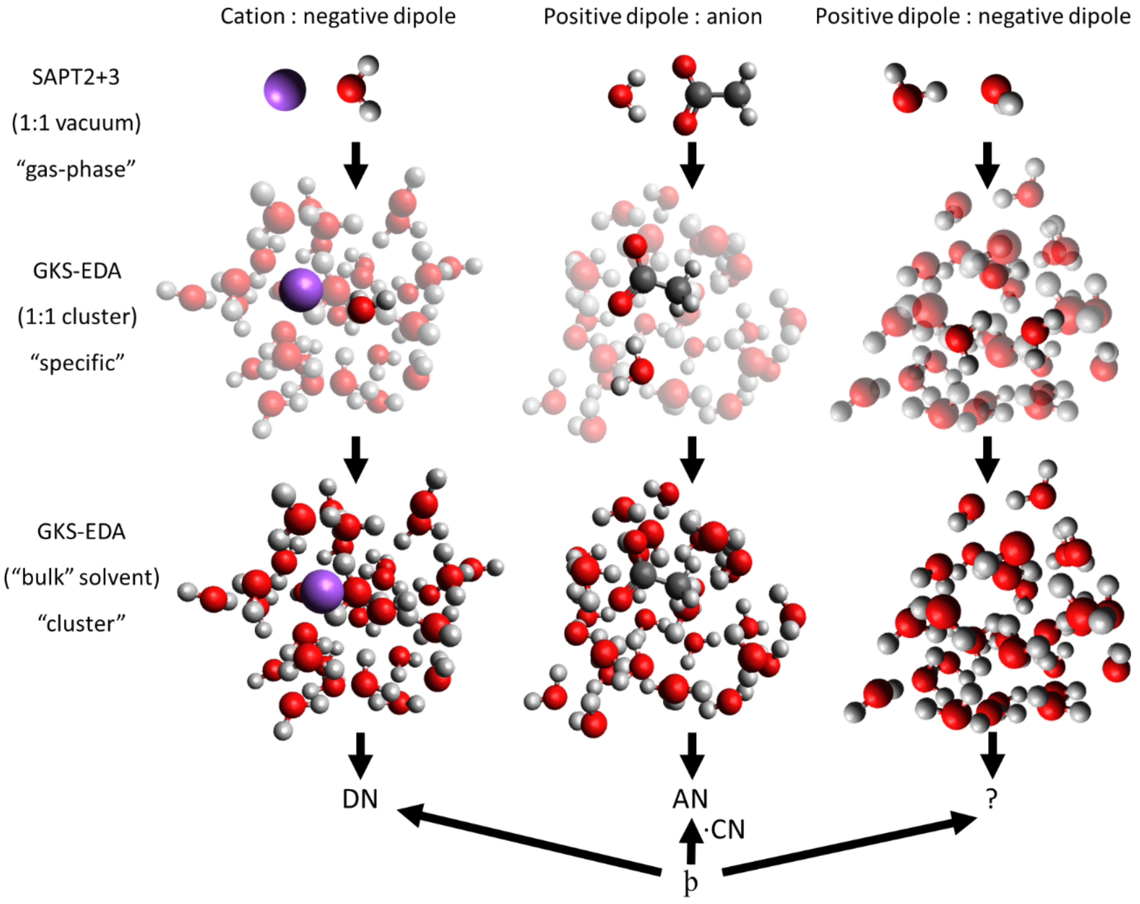

Figure S3: The interactions of (left) cations with a negative solvent dipole (§S4), (middle) anions with a positive solvent dipole (§S5) and (right) the positive and negative solvent dipoles (§S8) are investigated by increasing model complexity (top) 1:1 interactions in the gas phase (§S4.1,S5.1,S8.1) via SAPT2+3 calculations and (middle) 1:1 interactions in a solvent cluster (§S4.2,S5.2,S8.2) and (bottom) interactions with the entire solvent cluster (§S4.3,S5.3,S8.3) with an additional PCM environment in the GKS-EDA calculations.

The geometries used for the SAPT2+3 calculations are shown in Figure S4-Figure S6. These were collected from the lowest energy optimised geometry based on a small scan of 10 random starting geometries (which generally optimised to the same final geometry). In cases where the solvent geometry varied greatly between the different ions, such as for 1,2-dichloroethane (EDC), a further analysis to investigate the effects of these altered geometries of interaction was pursued in Figure S54.

While a similar sampling was done for the solvent clusters used in the GKS-EDA calculations. The geometries varied in each sample as a result of the higher degrees of freedom from a greater number of molecules. In these cases, averages and standard deviations were obtained for both the "specific" and "cluster" analyses. In the case of the specific interactions, only direct interactions (i.e., first solvation shell) of the measured solvent molecules were included in the analysis. These geometries are included in the supporting files.

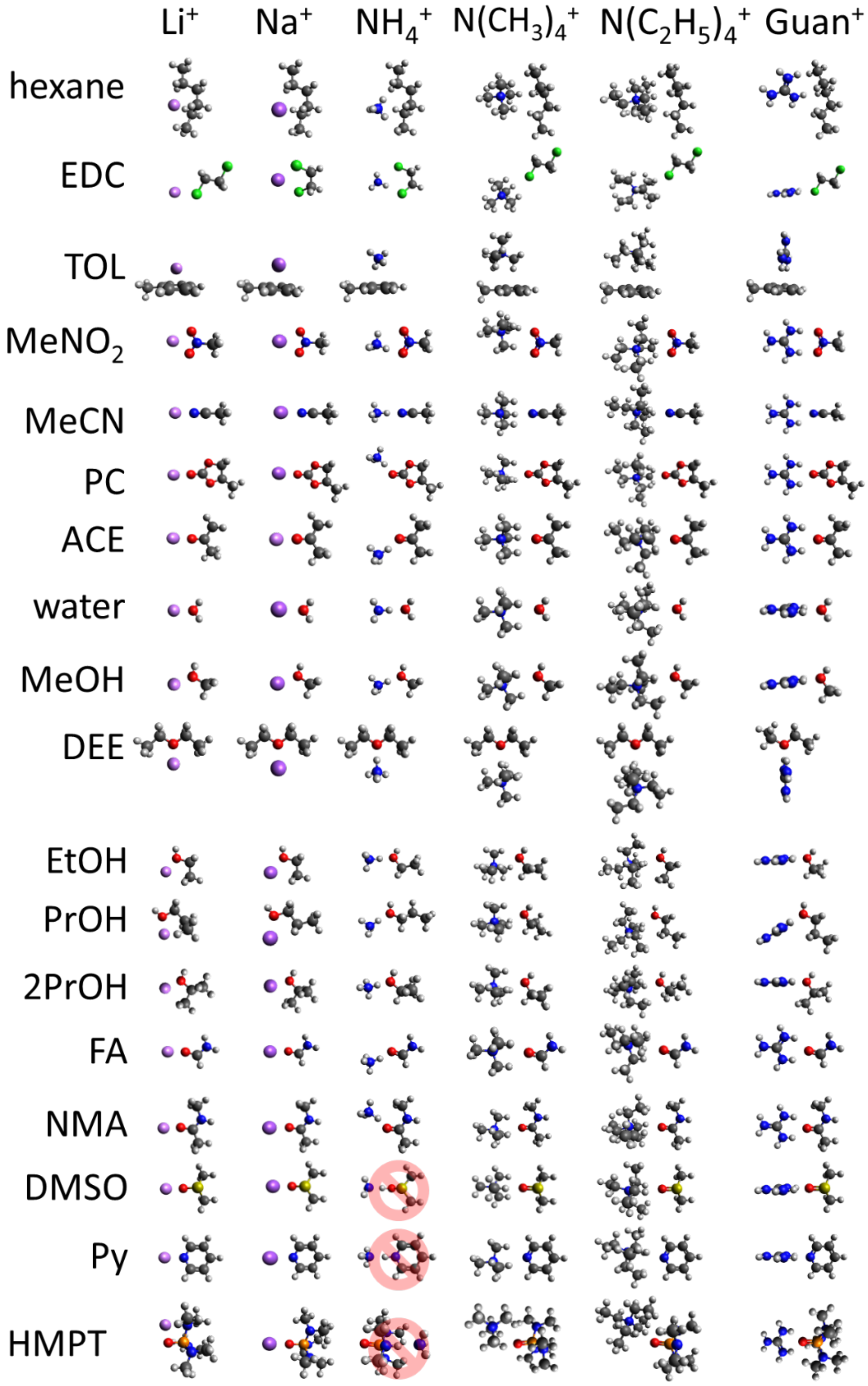

Figure S4: M06-2X/aug-cc-pVDZ geometries of cation-solvent structures used for SAPT2+3/aug-cc-pVDZ interaction energy analysis. Ordered by the Gutmann donor number of the solvent. Ammonium-solvent interactions where complete proton transfer has occurred have been excluded from the formal analysis. These have been indicated with the red prohibition symbol.

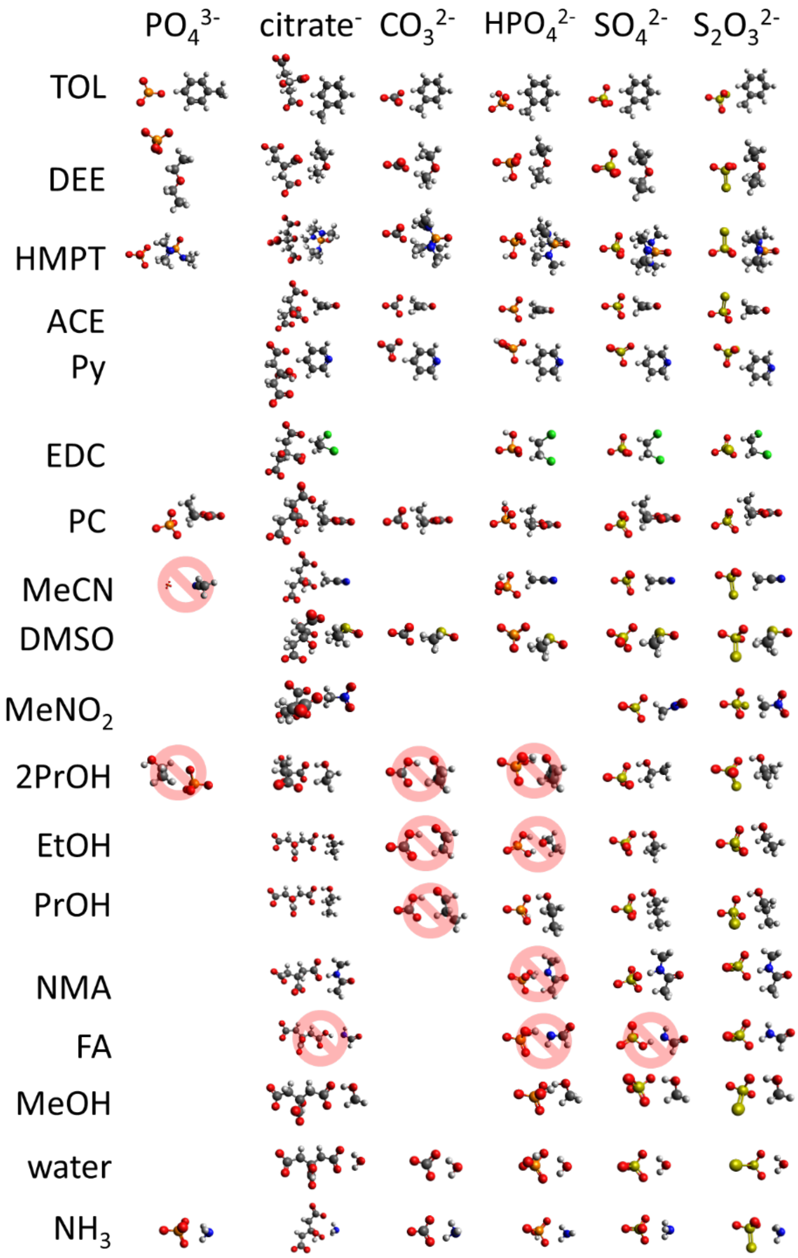

Figure S5: M06-2X/aug-cc-pVDZ geometries of polyvalent anion-solvent structures used for SAPT2+3/aug-cc-pVDZ interaction energy analysis.

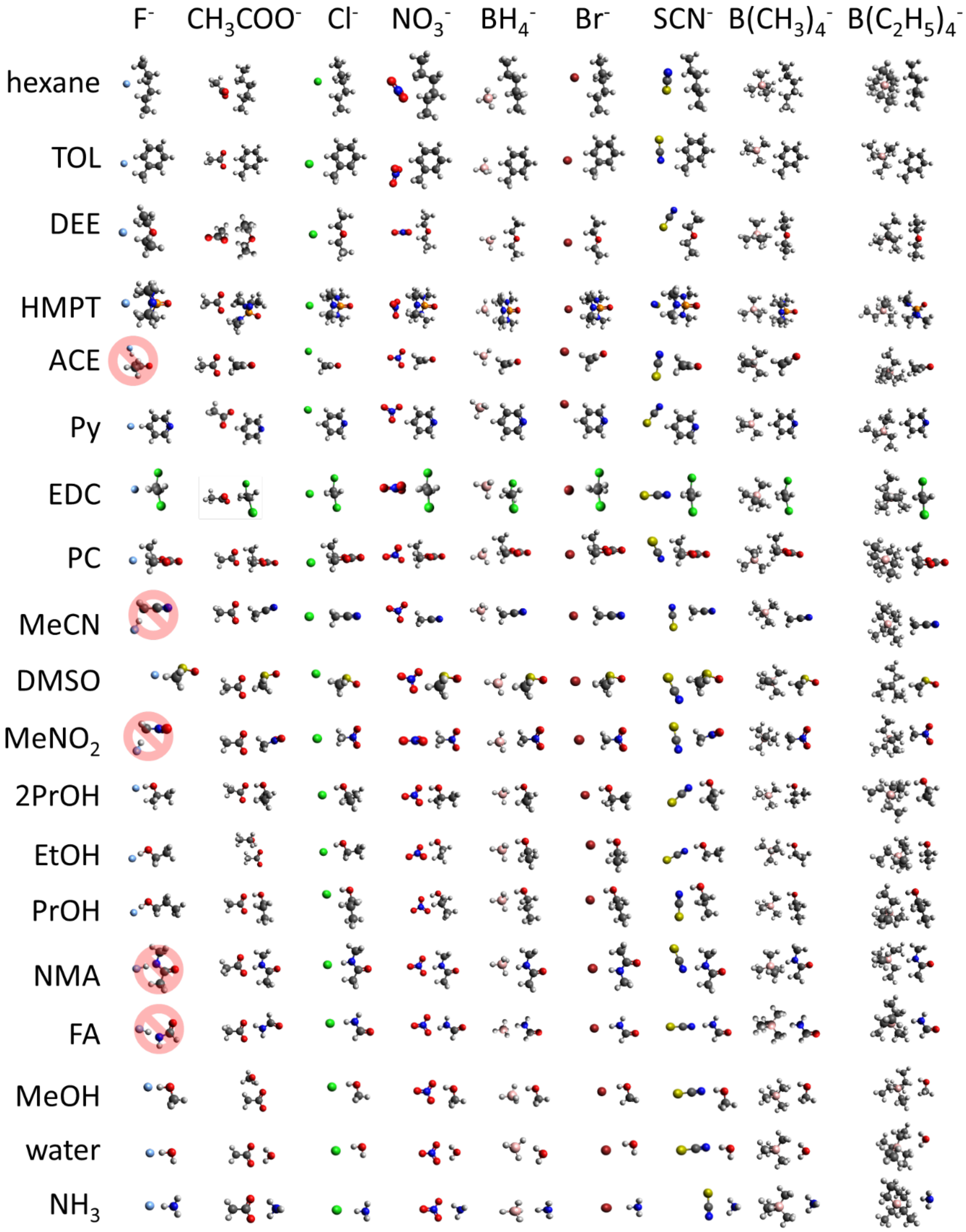

Figure S6: M06-2X/aug-cc-pVDZ geometries of monovalent anion-solvent structures used for SAPT2+3/aug-cc-pVDZ interaction energy analysis.

Figure S7(a-c) displays the correlations between the Gutmann donor number (DN) and cation-solvent total interaction energies for each of the three solvation models investigated (Figure S3). Figure S7(d-f) shows the correlations between the Gutmann-Mayer acceptor number (AN) and anion-solvent total interaction energies for each of the three solvation models. The specific interaction has the best correlation for the DN, while the cluster interaction has the best for the AN.

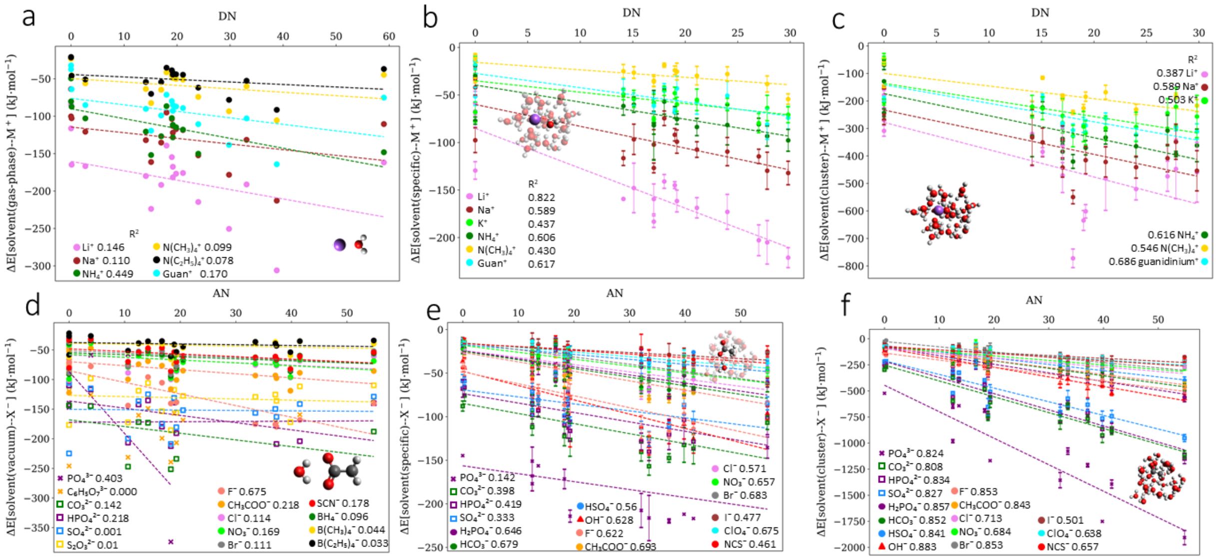

Figure S7: Correlation between the solvent basicity as measured via Gutmann donor and (a) the 1:1 cation-solvent interactions in the gas-phase calculated via M06-2X/aug-cc-pVDZ//SAPT2+3/aug-cc-pVDZ and (b) 1:1 cation-solvent and (c) cation-solvent shell interactions in a local solvent environment calculated with DFTB3-D3(BJ)/3-ob-3-1//GKS-EDA/M06-2X/cc-pVDZ. Correlation between the solvent acidity as measured via Gutmann-Mayer acceptor number and (d) the 1:1 anion-solvent interactions in the gas-phase calculated via M06-2X/aug-cc-pVDZ//SAPT2+3/aug-cc-pVDZ and (e) 1:1 anion-solvent and (f) anion-solvent shell interactions in a local solvent environment calculated with DFTB3-D3(BJ)/3-ob-3-1//GKS-EDA/M06-2X/cc-pVDZ. R^2 values for each energetic component with the donor numbers presented in Table S2 and with the acceptor numbers in Table S3.

The cation-solvent and anion-solvent coefficients of determination for each component energy, and each ion, are displayed in Table S2 and Table S3 respectively. These reveal the electrostatic component to be the most correlated energy component with the DN and AN parameters with few exceptions.

The electrostatic energy itself is revealed to correlate strongly with the total interaction energy for these important cation-solvent specific and anion-solvent cluster interactions (Figure S8 and Figure S9), and indeed more generally for each interaction investigated (Figure S10-Figure S11).

Table S2: The coefficients of determination (R^2) for each of the cation-solvent energetic contributions (Total, Electrostatic, Exchange, Repulsion, Induction/Polarisation, Desolvation and Dispersion/Correlation) with the Gutmann donor number in SAPT gas phase interactions and the GKS-EDA specific and cluster interactions. Bolded values represent the R^2 values for Figure 2(a).

Cation	Total	Elec	Exch	Rep	Ind/ Pol	Desol	Disp/ Corr
Gas phase (SAPT)							
Li^+	0.146	0.331	0.358		0.032		0.007
Na^+	0.11	0.276	0.398		0.16		0.085
$N(CH_3)_4^+$	0.099	0.157	0.08		0.034		0.002
$N(C_2H_5)_4^+$	0.078	0.148	0.037		0.059		0.013
NH_4^+	0.449	0.566	0.751		0.671		0.215
Guan$^+$	0.17	0.281	0.342		0.189		0.009
Specific (GKS-EDA)							
Li^+	**0.822**	0.879	0.701	0.785	0.121	0.162	0.71
Na^+	**0.589**	0.752	0.447	0.523	0.072	0.204	0.459
K^+	**0.437**	0.47	0.348	0.365	0.382	0.193	0.594
$N(CH_3)_4^+$	**0.43**	0.535	0.097	0.094	0.157	0.118	0.033
NH_4^+	**0.606**	0.805	0.362	0.415	0.032	0.214	0.326
Guan$^+$	**0.617**	0.606	0.208	0.334	0.036	0.09	0.21
Cluster (GKS-EDA)							
Li^+	0.387	0.586	0.649	0.626	0.49	0.253	0.699
Na^+	0.589	0.609	0.531	0.532	0.026	0.182	0.509
K^+	0.503	0.501	0.404	0.402	0.249	0.274	0.621
$N(CH_3)_4^+$	0.546	0.736	0.513	0.502	0.112	0.263	0.097
NH_4^+	0.616	0.781	0.759	0.751	0.161	0.194	0.198
Guan$^+$	0.686	0.819	0.24	0.242	0.208	0.219	0.021

Table S3: The coefficients of determination (R^2) for each of the anion-solvent energetic contributions (Total, Electrostatic, Exchange, Repulsion, Induction/Polarisation, Desolvation and Dispersion/Correlation) with the Gutmann acceptor number in SAPT gas phase interactions and the GKS-EDA specific and cluster interactions. Bolded values represent the R^2 values for Figure 2(b).

Anion	Total	Elec	Exch	Rep	Ind/ Pol	Desol	Disp/ Corr
Gas phase (SAPT)							
PO_4^{3-}	0.403	0.287	0.053	N/A	0.768	N/A	0
$C_6H_5O_7^{3-}$	0	0.179	0.149	N/A	0.013	N/A	0.021
CO_3^{2-}	0.142	0.513	0.28	N/A	0.01	N/A	0.005
HPO_4^{2-}	0.218	0.602	0.368	N/A	0.162	N/A	0.058
SO_4^{2-}	0.001	0.124	0.063	N/A	0	N/A	0.01
$S_2O_3^{2-}$	0.01	0.2	0.168	N/A	0.004	N/A	0.035
F^-	0.675	0.793	0.697	N/A	0.625	N/A	0.165
CH_3COO^-	0.218	0.528	0.436	N/A	0.211	N/A	0.012
Cl^-	0.114	0.247	0.133	N/A	0.022	N/A	0.009
NO_3^-	0.169	0.417	0.309	N/A	0.107	N/A	0.036
Br^-	0.111	0.219	0.077	N/A	0.005	N/A	0.009
SCN^-	0.178	0.464	0.448	N/A	0.325	N/A	0.031
BH_4^-	0.096	0.254	0.136	N/A	0	N/A	0.004
$B(CH_3)_4^-$	0.044	0.114	0.043	N/A	0.028	N/A	0.162
$B(C_2H_5)_4^-$	0.033	0.135	0.022	N/A	0	N/A	0.136
Specific (GKS-EDA)							
PO_4^{3-}	0.142	0.006	0.418	0.417	0.45	0.131	0.486
CO_3^{2-}	0.398	0.229	0.148	0.13	0.347	0.09	0.382
HPO_4^{2-}	0.419	0.235	0.079	0.059	0.267	0.124	0.434
SO_4^{2-}	0.333	0.157	0.152	0.131	0.389	0.166	0.402
$H_2PO_4^-$	0.646	0.347	0.016	0.028	0.166	0.375	0.267
HCO_3^-	0.679	0.388	0.005	0.02	0.087	0.186	0.313
HSO_4^-	0.5	0.501	0.083	0.134	0.246	0.184	0.26
OH^-	0.628	0.592	0.139	0.185	0.077	0.075	0.006
F^-	0.622	0.636	0.012	0.039	0.023	0.05	0.11
CH_3COO^-	0.693	0.638	0.042	0.076	0.038	0.091	0.144
Cl^-	0.571	0.614	0.211	0.321	0.005	0	0.021
NO_3^-	0.657	0.517	0.01	0.012	0.01	0.081	0.191
Br^-	0.683	0.75	0.232	0.318	0.173	0.087	0.32
I^-	0.477	0.403	0.072	0.135	0.102	0.002	0.007
ClO_4^-	0.675	0.516	0.049	0.11	0.025	0.007	0.045
SCN^-	0.461	0.356	0.008	0	0.106	0.001	0.121
Cluster (GKS-EDA)							
PO_4^{3-}	**0.824**	0.726	0.327	0.357	0.222	0.008	0.454
CO_3^{2-}	**0.808**	0.71	0.395	0.438	0.247	0.012	0.333
HPO_4^{2-}	**0.834**	0.77	0.618	0.657	0.515	0.016	0.019
SO_4^{2-}	**0.827**	0.692	0.534	0.571	0.256	0.001	0.043
$H_2PO_4^-$	**0.857**	0.858	0.746	0.764	0.817	0.074	0.244
HCO_3^-	**0.852**	0.85	0.643	0.673	0.76	0.025	0.023
HSO_4^-	**0.77**	0.802	0.682	0.708	0.71	0.096	0.429
OH^-	**0.883**	0.86	0.643	0.697	0.663	0.123	0.434
F^-	**0.853**	0.809	0.277	0.366	0.083	0.28	0.772
CH_3COO^-	**0.843**	0.847	0.61	0.644	0.682	0.161	0.072
Cl^-	**0.713**	0.807	0.582	0.659	0.197	0.126	0.104
NO_3^-	**0.684**	0.778	0.61	0.628	0.528	0.006	0.322
Br^-	**0.853**	0.762	0.308	0.322	0.276	0.034	0.269
I^-	**0.501**	0.706	0.39	0.432	0.136	0.201	0.3
ClO_4^-	**0.638**	0.779	0.625	0.649	0.526	0.026	0.393
SCN^-	**0.657**	0.694	0.24	0.283	0.183	0.138	0.038

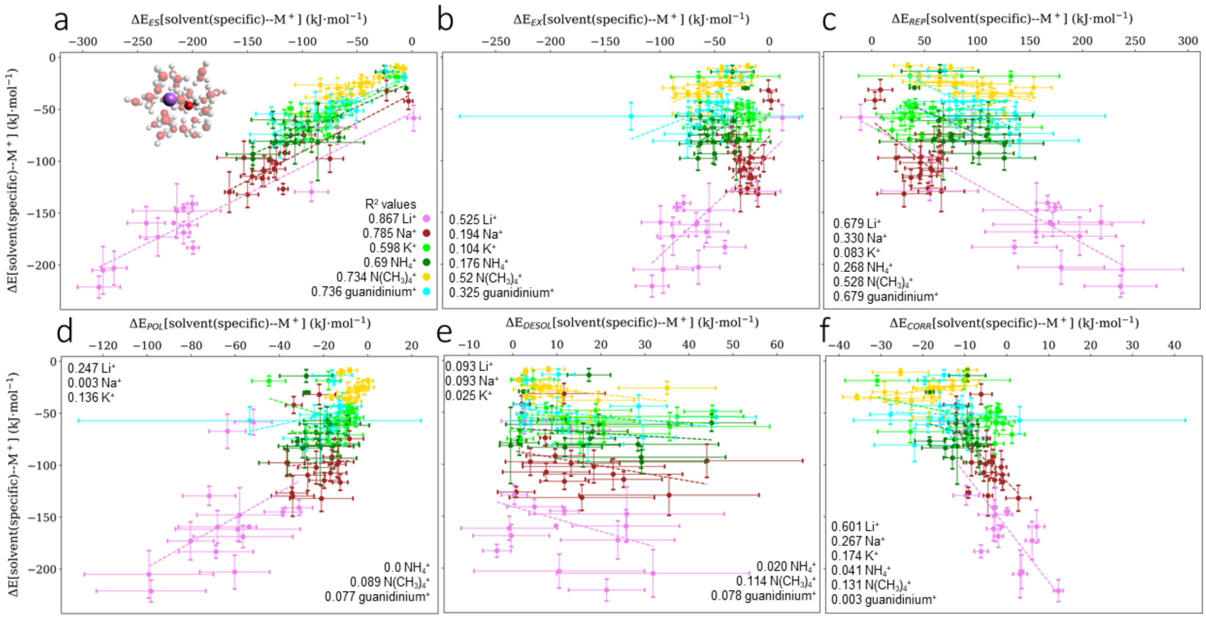

Figure S8: Comparison of the GKS-EDA (DFTB3(D3-BJ)/3-ob-3-1//M06-2X/cc-pVDZ) total *cation-solvent 1:1 pairwise interactions in the cluster model (including a PCM solvent environment)* interaction energy with the (a) electrostatic, (b) exchange, (c) repulsion, (d) polarisation, (e) desolvation and (f) correlation component energies. All data is averaged across multiple independent configurations; error bars denote 1 standard deviation. This figure emphasises the solvent trends for a particular cation, as opposed to the cation trends for a particular solvent (see, Figure S18).

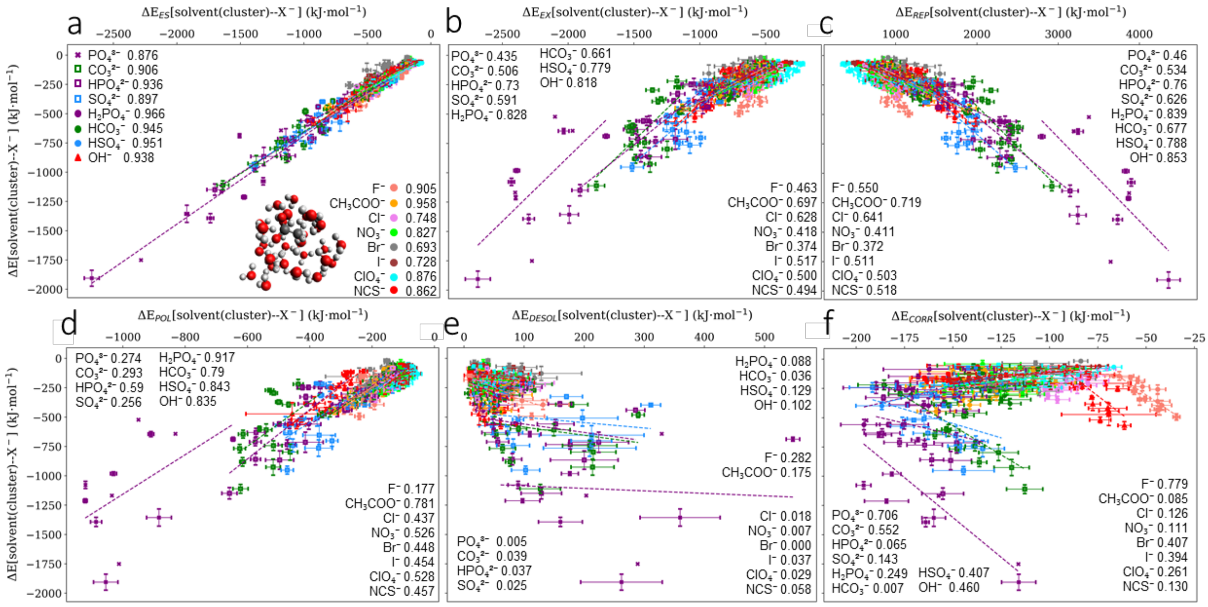

Figure S9: Comparison of the GKS-EDA (DFTB3(D3-BJ)/3-ob-3-1//M06-2X/cc-pVDZ) total *anion and its solvating shell in the cluster model (including a PCM solvent environment)* interaction energy with the (a) electrostatic, (b) exchange, (c) repulsion, (d) polarisation, (e) desolvation and (f) correlation component energies. All data is averaged across multiple independent configurations; error bars denote 1 standard deviation. This figure emphasises the solvent trends for a particular anion, as opposed to the anion trends for a particular solvent (see, Figure S25).

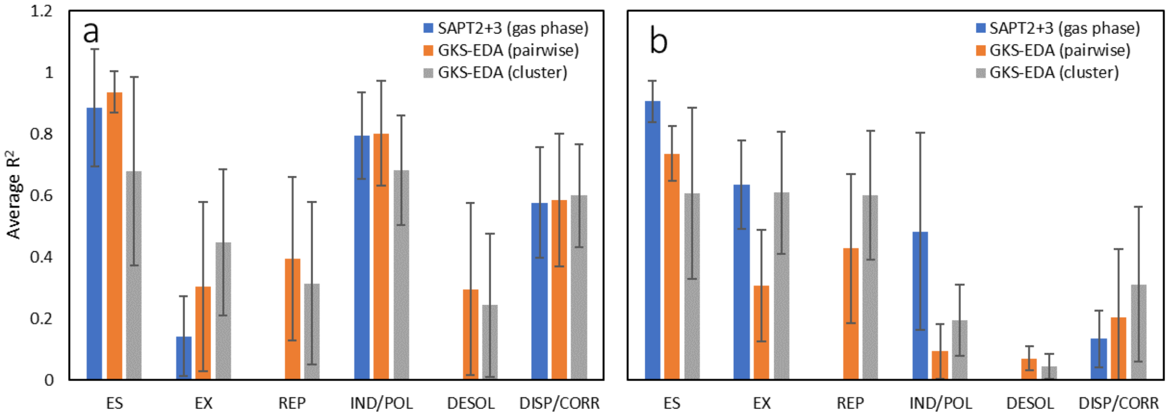

Figure S10: The average of all coefficients of determination (R^2) for each of the cation-solvent energetic contributions (electrostatics – ES, exchange – EX, repulsion - REP, induction or polarisation – IND/POL, desolvation – DESOL and dispersion or correlation – DISP/CORR) with the total energy in the three different ion-solvent models for (a) constant solvents and (b) constant cations. Error bars represent the standard deviation of all coefficients of determination (R^2). Note that in SAPT2+3 exchange and repulsion is combined into the exchange term, induction is used, rather than GKS-EDA's polarisability term and SAPT2+3 does not have the desolvation term as there is no implicit solvation present. These R^2 values relate to Figure S12-Figure S20.

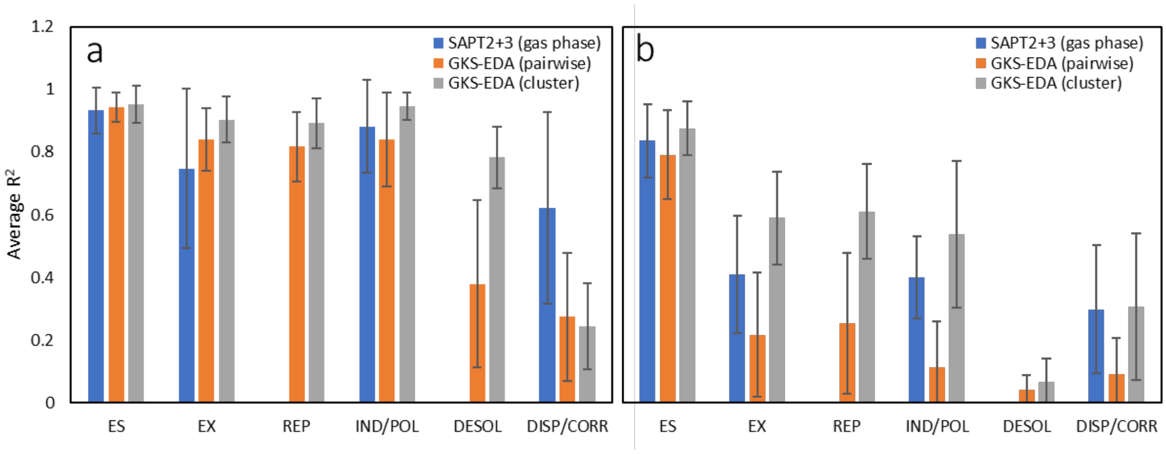

Figure S11: The average of all coefficients of determination (R^2) for each of the anion-solvent energetic contributions (electrostatics – ES, exchange – EX, repulsion - REP, induction or polarisation – IND/POL, desolvation – DESOL and dispersion or correlation – DISP/CORR) with the total energy in the three different ion-solvent models for (a) constant solvents and (b) constant cations. Error bars represent the standard deviation of all coefficients of determination (R^2). Note that in SAPT2+3 exchange and repulsion is combined into the exchange term, induction is used, rather than GKS-EDA's polarisability term and SAPT2+3 does not have the desolvation term as there is no implicit solvation present. These R^2 relate to Figure S9,Figure **S21**-Figure **S25**.

S4. Cation-Solvent Interactions

S4.1 Gas phase cation-solvent interactions and their component energies

SAPT2+3/aug-cc-pVDZ electrostatic, induction, exchange, and dispersion components of the pairwise ion-solvent interaction energies for cations (Li^+, Na^+, NH_4^+, $N(CH_3)_4^+$, $N(C_2H_5)_4^+$ and guanidinium$^+$) and the solvents listed in Table 2 are presented in Figure S12(a), (b), (c) and (d), respectively. Corresponding minimum energy structures are shown in Figure S4 and are the basis of the following discussion. For all monovalent cation-solvent combinations investigated here a general correlation exists between the total interaction energy and the electrostatic contribution (Figure S12(a)). This indicates that the total cation-solvent pairwise interactions might be approximated by the electrostatic contribution. Considering the presence of a charged species in these complexes, the dominance of the electrostatic contribution is unsurprising. It is nevertheless striking that the same correlation appears generally across multiple ions and solvents. The exception here is for the cation-toluene, cation-hexane, and to a lesser extent, cation-EDC interactions which exhibit weaker electrostatic contributions than the general trend. In these cases, the induction behaviour is instead the dominant intermolecular force (Figure S12(b)). To exemplify these exceptions, the strongest Na^+ solvent or cation formamide interactions, representing a relatively charge dense cation and Lewis basic solvent respectively, are dominated by the electrostatic contribution (Figure S26 and Figure S28 respectively). However, the strongest cation toluene interaction, representing a weakly Lewis basic solvent, is induction dominated (Figure S29). Of note here is the fact that for both a charge dense and charge diffuse cation (*e.g.*, Na^+ and $N(C_2H_5)_4^+$) the solvent's radial charge density of the negative dipolar atom (þ$^{-}_{\text{solvent}}$) correlates well with the electrostatic energy contribution for the majority of the solvents (Figure S26(b), Figure S27(b)). A more extensive electrostatic analysis reveals that the outliers can be accounted for as well (Figure S49-Figure S54).

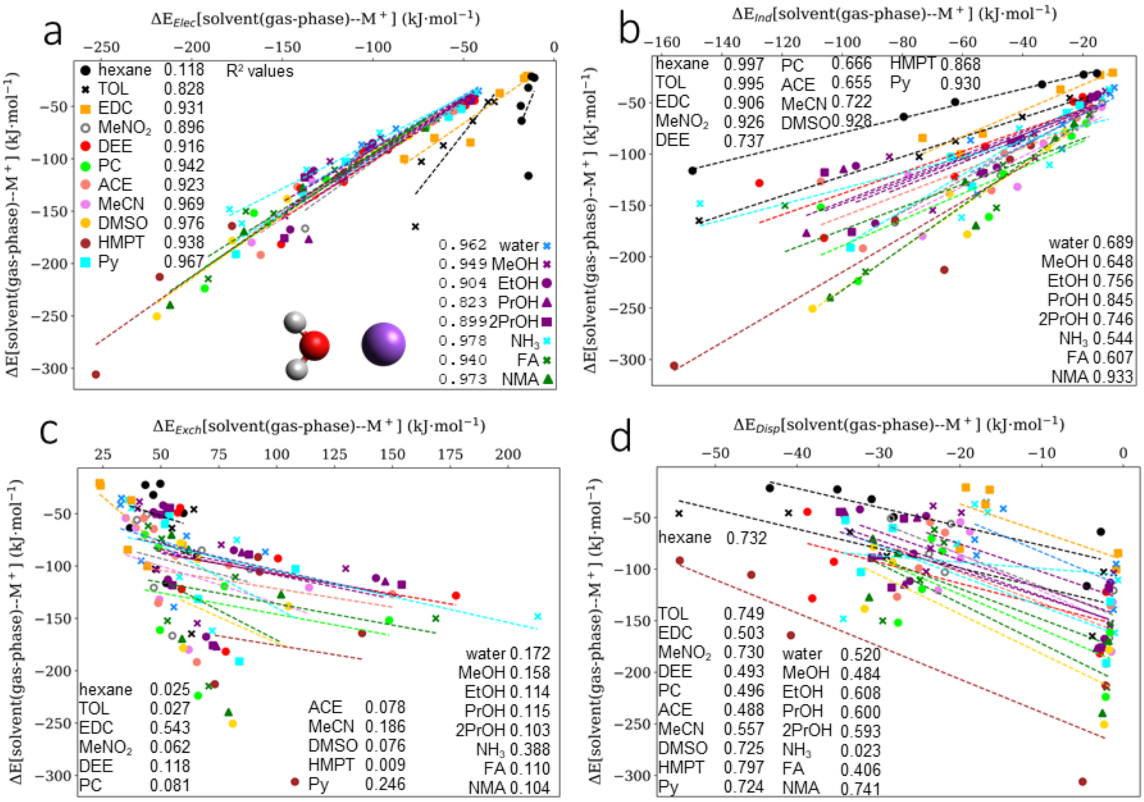

Figure S12: Comparison of the M06-2X/aug-cc-pVDZ//SAPT2+3/aug-cc-pVDZ total *cation-solvent pairwise interactions* interaction energy for with the a) electrostatic, b) induction, c) exchange and d) dispersion component energies. This figure emphasises the cation trends for a particular solvent, as opposed to the solvent trends for a particular cation (see, Figure S13). Here we can see that for any protic or polar solvent (with few exceptions) there is a strong trend between the (a) electrostatic contribution and the total energy. It appears that for the non-polar solvents, this trend is strongest for the (b) induction contribution. For the (c) exchange contribution there appears are no obvious trends occurring for each solvent. A weaker inverse correlation is seen for the (d) dispersion contribution. All geometries in Figure S4.

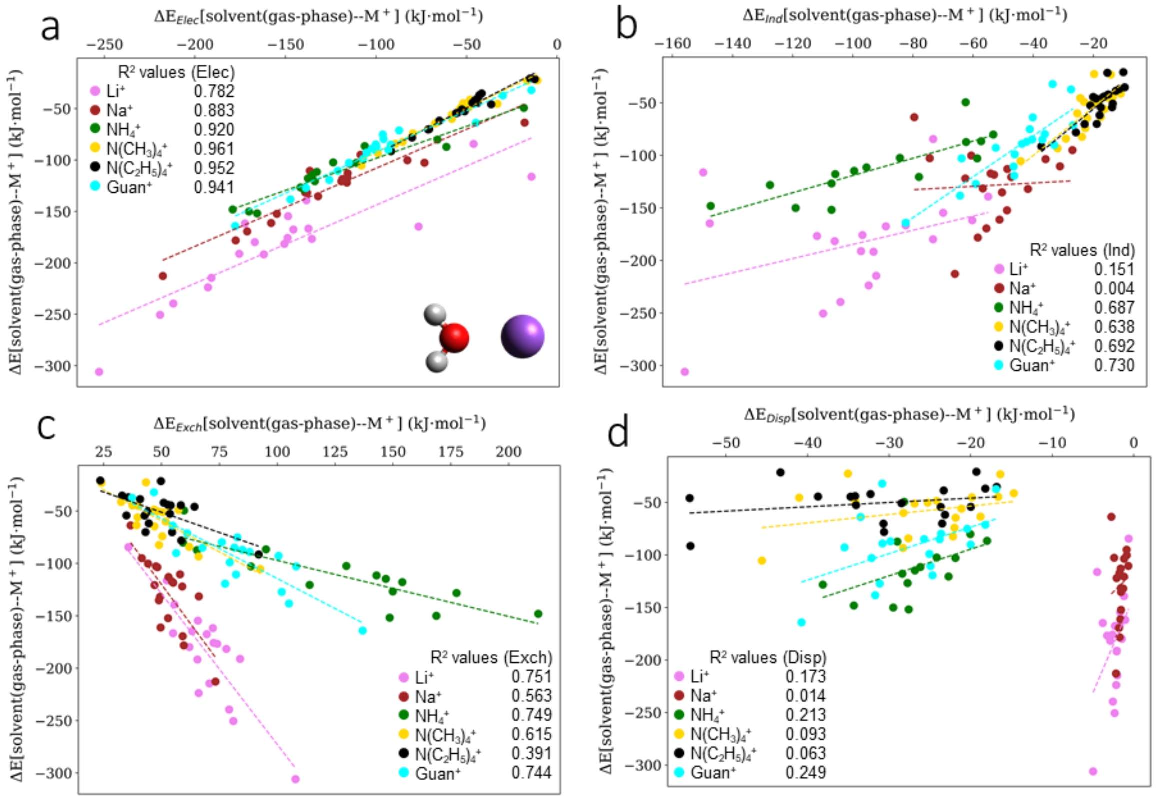

Figure S13: Comparison of the M06-2X/aug-cc-pVDZ//SAPT2+3/aug-cc-pVDZ total *cation-solvent pairwise interactions* interaction energy for with the a) electrostatic, b) induction, c) exchange and d) dispersion component energies. This figure emphasises the solvent trends for a particular cation, as opposed to the cation trends for a particular solvent (see, Figure S12). All geometries in Figure S4.

In general, the induction components (Figure S12(b)) present a similar, yet slightly weaker and more solvent-dependent trend to those observed for the electrostatic component. Both the induction and electrostatic component are ultimately determined by the charge densities of the interacting species (As seen in Figure S26 and Figure S9 (b) of ref 4, respectively), and so this overall trend is unsurprising. An example of the solvent dependence is seen here for cation-toluene interactions, which deviates from the more common trend due to the increased induction contribution inherent to the cation-π interaction.[6] Similarly, cation-hexane interactions also have increased induction contributions, as they form an alkyl chain "pocket", through which they interact directly with the carbon atoms (Figure S4). The solvent-dependence of the induction is consistent with the solvent molecule's average polarisability (α_{solvent}), perhaps with a dual dependence on the degree of contact of the solvent's polarisable atoms with the cation (Figure S26(c), Figure S27(c), Figure S30). For Na$^+$, the induction energy ordering follows the order: hexane > TOL > HMPT > DEE > EDC > DMSO > Py > NMA > PrOH > 2PrOH > PC ≈ ACE > FA ≈ EtOH > MeNO$_2$ > MeCN > MeOH > NH$_3$ > water (see structures in Figure S26(a)). Exceptions to the solvent polarisability – induction energy relationship appear to arise for solvents where the cation-solvent interaction geometry (Figure S4) does not fully utilise the most polarisable atoms in its structure. For instance, the Li$^+$-EDC interaction here occurs orthogonally through only one chlorine atom, whereas the Na$^+$ EDC interaction occurs via two chlorine atoms. In the former case EDC does not fall in trend with the solvent polarizability (Figure S30(c)), whereas for the Na$^+$ interactions it does (Figure S30(d)). The generality of this trend also appears to weaken for the larger polyatomic cations which are less charge-dense and have more conformational degrees of freedom (Figure S30), as well as protic cations, which are susceptible to partial proton transfer events in these gas phase optimisations. While induction appears to relate to the solvent's polarisability, the magnitude of the induction component for each ion, (characterised by the gradient of each series Figure S30), correlates with the ion's electrostatic properties (Figure S14). In this regard, the cation TOL induction contributions to the interactions (Figure S29(c)), correlate strongly with þ$^{+}_{\text{cation}}$. However, for the more Lewis basic FA (Figure S28(c)), the cation-FA induction energy component deviates for both the protic solvents, NH_4^+ and guanidinium$^+$, with respect to þ$^{+}_{\text{cation}}$.

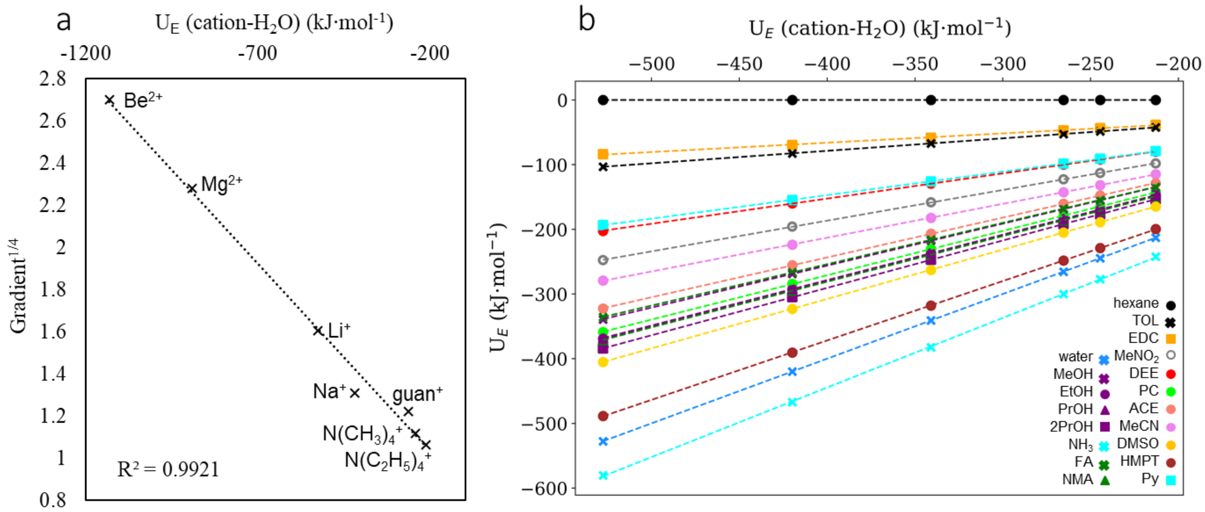

Figure S14: (a) The cations electrostatic potential energy with water (calculated via DDEC6 charges and effective radial moments using Eq. S4) compared to the fourth root of the induction energy-solvent polarisability gradients (excluding NH_4^+) obtained from the correlations in Figure S30 for all solvents. The fourth root is taken here given both charge dipole and charge-non-polar interactions scale with $1/r^4$ according to Israelachvili,[7] whereas U_E scales with 1/r. (b) The cation-water U_E is used as a proxy for all solvents given the covariance ($R^2 > 0.999$) with the cation-nonaqueous solvent, whereas a cations þ values are non-linear and charge dependent with respect to its U_E with water.[4]

Correlations between the exchange component energy and the total interaction energy exhibit limited trends, in terms of the cation trends (Figure S12(c)), though stronger correlations exist in terms of the solvent trends (Figure S13(c)). As an example, the exchange contribution for Na^+-solvent interactions has a comparably low correlation with the total energy value ($R^2 = 0.563$, Figure S13(c)), with little variance between each solvent where the average exchange component is 50.9 ± 8.4 kJ·mol^{-1}. This also has little correlation with the solvent or cation þ values (Figure S26-Figure S29(d)). For $N(C_2H_5)_4^+$solvent interactions, the exchange energy varies more substantially than it did for Na^+, and becomes a significant contributor to the overall interaction energies investigated here (Figure S26-Figure S27(d)). This is not due to an increase in the average exchange contribution of 46.7 ± 17.3 kJ·mol^{-1} however, merely a reduction in the other energy components. The exchange component does seem to exhibit cation "family" based trends (Figure S13(c)) when considering the proticity of the cations or whether they are polyatomic. The exchange contributions to the total interaction energies (Figure S13(c)) are larger for protic cations (*i.e.*, NH_4^+ and guanidinium$^+$), and largest for the interaction between NH_4^+ and NH_3 which exist in vacuum as two NH_3 molecules equally sharing the proton, and thus have a strong induction contribution (Figure S12(b)). This increase in the exchange component has been seen previously for proton transfer between formamide, formamidine and formic acid.[8]

The dispersion component similarly has a limited correlation with the total interaction energy (Figure S31(d)). A notable difference in the dispersion contribution is evident when comparing the monatomic and ammonium cation families (Figure S15). For the small monatomic cations investigated here, dispersion is approximately negligible (< 5 kJ·mol^{-1} in magnitude, or < 5% of the total interaction energy), whereas for alkyl-ammonium cations, dispersion becomes significant (up to 90% for TOL-$N(CH_3)_4^+$), and can exceed the total interaction energy itself (e.g. TOL-$N(C_2H_5)_4^+$, hexane-$N(CH_3)_4^+$ and hexane-$N(C_2H_5)_4^+$ for which the dispersion components are 119%, 155% and 202% of the total interaction energy respectively). The dispersion component would be expected to increase further still with longer alkyl chain lengths on the ammonium cations, as there is a relationship between ΔE_{Disp} and the SA of the cation molecules (Figure S34(e)). However, consideration of the interaction geometry (Figure S4) is also required. For example, formamide interacts with each cation in an orthogonal manner (Figure S28(a)), and has dispersion contributions of near equal magnitude for each polyatomic cation (Figure S28(e)). On the other hand, for solvents interacting with the cation in a planar fashion (e.g. TOL), the dispersion contribution increases simply with the ion's surface area (Figure S29(e)).

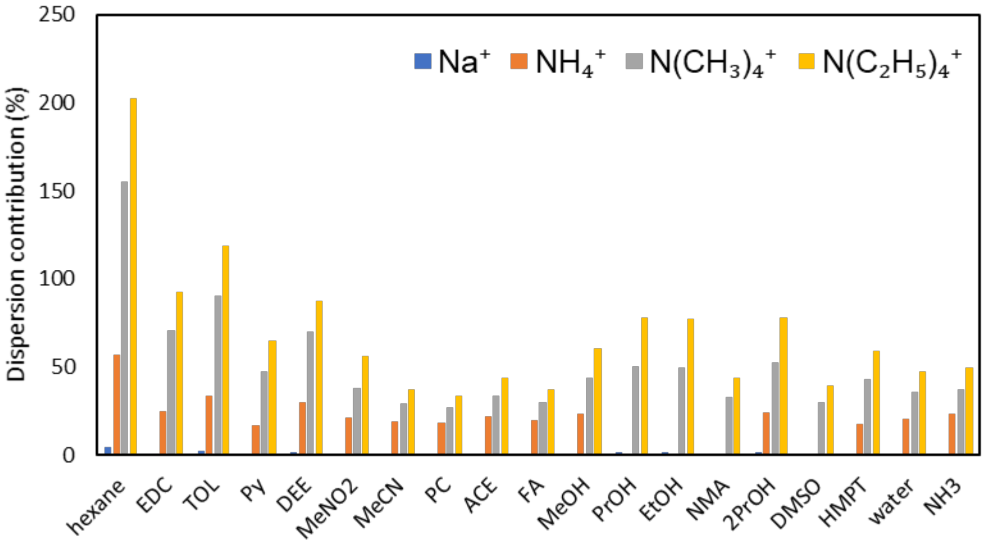

Figure S15: The percent of the total energy that the dispersion contribution takes up for the ammonium cations. Sodium (blue) represents how insignificant this contribution is for the monatomic cations, whereas these become substantial for the polyatomic cations, exceedingly so with larger and larger cations. Solvents ordered by their $þ^{-}_{\text{solvent}}$.

When instead investigating the interactions of different solvents with a constant cation, the dispersion contribution roughly correlates with the SA of each isolated solvent molecules (Figure S31). As was the case for a constant solvent, considering the interaction geometries of each cation-solvent interaction (Figure S27(a), or Figure S4), provides further insight into the physical basis of this correlation. For a constant $N(C_2H_5)_4^+$ cation (Figure S27(e)) SA exhibits a linear correlation with the overall interaction energy for water, NH_3, MeOH, FA, $MeNO_2$, PrOH, 2PrOH and DEE (black crosses). In these cases, a significant portion of the solvent electron density can interact with that of the $N(C_2H_5)_4^+$ cation. On the other hand, for MeCN, ACE, PC, EDC and HMPT there is a significant portion of the solvent that does not directly interact with the cation. TOL is unique in this dataset as the cation-π interaction, and this appears to increase its dispersion interaction with respect to the surface area. Notably, MeOH, FA, ACE and PC each have dispersion energy contributions of approximately equal magnitudes (-23.3, -23.2, -23.7, -23.5 kJ·mol^{-1} respectively), whilst also sharing similar oxygen interaction geometries. Even for the negligible Na^+-solvent dispersion energy contributions (Figure S27(e)), for most solvents there is a strong correlation with the solvent surface area. Indeed, looking directly at the cation-solvent contact surface area reveals a strong correlation (Figure S32), especially for the largest cation, $N(C_2H_5)_4^+$. Alternatively, the cubed root of the C_6 dispersion coefficient appears to also be another effective parameter in this regard (Figure S34), sharing a strong correlation with the surfaces area of these solvents and ions (Figure S33). These results formalise the assertion that dispersion increases with molecular size.

S4.2 Pairwise Cation-Solvent Interactions in a Solvent Cluster

Whilst pairwise interactions in the gas-phase (§S4.1) are highly useful at informing us of the key fundamental forces involved in these interactions, it is important to also consider these interactions in a larger cluster model with a solvent shell (or two). The effects of solvent crowding and solvent-solvent interactions may diminish (or enhance) any single ion-solvent interaction. This might also be affected by the coordination number (CN) as a cation's intermolecular forces are spread in each direction, for instance, solvent stabilisation could occur, where inductive forces are spread across multiple solvent molecules, given their directionality (*i.e.*, the likelihood of proton transfer in NH_4^+ decreases from the gas-phase to the cluster model (Figure S16)).

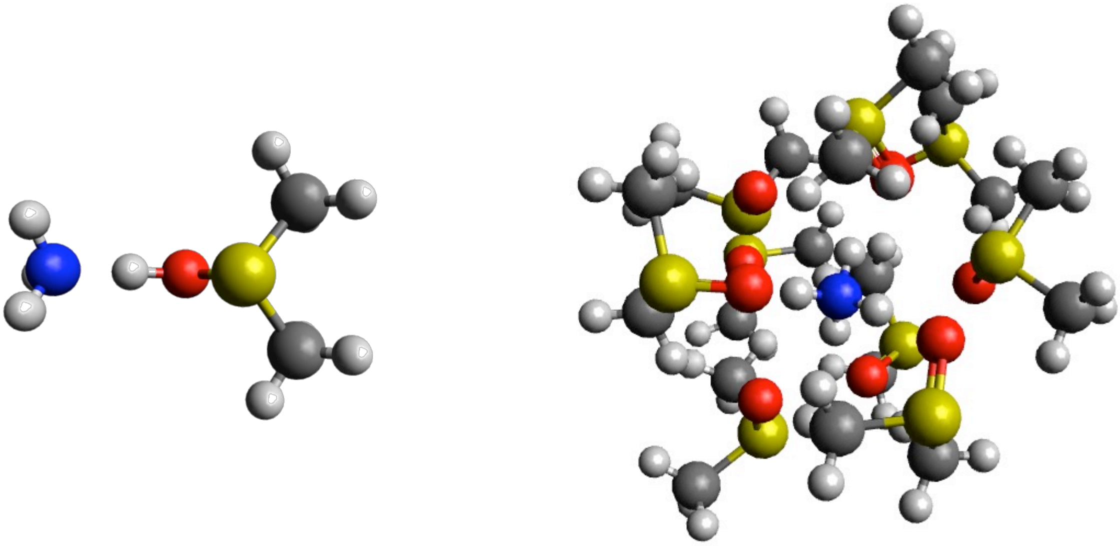

NH_4^+-DMSO
Gas-phase interaction

NH_4^+-DMSO
Cluster interaction

Figure S16: In the gas-phase optimisations, NH_4^+ is deprotonated by a DMSO solvent molecule, whereas this doesn't occur in the cluster model optimisations (notably these are optimised with M06-2X/aug-cc-pVDZ and DFTB/3ob-3-1 respectively).

Given the high throughput nature of this analysis, in conjunction with inhibitive scaling of SAPT2+3 when considering this solvent cluster model, GKS-EDA is employed for its lower computational cost in conjunction with the ability to incorporate implicit solvation, as used by us previously.[4,9] The component energies from GKS-EDA(sol) (e.g. Figure S17(d)) differ slightly from SAPT, in that they are decomposed into the electrostatic, exchange, repulsion, polarisation, desolvation and correlation contributions. Nonetheless, the trends considered here (Figure S18) follow those that were seen in the gas-phase SAPT2+3 interactions in §S4.1.

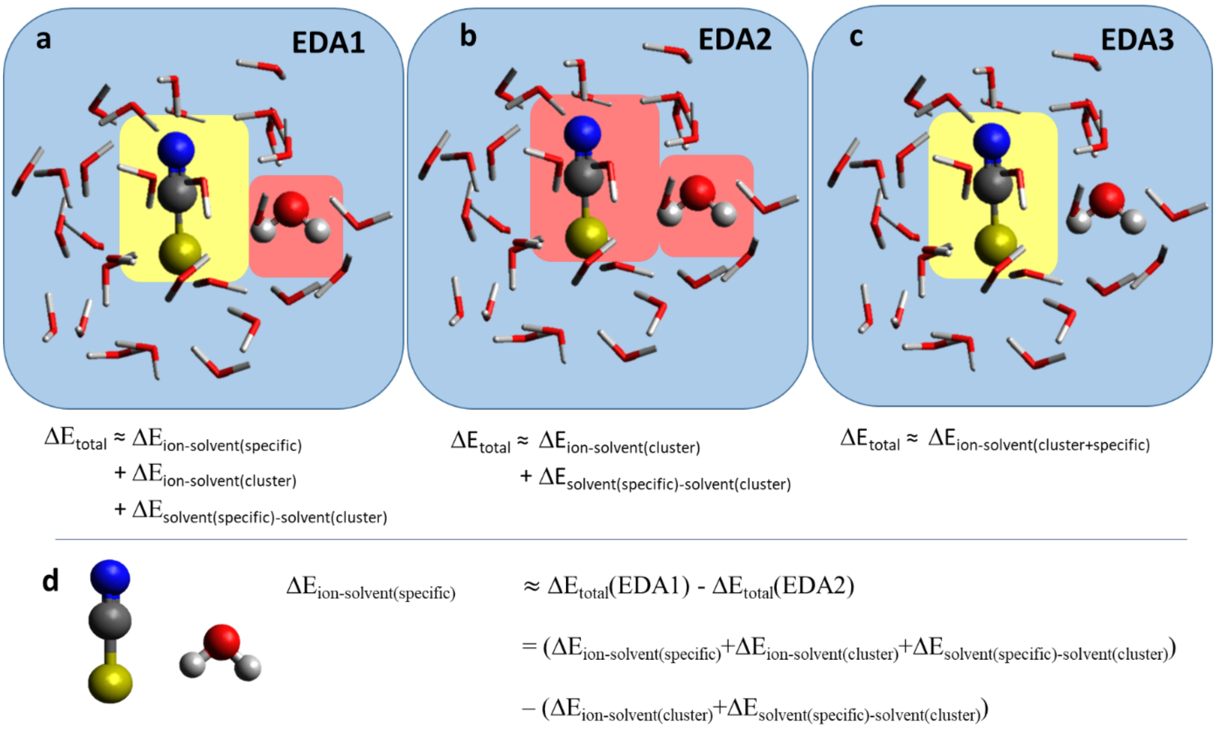

$\Delta E_{\text{total}} \approx \Delta E_{\text{ion-solvent(specific)}} + \Delta E_{\text{ion-solvent(cluster)}} + \Delta E_{\text{solvent(specific)-solvent(cluster)}}$

$\Delta E_{\text{total}} \approx \Delta E_{\text{ion-solvent(cluster)}} + \Delta E_{\text{solvent(specific)-solvent(cluster)}}$

$\Delta E_{\text{total}} \approx \Delta E_{\text{ion-solvent(cluster+specific)}}$

$$\begin{aligned}\Delta E_{\text{ion-solvent(specific)}} &\approx \Delta E_{\text{total}}(\text{EDA1}) - \Delta E_{\text{total}}(\text{EDA2})\\ &= (\Delta E_{\text{ion-solvent(specific)}} + \Delta E_{\text{ion-solvent(cluster)}} + \Delta E_{\text{solvent(specific)-solvent(cluster)}})\\ &\quad - (\Delta E_{\text{ion-solvent(cluster)}} + \Delta E_{\text{solvent(specific)-solvent(cluster)}})\end{aligned}$$

Figure S17. EDA schemes for elucidating ion-solvent interaction free energies (ΔE), illustrated for a water solvent and SCN^- ion. (a) EDA1 partitions the system into the bulk solvent, ion and single specifically interacting solvent molecule. (b) EDA2 partitions the system into bulk solvent and ion-solvent complex. (c) EDA3 partitions the system into the ion and the solvent fragments. (d) The one-to-one ion-solvent interaction may be approximated as the difference between EDA1 and EDA2.

Figure S18(a) shows that, similarly to gas-phase interactions, the electrostatic interaction is the main contributing energy for pairwise cation-solvent interactions in a cluster model. In fact, in many cases the electrostatic interaction is of larger magnitude than the total interaction energy itself. This is possible due to comparably strong repulsive contributions (Figure S18(c)). Broad, yet weaker trends also exist for the exchange (Figure S18(b)) and polarisation (Figure S18(d)) energies. Indeed, two exceptions to the electrostatic dominance generality are hexane and EDC, both with a DN of 0. In these circumstances, the polarisation term is dominant, consistent with the pairwise SAPT2+3 induction term for these solvents. The desolvation contribution (Figure S18(e)) in these cases is more of an indicator of how well (explicitly) solvated the interacting site of the ion and solvent molecule is. Ideally this will be small, however it can become increasingly large (in comparison to the total energy) when an ion (or interacting solvent) has a solvent accessible surface for the PCM (*i.e.*, many of the PC interactions where only five solvent molecules were used have larger desolvation penalties). The correlation contribution (Figure S18(f)) follows an inverse trend with the total interaction energy being dominant. For the strongest interactions, the correlation energy is almost negligible (*e.g.*, Li^+ with DMSO (-52.9 ± 2.5 kJ·mol^{-1} total energy; 2.9 ± 0.3 kJ·mol^{-1} correlation energy)), yet for weaker interactions (*i.e.*, large cations) it makes a significant contribution to the total energy (*e.g.*, $N(CH_3)_4^+$ with toluene (-8.3 ± 0.6 kJ·mol^{-1} total energy; -8.5 ± 0.8 kJ·mol^{-1} correlation energy)). Whilst the correlation energy is not directly comparable to the dispersion energy, it shares similar electronic origins, and as such are qualitatively consistent with the results in (Figure S12(d)).

Electrostatics are usually the driving force and somewhat predictive of the overall energy in most cases. However, van der Waals interactions become significant contributors for large bulky cations. This supports the hypothesis that the non-linear trends between þ and experimental data observed for cations in previous work[4] originate due to non-electrostatic forces becoming non-negligible or even competitive with the electrostatics.[4] None-the-less, for each cation the most pronounced solvent correlation with the total energy is with the electrostatic component (Figure S8(a)). This is consistent with the SAPT2+3 gas-phase interactions. Given Gutmann donor numbers[10,11] were developed from 1:1 interactions with the strong Lewis acid, $SbCl_5$, it should follow that the 1:1 interaction energy predominantly correlates with these and therefore may be parameterised via an electrostatic measure.

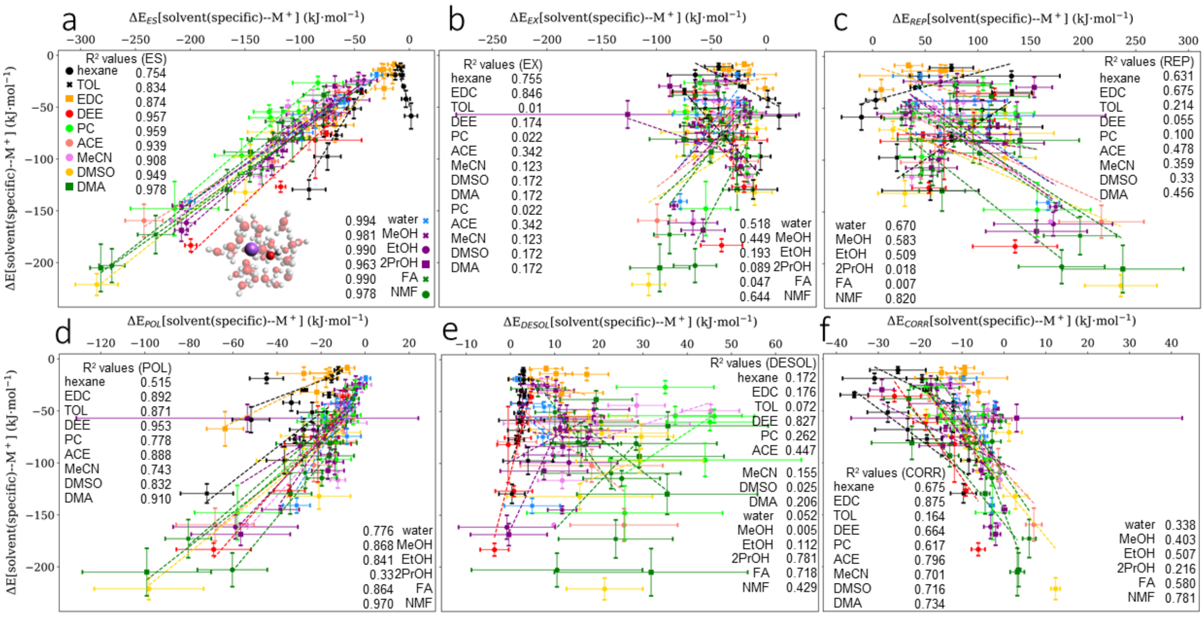

Figure S18: Comparison of the GKS-EDA (DFTB3(D3-BJ)/3-ob-3-1//M06-2X/cc-pVDZ) total *anion-solvent 1:1 pairwise interactions in the cluster model (including a PCM solvent environment)* interaction energy with the (a) electrostatic, (b) exchange, (c) repulsion, (d) polarisation, (e) desolvation and (f) correlation component energies. All data is averaged across multiple independent configurations; error bars denote 1 standard deviation. This figure emphasises the cation trends for a particular solvent, as opposed to the solvent trends for a particular cation (see, Figure S8).

S4.3 Cation-Solvent Cluster Interactions

While the Gutmann Donor number is a useful solvent parameters for the quantification of 1:1 Lewis acid-solvent interactions (albeit being empirical limits its understanding for generality and universal transferability), many interactions such as cation solvation energy and viscosity B coefficients are affected by (or a result of) the whole solvent shell.[4] Therefore, it would be useful to know the level of additivity from single interactions toward ion-bulk interactions, as well as verify the use of the Gutmann donor number for such interactions. Additionally, investigating how intermolecular forces differ from uni-directional interactions to radial many-body interactions aids our fundamental understanding, and should aid in comparisons with anionic solvent properties, something that may not be possible for Gutmann DN and AN given their dissimilar origins.

Using the same cation-solvent cluster structures presented in §S4.2, as opposed to isolating a 1:1 cation-solvent interaction from the system (via Figure S17(d)), the interaction is instead calculated between the cation and the entire surrounding solvent (via Figure S17(c)). Effectively, this allows us to inspect the interaction energy between the ion and its first solvation shell. As was the case in §S4.1-S4.2, electrostatics (Figure S19(a)) broadly represents the total interaction energy, given the overall gradient is approximately 1. Although of course there are some outliers here, the trends themselves are comparatively ion independent (Figure S20(a)). Where the trends look starkly different in comparison to the 1:1 interaction is the exchange contribution (Figure S18(b) and Figure S19(b)). For the specific 1:1 model the gradients of each specific ion were quite similar, whereas in the cluster model there is a difference for each ion, which appears size dependent (Figure S20 (b)). For example, the largest ion investigated here, $N(CH_3)_4^+$, has exchange contributions ranging from ~150-300% of the total energy (made possible by the similarly large repulsion energy contributions). Similarly, guanidinium$^+$ (~100-250%) and NH_4^+ (~50-200%) have significant exchange contributions. In contrast, the monatomic Li^+

(~10-50%) and Na$^+$ (~10-30%) ions have much smaller exchange contributions. Repulsion (Figure S19(c)), given its usual pairing with exchange, shares these trends, albeit even stronger and more repulsive. The polarisation contribution (Figure S19(d), Figure S20(d)) has a weak overall correlation with the total energy, while the correlation energy itself has an inverse correlation with the total energy.

While electrostatics are usually the driving force and somewhat predictive of the overall energy in most cases, van der Waals interactions become significant contributors for large bulky cations (Figure S20). This supports the hypothesis that the non-linear trends between þ and experimental data observed in the cations in prior work originate due to non-electrostatic forces becoming non-negligible or even competitive with the electrostatics.[4] The desolvation contribution in these cases is more of an indicator of how well (explicitly) solvated the interacting site of the ion and solvent molecule is. Ideally this will be small, however it can become increasingly large (in comparison to the total energy) when an ion (or interacting solvent) has a solvent accessible surface for the PCM (*i.e.*, many of the PC interactions where only five solvent molecules were used have larger desolvation penalties).

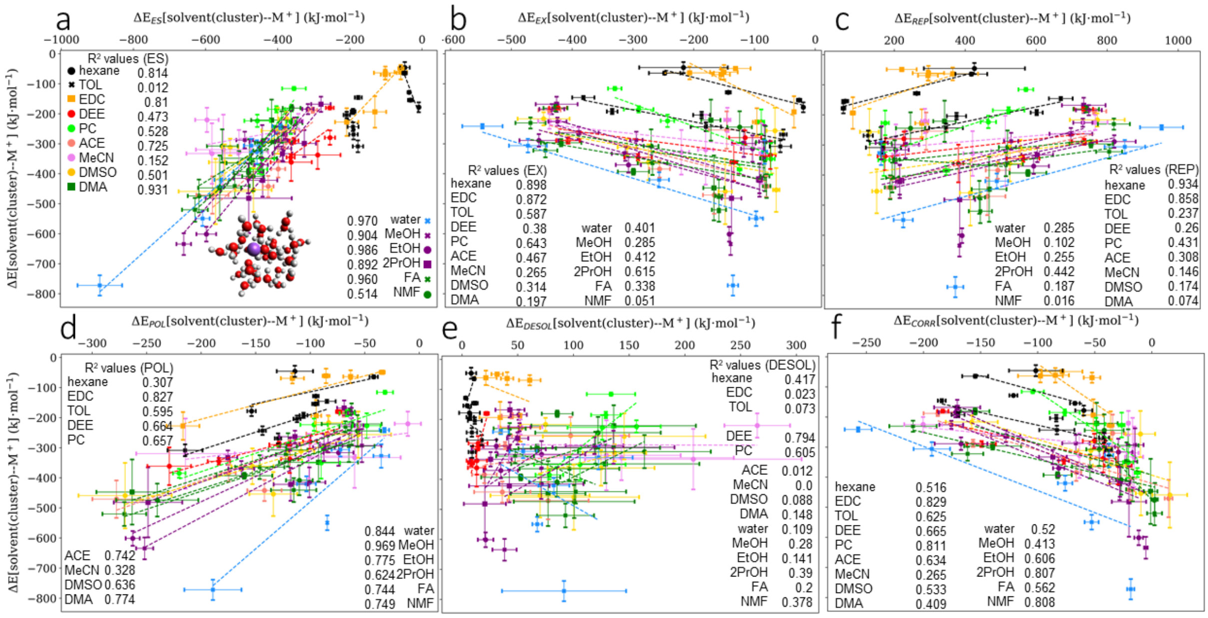

Figure S19: Comparison of the GKS-EDA (DFTB3(D3-BJ)/3-ob-3-1//M06-2X/cc-pVDZ) total *cation and its solvating shell the cluster model (including a PCM solvent environment)* interaction energy with the (a) electrostatic, (b) exchange, (c) repulsion, (d) polarisation, (e) desolvation and (f) correlation component energies. All data is averaged across multiple independent configurations; error bars denote 1 standard deviation. This figure emphasises the cation trends for a particular solvent, as opposed to the solvent trends for a particular cation (see, Figure S20).

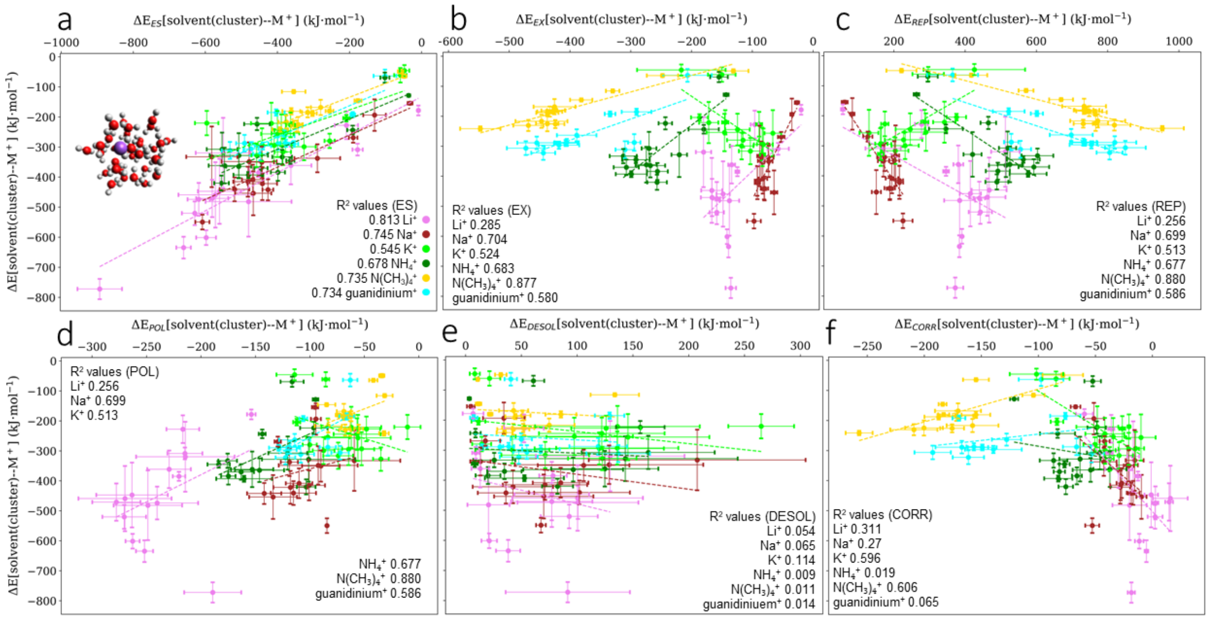

Figure S20: The GKS-EDA (DFTB3(D3-BJ)/3-ob-3-1//M06-2X/cc-pVDZ) (a) electrostatic, (b) exchange, (c) repulsion, (d) polarisation, (e) desolvation and (f) correlation energy components compared to the overall energy, between an ion and its solvating shell, for aqueous and nonaqueous solvents. This figure emphasises the solvent trends for a particular cation, as opposed to the cation trends for a particular solvent (see, Figure S19).

One example of these non-linear trends was for the Gibbs energy of transfer from water to methanol. In these two solvents, taking the difference in the electrostatic interaction between water and MeOH ($\Delta\Delta E_{ES}$ (water-MeOH)), for Na$^+$ a value of -5.7 kJ·mol^{-1} was obtained, while for $N(CH_3)_4^+$ this value was -9.3 kJ·mol^{-1} favouring water in both cases. In the former case the sum of the non-electrostatic interactions between water and MeOH ($\Delta\Delta E_{non\text{-}ES}$ (water-MeOH)) was found to be a water favourable -16.0 kJ·mol^{-1} for Na$^+$, yet a MeOH favourable value of 5.6 kJ·mol^{-1} was found for $N(CH_3)_4^+$. As discussed in §S4.2, the solvent properties primarily attributed to cation solvation are Lewis basicity (or hydrogen bond acceptor capability), and in this case the Gutmann donor number (DN) will be used as a representative example. As expected, there are correlations between the solvent-ion electrostatic component of the interaction strength and the solvent's DN for each ion (**Error! Reference source not found.**(a-c)), where the linear trends are generally stronger (higher R^2 value) for the smaller cations in the specific 1:1 interactions. For the ion-cluster interaction, the correlation is instead strongest for the larger cations (**Error! Reference source not found.**(c)).

S5. Anion-Solvent Interactions

S5.1 Gas phase anion-solvent interactions and their component energies

Investigating the energetic contributions of anion-solvent pairwise interactions (Figure S21) presents similar trends to those observed in cation-solvent interactions (Figure S12). Anions have a strong correlation between the total energy and its electrostatic component for all the anions and solvents investigated here (Figure S21(a)). This supports the conclusions that the electrostatic origins of specific ion effects are applicable, beyond water, to nonaqueous solvents.[4] In general, the minimum energy interaction site for a given solvent is consistent for each anion (Figure S5-Figure S6). One exception is the PO_4^{3-}-toluene interaction which is an outlier for each interaction component, and the probable origin for the weakened correlation observed for TOL. When investigating the $\text{þ}^{-}_{\text{anion}}$ relationship with the electrostatic component of the interaction energy for both a protic solvent, formamide (Figure S35(b)) and aprotic solvent, toluene (Figure S36(b)), a strong correlation exists. Alternatively, when considering a given anion for a range of solvents, the interaction geometries have more variability given each solvent has a differing number of contact-points with the ion (*e.g.*, Figure S37(a) and Figure S38(a)). This means that a single solvent $\text{þ}^{+}_{\text{solvent}}$ value may be insufficient for correlating with its electrostatic contribution, and this is the indeed case for both Cl^- (Figure S37 (b)) and $B(C_2H_5)_4^-$ (Figure S38(b)). It would appear for these lone anion-solvent interactions, a more comprehensive electrostatic analysis is required (Figure S60(d)). Nonetheless, $\text{þ}^{+}_{\text{solvent}}$ does correlate with empirical solvent properties such as the acceptor number (Figure S62) once coordination is accounted for, likely due to the non-specific interactions occurring in AN measurements. Similarly, for direct comparisons with these computational results, the correlation is stronger with $\text{þ}^{+}_{\text{solvent}}$ when in a cluster environment (Figure S48(d-f)).

As was the case with the cation-solvent interactions, the induction contribution of the total energy has a strong correlation that is slightly more solvent dependent (Figure S21(b)). For example, nonpolar solvents such as TOL and hexane, or solvents with larger hydrophobic groups, such as PrOH, have larger gradients for their induction contribution than some of the smaller solvents such as water, NH_3 and $MeNO_2$. In line with previous work,[4] in which there was also a strong relationship between $\text{þ}^{-}_{\text{anion}}$ and its induction contribution for anion-water interactions, a similarly strong relationship exists for both the protic FA (Figure S35(c)) and aprotic TOL (Figure S36(c)) nonaqueous examples. However, the strong relationship between the solvent's polarizability and the pairwise cation-solvent induction contribution (Figure S26 and Figure S27), does not similarly persist for the anions (Figure S35(b)) and (Figure S36(b)). By the very nature of these anion-solvent interactions taking place at electron deficient hydrogen atoms, the polarisability of the solvent is of less relevance.

For the exchange contribution, (Figure S21(c)) a stronger correlation with the total energy persists for anions than was observed for the cations (except for HMPT, DEE and TOL which are skewed by PO_4^{3-} outliers). $\text{þ}^{-}_{\text{anion}}$ once again has a strong correlation with the exchange energy contribution for both the protic FA (Figure S35(d)) and aprotic TOL (Figure S36(d)) nonaqueous examples. When observing Figure S35-Figure S36 (b-d), it is perhaps unsurprising that $\text{þ}^{-}_{\text{anion}}$ can quantify many experimental SIE, given the covariance between these three stronger terms. No direct correlation exists for $\text{þ}^{+}_{\text{solvent}}$ with the exchange energy contribution for either Cl^- (Figure S37(d)) or $B(C_2H_5)_4^-$ (Figure S38(d)). So, as was the case of the cations, and negative solvent dipoles, the exchange contribution does not correlate with these simple descriptors.

Finally, the dispersion contribution (Figure S21(d)) for the anions follows a direct correlation (again with PO_4^{3-} outliers) with the overall interaction energy**.** This is the opposite to the inverse correlation observed for cations (Figure S12(d)). Likely this is one manifestation of the polyatomic nature of the multivalent anions included in this dataset. For example, citrate^{3-} and PO_4^{3-} are the most charge dense anions in this dataset, yet they are also some of the larger anions. Conversely, the most charge-dense cation considered here is Li^+, which is also the smallest cation. The opposing behaviour of cations and anions with respect to dispersion is consistent with work by Duignan *et al.*[12] as well as those observed in our own previous work.[4] Using surface areas (SA) to approximate either the anion (Figure S35-Figure S36(e)), or solvent (Figure S37-Figure S38(e)) dispersion contributions shows less of a correlation for anion-solvent interactions than it did for cation-solvent interactions. For $B(C_2H_5)_4^-$ (Figure S38(e)), dispersion becomes a significant contribution to the total interaction energy and if the geometries of the interactions are considered, solvents that had lower dispersion contributions than the overall trend all share the fact that a large portion of the solvent is not in direct contact with the anion. Indeed, the contact surface area correlates well with the dispersion contribution for most anions (Figure S39), especially the more charge diffuse anions such as $B(C_2H_5)_4^-$.

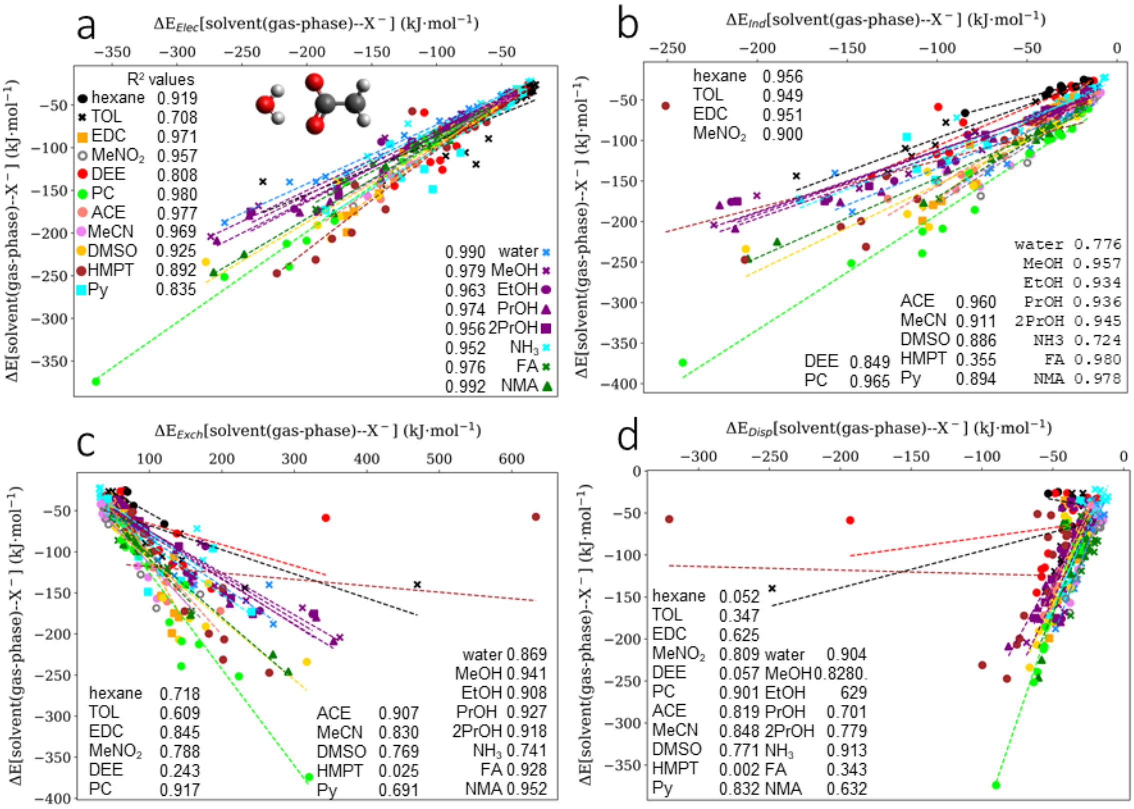

Figure S21: Comparison of the M06-2X/aug-cc-pVDZ//SAPT2+3/aug-cc-pVDZ total *anion-solvent pairwise interactions* interaction energy for with the a) electrostatic, b) induction, c) exchange and d) dispersion component energies. This figure investigates the anion trends for a particular solvent, as opposed to the solvent trends for a particular anion (see, Figure S22). Here we can see that for any protic or polar solvent (with few exceptions) there is a strong trend between the (a) electrostatic contribution and the total energy. Similarly, strong trends are observed for the (b) induction contribution, albeit with a larger solvent dependence. For the (c) exchange contribution there appears to be general trends with the total interaction energy that was not observed for the cations. A weak inverse correlation is seen for the (d) dispersion contribution, with large outliers observed for PO_4^{3-} interactions. All geometries in Figure S5-Figure S6.

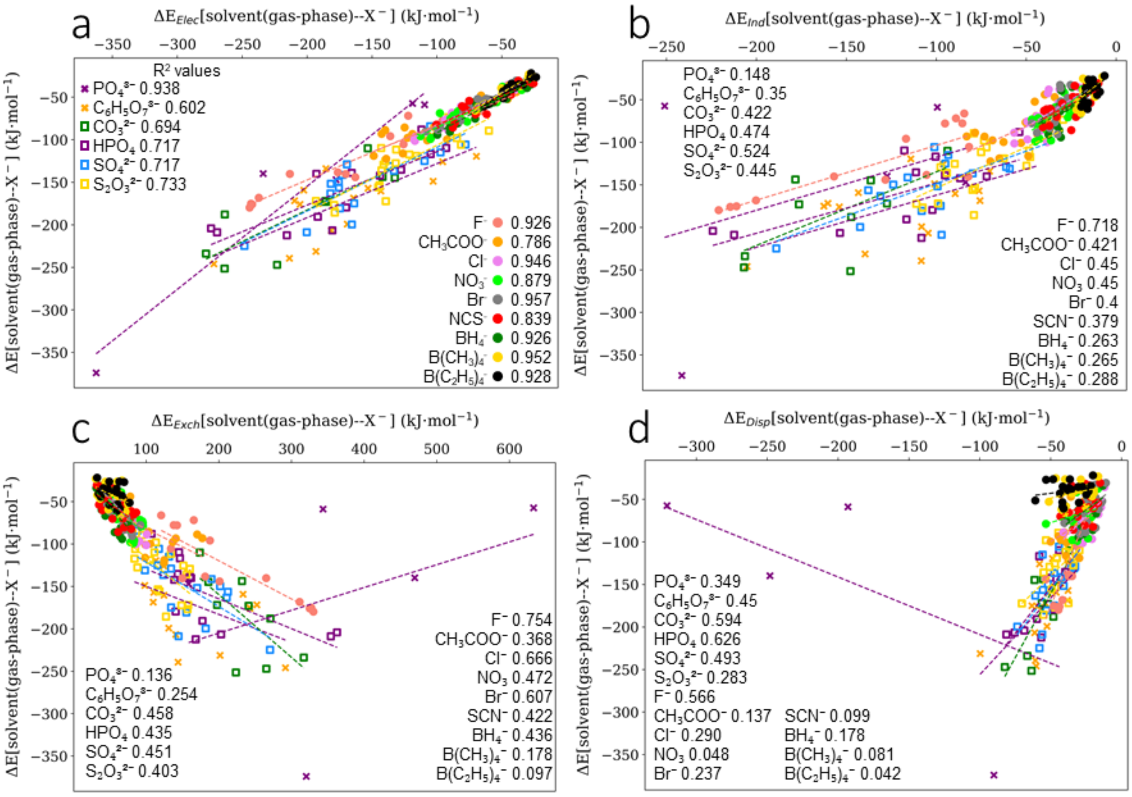

Figure S22: Comparison of the M06-2X/aug-cc-pVDZ//SAPT2+3/aug-cc-pVDZ total *anion-solvent pairwise interactions* interaction energy with the a) electrostatic, b) induction, c) exchange and d) dispersion component energies. Separated by anion. This figure investigates the solvent trends for a constant anion, as opposed to the solvent trends for a particular anion (see, Figure S21). All geometries in Figure S5-Figure S6.

S5.2 Pairwise Anion-Solvent Interactions in a Solvent Cluster

For many anion effects, the Gutmann-Mayer acceptor number has been shown as a sufficient solvent parameter for approximating the solvent's effect on the magnitude of the observed SIE.[4] However, given AN has such a poor correlation with the specific-interaction in the gas phase (Figure S57), its likely multiple solvent molecules are required for practical purposes (as it is not definitionally a 1:1 interaction like the DN). This may be a result of the ~additive and non-directional nature of electrostatics[13] that should increase comparatively faster than the other intermolecular forces as there are more surrounding solvent molecules (*e.g.*, induction requires the warping of the anion's electron density and is therefore directional and non-additive).

As seen in all previous cases, electrostatics has a strong correlation with the overall interaction strength (Figure S23 (a)). However, in this case, the exchange interaction (Figure S23 (b)) is of a comparative magnitude and is more solvent dependent than the electrostatic contribution. This is counteracted by the strong repulsive force (Figure S23 (c)) that is inherently linked to the exchange. The polarisation interaction (Figure S23 (d)) replicates what was observed in §S5.1 for the analogous induction contribution, where there is a strong solvent dependent correlation with the total energy, and especially strong for polarisable non-polar solvents such as toluene and hexane. The desolvation term (Figure S23 (e)) is negligible for many solvents, as this should be quenched by the explicit hydration model, but solvents such as PC and DMA (which were computationally costly to use excessive solvent molecules – Table 2) had large desolvation energies. The correlation energy (Figure S23 (f)) revealed very little correlation with the total interaction energy for most solvents, especially the protic solvents in this dataset.

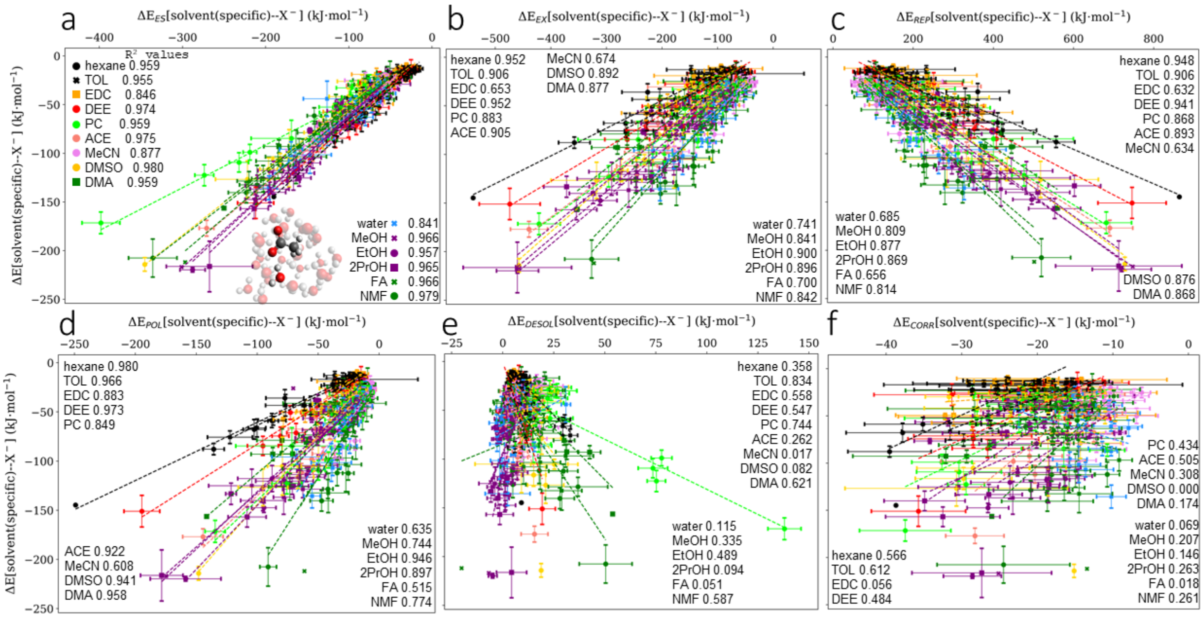

Figure S23: Comparison of the GKS-EDA (DFTB3(D3-BJ)/3-ob-3-1//M06-2X/cc-pVDZ total *anion-solvent 1:1 pairwise interactions in the cluster model (including a PCM solvent environment)* interaction energy with the (a) electrostatic, (b) exchange, (c) repulsion, (d) polarisation, (e) desolvation and (f) correlation component energies. All data is averaged across multiple independent configurations; error bars denote 1 standard deviation. This figure investigates the anion trends for a particular solvent, as opposed to the solvent trends for a particular anion (see, Figure S24).

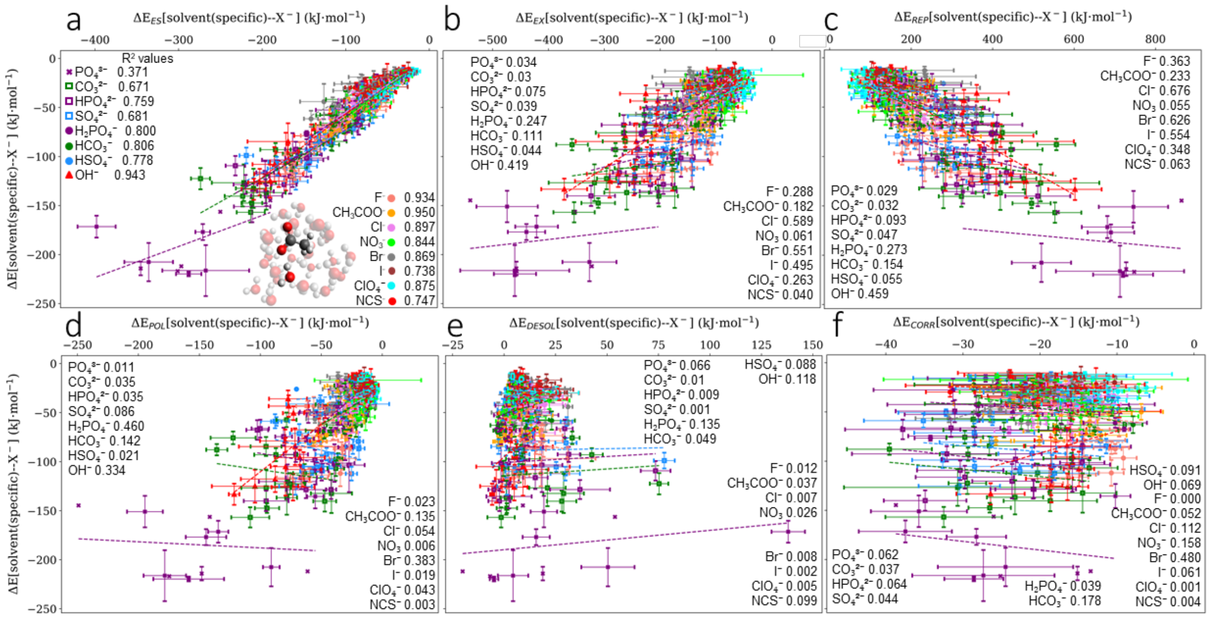

Figure S24: Comparison of the GKS-EDA (DFTB3(D3-BJ)/3-ob-3-1//M06-2X/cc-pVDZ) total *anion-solvent 1:1 pairwise interactions in the cluster model (including a PCM solvent environment)* interaction energy with the (a) electrostatic, (b) exchange, (c) repulsion, (d) polarisation, (e) desolvation and (f) correlation component energies. All data is averaged across multiple independent configurations; error bars denote 1 standard deviation. This figure investigates the solvent trends for a particular anion, as opposed to the anion trends for a particular solvent (see, Figure S23).

S5.3 Anion-Solvent Cluster Interactions

Figure S25 supports the previous trends for anion-solvent interactions from §S5.1-S5.2, yet is perhaps even more solvent-independent in its electrostatic contribution (Figure S25(a)). Indeed, the trends in the other component energies also become stronger (Figure S25(b-f)). For example, the exchange component (Figure S25(b)) has a stronger correlation with the protic solvents than it did in the pairwise cluster model (Figure S23(b)). Furthermore, the exchange energy component is generally as strong, if not stronger than the total energy or the electrostatic energy component (Figure S23(a)). This is consistent with the pairwise interactions in the cluster model. Additionally, these anion-solvent exchange interactions have a direct linear correlation with the total energy, whereas the comparable cation-solvent interactions follow an inverse relationship (Figure S19(b)). The repulsion contribution (Figure S23(c)) follows a similar trend to those observed in exchange, but of a larger magnitude, and repulsive. The polarisation contribution (Figure S23(d)), with similarity to the previous interactions, shows a solvent dependence in the anion-gradient. More specifically, the non-polar, polarisable solvents such as hexane, TOL, DEE, DMA and EDC have a large polarisation component in comparison to their total interaction energy, with respective gradients of 1.80, 1.81, 1.40, 1.31 and 1.55. Similarly, in terms of alkyl chain length the alcohols provide a useful test case for a common functional group. The polarisation-total energy gradient larger for 2PrOH than EtOH with respective gradients of 1.06 and 0.95, and greater for EtOH than MeOH which has a gradient of 0.78. The desolvation energy (Figure S23(e)) has a solvent dependence that displays one of the limitations of the hybrid explicit/implicit solvation environment. This is with respect to the explicit/implicit solvation boundary where artefacts can arise.[14] In particular, PC generally has the largest desolvation component for any given ion. Given the number of atoms in PC only a limited number of explicit solvent molecules were computationally feasible. This appears to have been insufficient for large charge dense anions such as PO_4^{3-} and SO_4^{2-}, especially given the lack of conformational freedom exhibited by PC. Hence, a larger contribution is made by the implicit solvent, and therefore larger desolvation contribution. This will additionally be larger for a given solvent accessible surface area for larger dielectric constant solvents, of which PC has a relative permittivity of 64.92. NMF also has a large desolvation contribution and a relative permittivity value 182.4. So, despite the extra four NMF solvent molecules each ion has in comparison to PC, there is still a strong desolvation penalty. Finally, Figure S23(f) shows that there is very little correlation between the total energy and its correlation component for any given ion. However, when considering different ions (Figure S9) there is some degree of clustering for some ions, most notably PO_4^{3-} and HPO_4^{2-} which have relatively strong correlation component, and F^- and OH^- which have relatively weak correlation contributions.

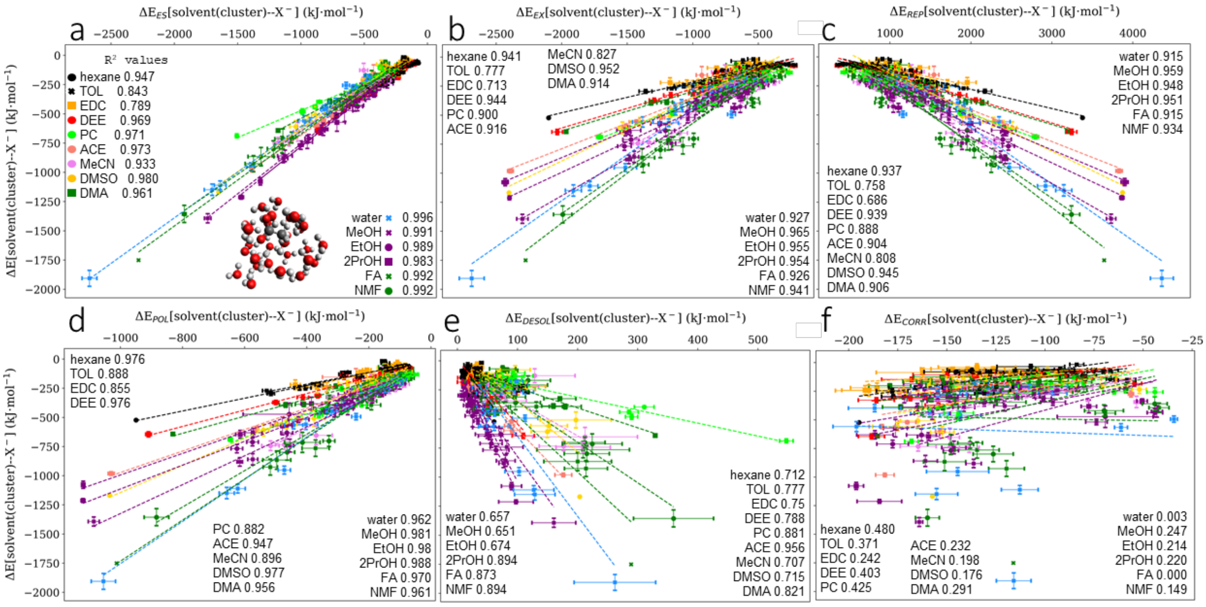

Figure S25: Comparison of the GKS-EDA (DFTB3(D3-BJ)/3-ob-3-1//M06-2X/cc-pVDZ) total *anion and its solvating shell in the cluster model (including a PCM solvent environment)* interaction energy with the (a) electrostatic, (b) exchange, (c) repulsion, (d) polarisation, (e) desolvation and (f) correlation component energies. All data is averaged across multiple independent configurations; error bars denote 1 standard deviation. This figure emphasises the anion trends for a particular solvent, as opposed to the solvent trends for a particular anion (see, Figure S9).

S6. Non-electrostatic parameters

Accompanying discussion for these Figure in §S4.1and §S5.1.

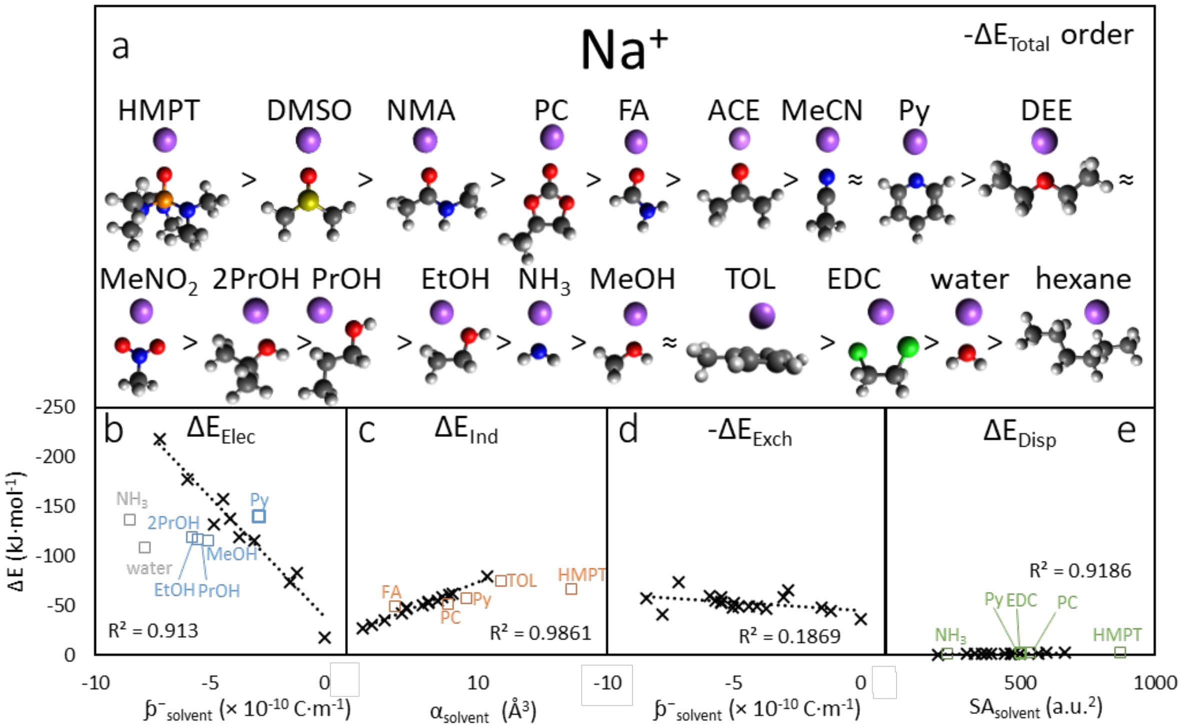

Figure S26: Specific 1:1 Na^+-solvent complexes in the gas phase and their interaction energy contributions. Na^+ here serves as a model monovalent monatomic charge dense cation to more fully understand the effects of changing the solvent. (a) M06-2X/aug-cc-pVDZ optimised sodium-solvent structures are ordered in terms of their overall interaction energy, with the Lewis basic HMPT having the strongest interaction and the non-polar aprotic hexane the weakest. For these Na^+-solvent interactions the solvent's radial charge densities ($ϸ^-_{\text{solvent}}$) at its negative dipole atom are compared to the SAPT2+3/aug-cc-pVDZ (b) electrostatic and (d) exchange energy contributions, the solvent's polarisability with the induction contribution and (e) the solvent's surface area is compared to the SAPT2+3/aug-cc-pVDZ dispersion interaction energy (while the trend here is strong, see Figure S31, the dispersion contribution is negligible). The predominant solvent trends appear to originate from the electrostatic contribution. Squares are outliers from the overarching trend.

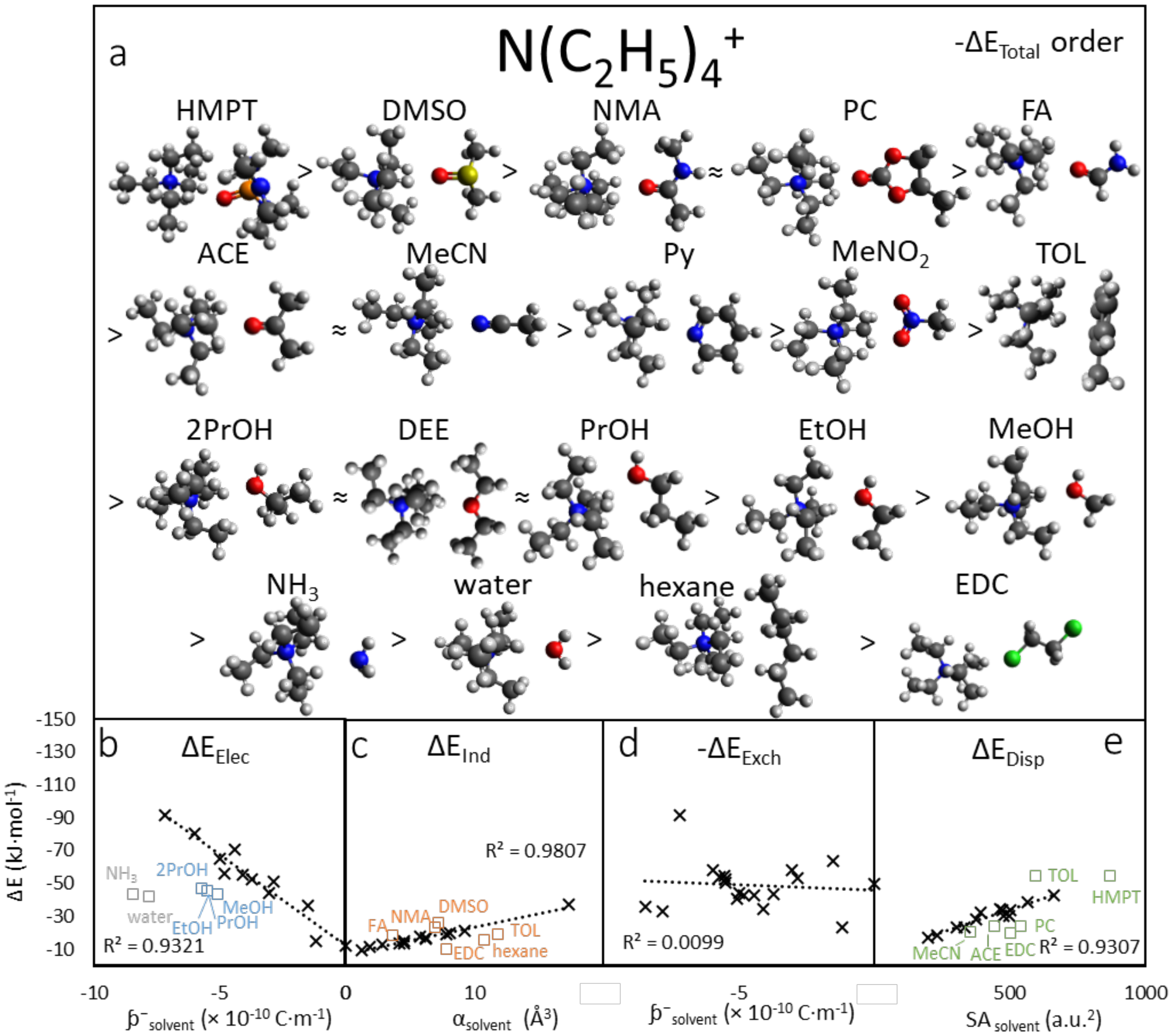

Figure S27: Specific 1:1 $N(C_2H_5)_4^+$-solvent complexes in the gas phase and their interaction energy components. $N(C_2H_5)_4^+$ here serves as a model polyatomic charge diffuse cation to more fully understand the effects of changing the solvent for such cations. (a) M06-2X/aug-cc-pVDZ optimised $N(C_2H_5)_4^+$-solvent structures are ordered in terms of their overall interaction energy, with the Lewis basic HMPT having the strongest interaction and the non-polar aprotic hexane the weakest. For these tetraethylammonium-solvent interactions the solvent's radial charge densities ($þ^-_{solvent}$) at its negative dipole atom are compared to the SAPT2+3/aug-cc-pVDZ (b) electrostatic and (d) exchange energy contributions, the solvent's polarisability with the induction contribution and (e) the solvent's surface area is compared to the SAPT2+3/aug-cc-pVDZ dispersion interaction energy (the dispersion contribution becomes significant, and even dominant (yet still small) for some of these interactions). The predominant solvent trends appear to originate from the electrostatic contribution. Squares are outliers from each overarching trend.

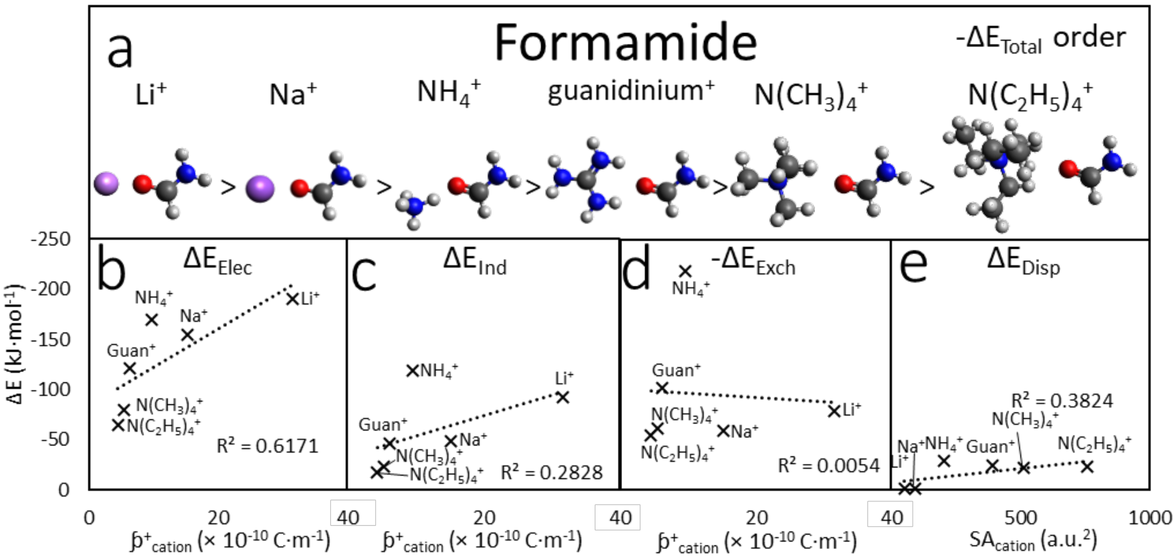

Figure S28: Specific 1:1 cation-formamide complexes in the gas phase and their interaction energy contributions. Formamide here serves as a model polar protic nonaqueous solvent to more fully understand the intermolecular interactions and their structure-energy relationship. (a) M06-2X/aug-cc-pVDZ optimised cation-formamide structures are ordered in terms of their overall interaction energy, with Li^+ having the strongest interaction and the two alkyl-ammonium cations the weakest. For these cation-formamide interactions the cation radial charge densities ($ϸ^+_{cation}$) are used to investigate the SAPT2+3/aug-cc-pVDZ (b) electrostatic, (c) induction and (d) exchange energy contributions and (e) the cation's surface area is compared to the cation-formamide SAPT2+3/aug-cc-pVDZ dispersion interaction energy (which follows an inverse cation Hofmeister series in this case).

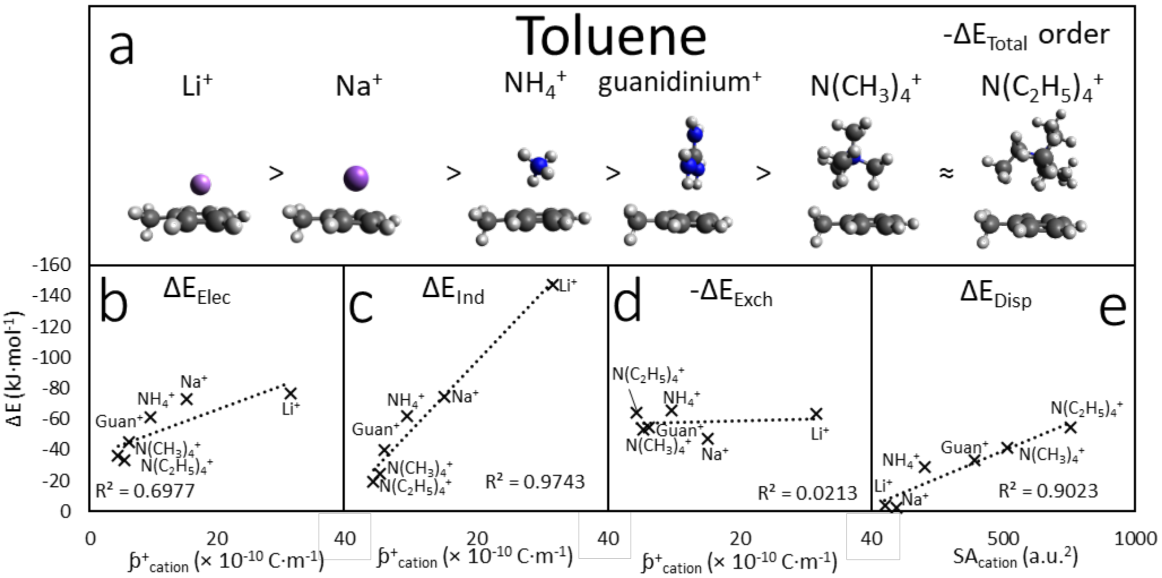

Figure S29: Specific 1:1 cation-toluene complexes in the gas phase and their interaction energy contributions. Toluene here serves as a model non-polar aprotic nonaqueous solvent to more fully understand the intermolecular interactions and their structure-energy relationship. (a) M06-2X/aug-cc-pVDZ optimised cation-toluene structures are ordered in terms of their overall interaction energy, with Li^+ having the strongest interaction and the two alkylammonium cations the weakest. For these cation-toluene interactions the cation radial charge densities ($ϸ^+_{cation}$) are used to investigated the SAPT2+3/aug-cc-pVDZ (b) electrostatic, (c) induction and (d) exchange energy contributions and (e) the cation's surface area is compared to the cation-toluene dispersion SAPT2+3/aug-cc-pVDZ interaction energy (which follows an inverse cation Hofmeister series in this case).

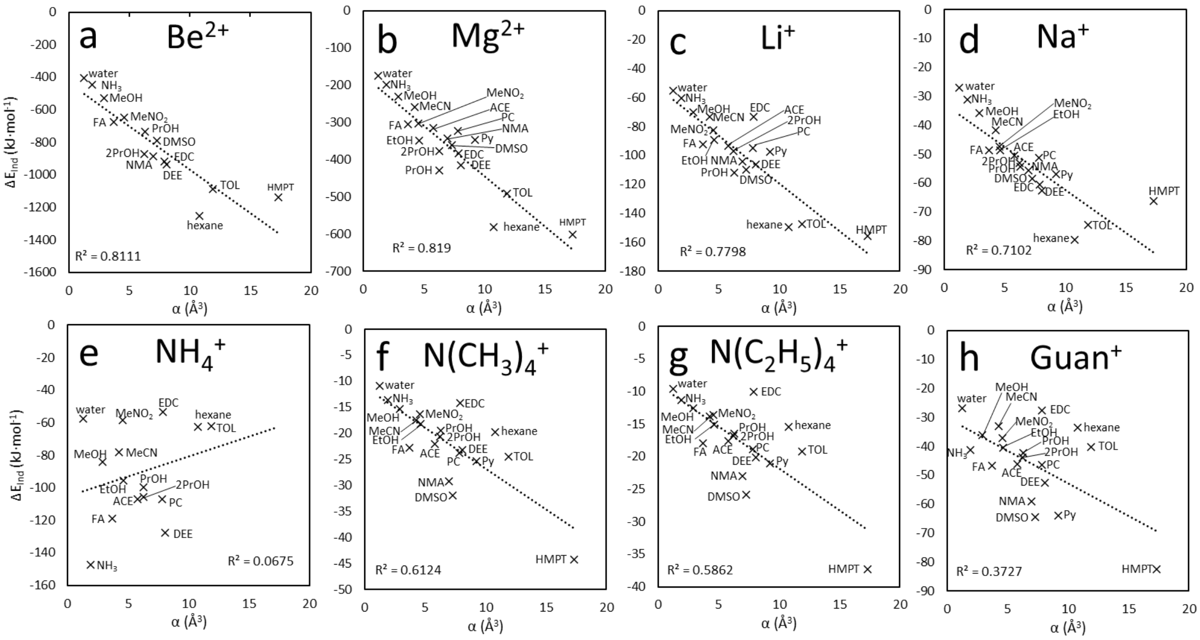

Figure S30: Comparison of the induction energy contribution (SAPT2+3/aug-cc-pVDZ) from cation-solvent pairwise interactions with the solvents average molecular polarisability for (a) Be^{2+}, (b) Mg^{2+}, (c) Li^+, (d) Na^+, (e) NH_4^+, (f) $N(CH_3)_4^+$, (g) $N(C_2H_5)_4^+$ and (h) guanidinium$^+$.

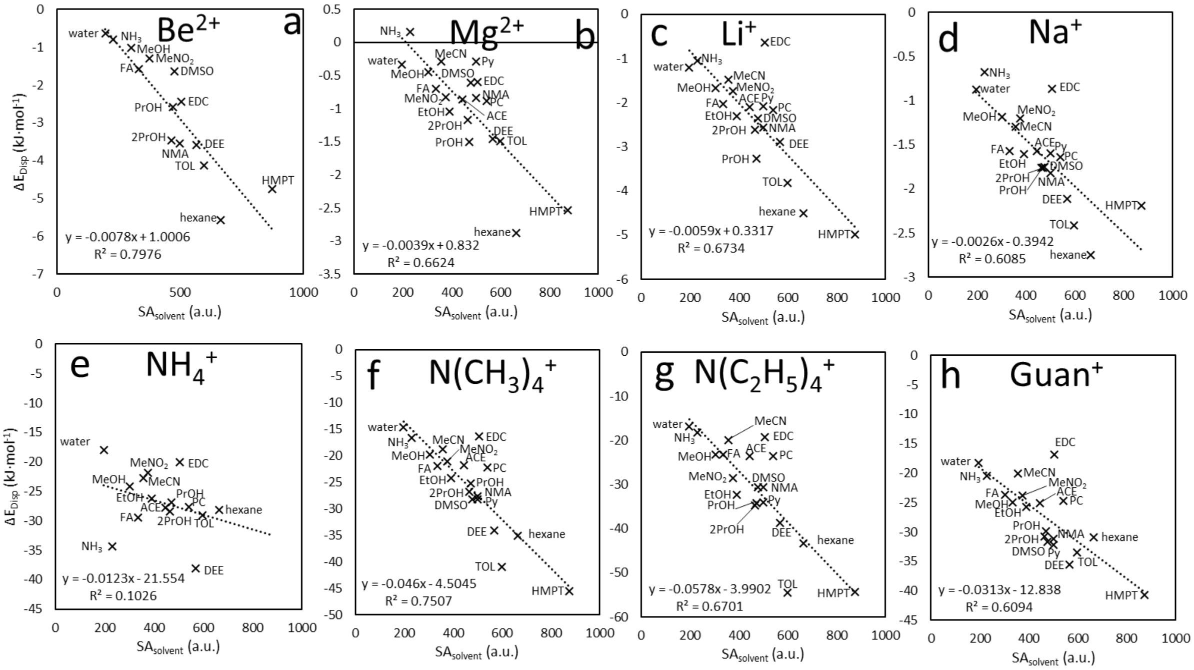

Figure S31: Comparison of the dispersion energy contribution (SAPT2+3/aug-cc-pVDZ) from cation-solvent pairwise interactions with the solvents surface area (Table S4) for (a) Be^{2+}, (b) Mg^{2+}, (c) Li^+, (d) Na^+, (e) NH_4^+, (f) $N(CH_3)_4^+$, (g) $N(C_2H_5)_4^+$ and (h) guanidinium$^+$. When the entire solvent surface is interacting with these ions (in a planar manner), the correlation is linear and strong, however weaker (deviating) dispersion energies are observed if the solvent interacts orthogonally through only a small portion of its surface area (see, Figure S32 in conjunction with Figure S4).

Table S4: Surface areas of cations, anions and solvents, calculated via AIMAll, ordered from smallest to largest.

Ion/Solvent	**Surface Area (a.u.^{2})**
Li^+	51.8
Na^+	95.0
water	161.0
NH_3	188.7
NH_4^+	202.6
MeOH	254.3
F^-	209.5
FA	283.6
Cl^-	300.3
MeCN	303.1
$MeNO_2$	323.2
BH_4^-	332.2
EtOH	334.0
NO_3^-	348.3
BH_4^-	366.9
ACE	382.9
guanidinium$^+$	393.1
2PrOH	401.6
PrOH	408.3
DMSO	412.4
SCN^-	415.1
CO_3^-	416.7
acetate$^-$	422.5
Py	432.2
NMA	435.2
EDC	438.1
SO_4^{2-}	465.0
PC	476.1
HPO_4^{2-}	492.0
DEE	493.5
$N(CH_3)_4^+$	514.6
TOL	520.6
$S_2O_3^{2-}$	545.6
PO_4^{2-}	556.3
hexane	585.7
$B(CH_3)_4^-$	641.4
$N(C_2H_5)_4^+$	757.3
HMPT	789.9
citrate$^-$	848.6
$B(C_2H_5)_4^-$	851.6

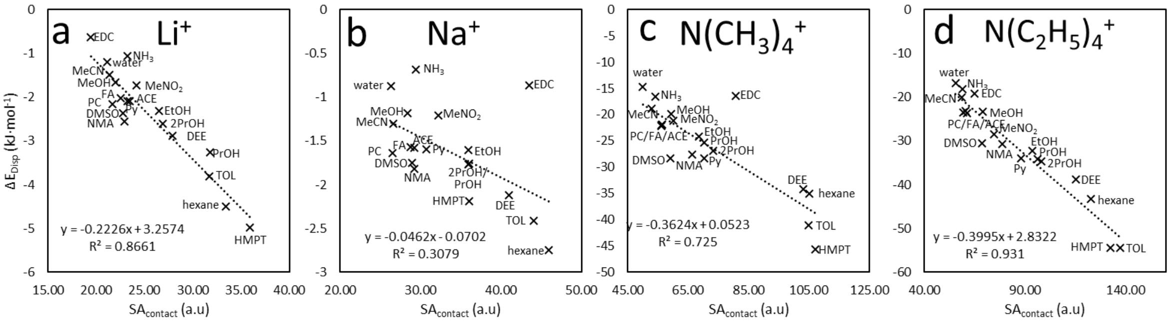

Figure S32: Comparison of the dispersion energy contribution (SAPT2+3/aug-cc-pVDZ) from cation-solvent pairwise interactions with the contact surface area for (a) Li^+, (b) Na^+, (c) $N(CH_3)_4^+$ and (d) $N(C_2H_5)_4^+$. The small ΔE_{Disp} values for Na^+ mean that intrinsic method errors won't be negligible, however it also means that the dispersion interactions for Na^+ will be negligible in the summation of ΔE_{Total} for this ion.

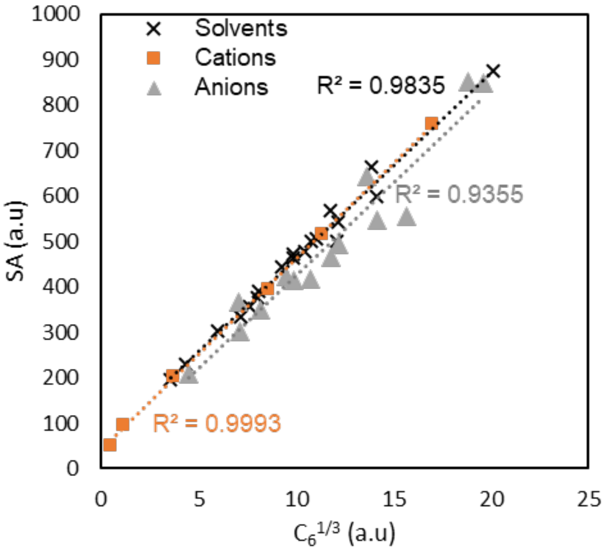

Figure S33: There is a strong relationship between the surface area (SA) of solvents, cations and anions and their respective $C_6^{1/3}$ dispersion coefficients.* The surface areas have been calculated using the AIMALL package[15] (M06-2X/aug-cc-pVDZ) using an IsoDensity surface of 0.0004.

---

* The cubed root of the C_6 to account for these interactions occurring in a single direction, rather than the radial three-dimensional interactions that would occur in bulk.

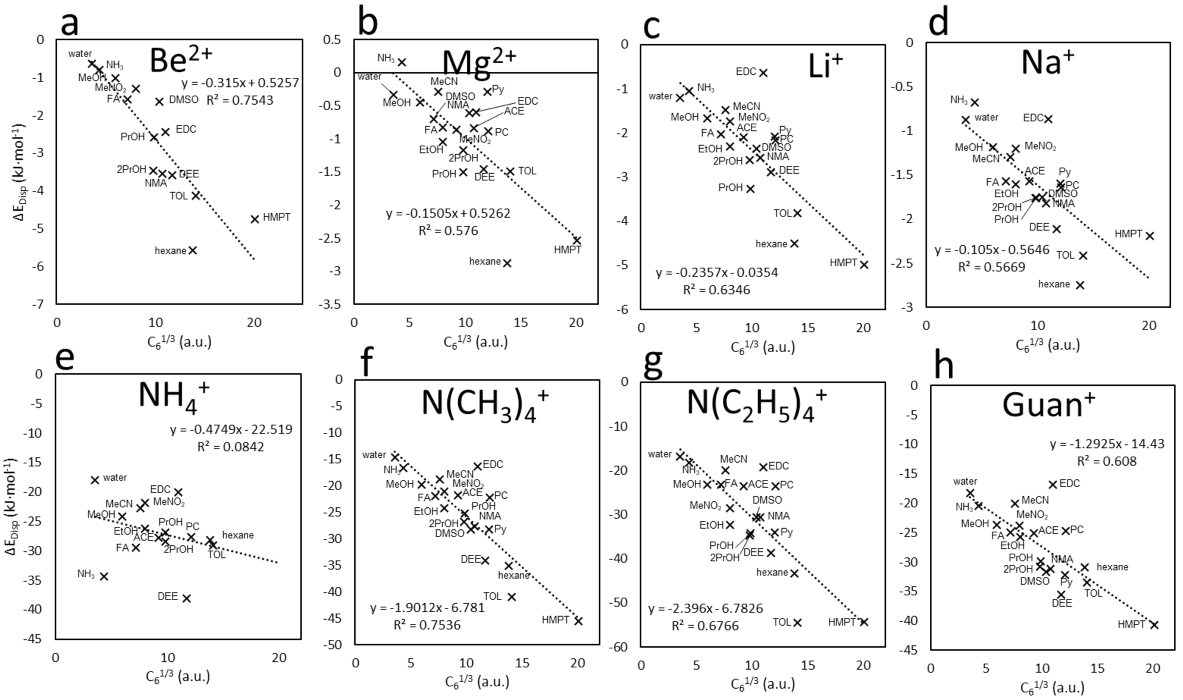

Figure S34: Comparison of the dispersion energy contribution (SAPT2+3/aug-cc-pVDZ) from cation-solvent pairwise interactions with the solvents $C_6^{1/3}$ for (a) Be^{2+}, (b) Mg^{2+}, (c) Li^+, (d) Na^+, (e) NH_4^+, (f) $N(CH_3)_4^+$, (g) $N(C_2H_5)_4^+$ and (h) guanidinium$^+$. When the entire solvent surface is interacting with these ions (in a planar manner), the correlation is linear and strong, however weaker (deviating) dispersion energies are observed if the solvent interacts orthogonally, through only a small portion of its surface area (see, Figure S4, Figure S32).

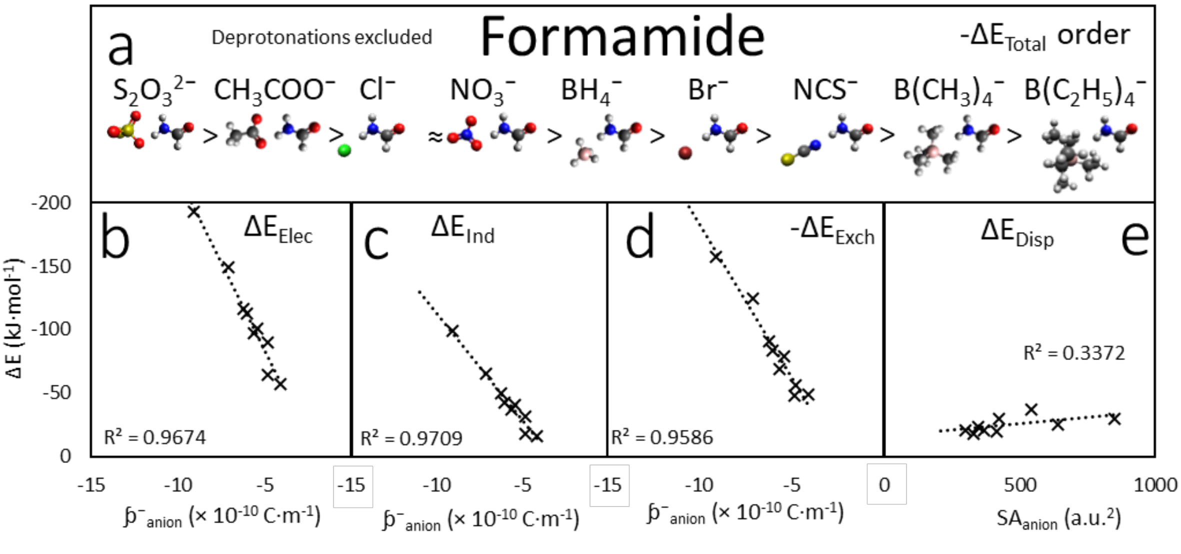

Figure S35: Specific 1:1 anion-formamide complexes in the gas phase and their interaction energy components. Formamide here serves as a model polar protic nonaqueous solvent to more fully understand the intermolecular anion-solvent interactions and their structure energy relationship. (a) M06-2X/aug-cc-pVDZ optimised anion-formamide structures are ordered in terms of their overall interaction energy, with $S_2O_3^{2-}$ having the strongest (non-deprotonated) interaction and the $B(C_2H_5)_4^-$ anion the weakest. For these anion-formamide interactions, þ$^-_{anion}$ values are used to investigate the SAPT2+3/aug-cc-pVDZ (b) electrostatic, (c) induction and (d) exchange energy contributions and (e) the anion's surface area is compared to the anion-formamide SAPT2+3/aug-cc-pVDZ dispersion interaction energy. Optimisations resulting in solvent deprotonation have been excluded.

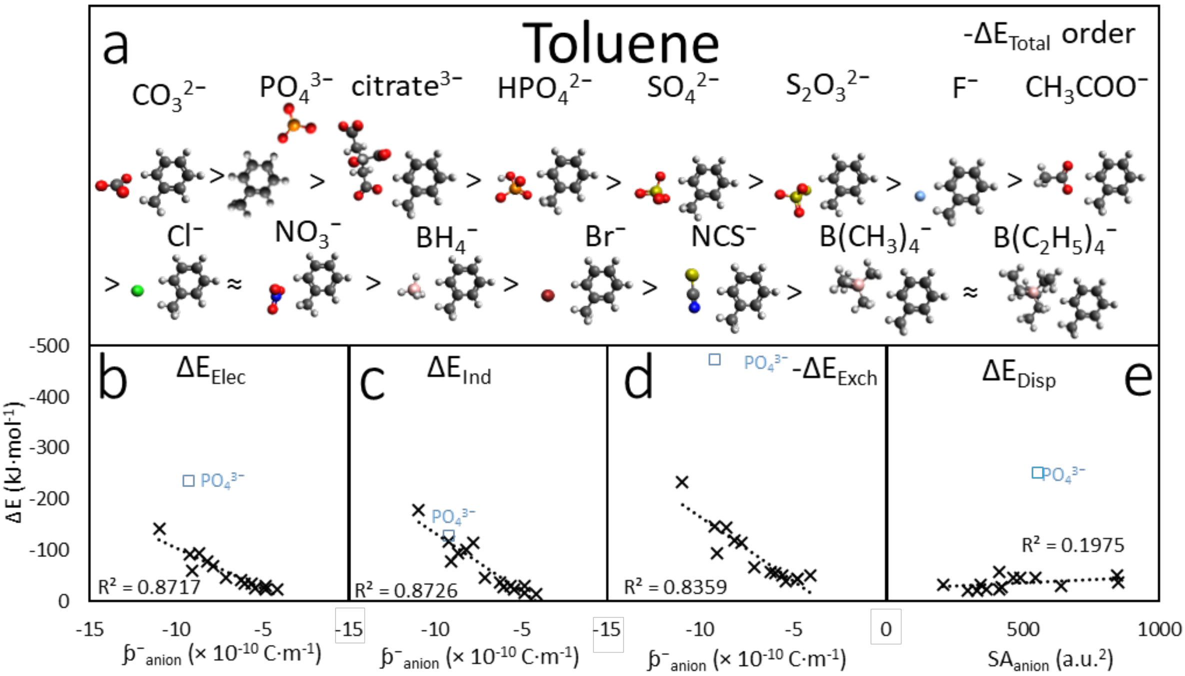

Figure S36: Specific 1:1 anion-toluene complexes in the gas phase and their interaction energy components. Toluene here serves as a non-polar aprotic nonaqueous solvent to more fully understand the intermolecular anion-solvent interactions and their structure energy relationship. (a) M06-2X/aug-cc-pVDZ optimised anion-toluene structures are ordered in terms of their overall interaction energy, with CO_3^{2-} having the strongest interaction and the two tetraalkylborate anions the weakest. For these anion-toluene interactions, $þ^{-}_{anion}$ values are used to investigate the SAPT2+3/aug-cc-pVDZ (b) electrostatic, (c) induction and (d) exchange energy contributions and (e) the anion's surface area is compared to the anion-toluene SAPT2+3/aug-cc-pVDZ dispersion interaction energy. PO_4^{3-} is not included in the R^2 values given its differing binding geometry and large difference from the other anions.

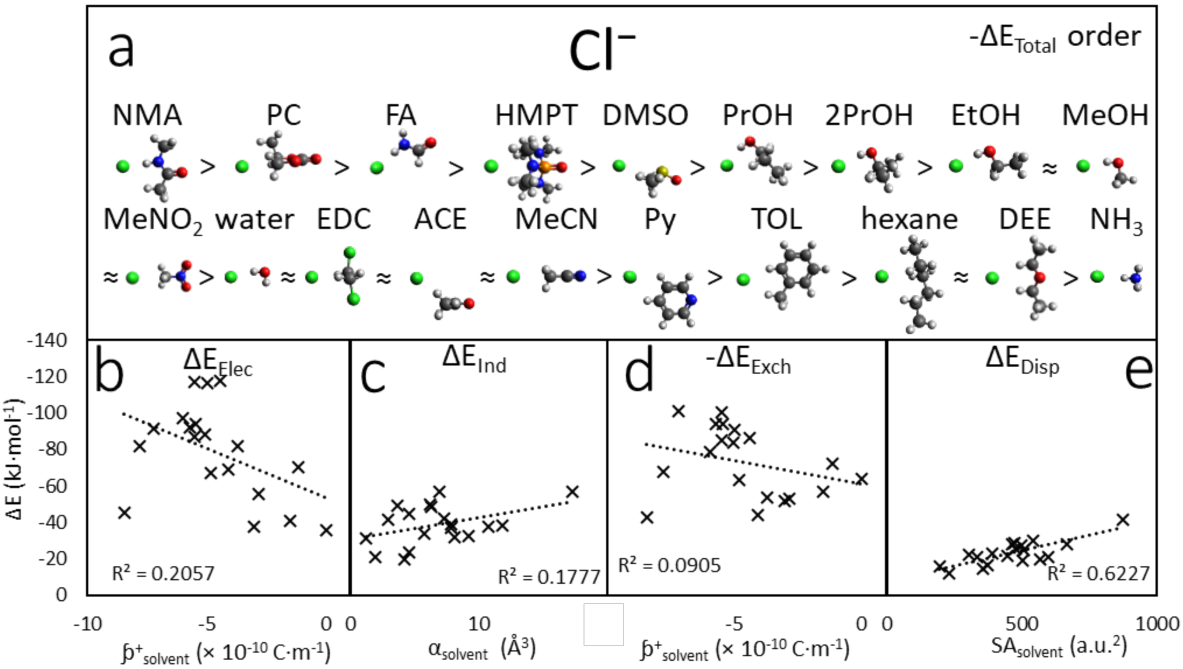

Figure S37: Specific 1:1 Cl⁻-solvent complexes in the gas phase and their interaction energy components. Cl⁻ here serves as a model monovalent monatomic charge dense anion to more fully understand the effects of changing the solvent. (a) M06-2X/aug-cc-pVDZ optimised Cl⁻-solvent structures are ordered in terms of their overall interaction energy, with the Lewis acidic NMA having the strongest interaction and the small ammonia molecule the weakest. As for the cation-solvent interactions, for these Cl⁻-solvent interactions, $þ^{+}_{\text{solvent}}$ values are compared to the SAPT2+3/aug-cc-pVDZ (b) electrostatic and (d) exchange energy contributions, (c) the solvent's polarisability with the SAPT2+3/aug-cc-pVDZ induction contribution and (e) the solvent's surface area compared to the SAPT2+3/aug-cc-pVDZ dispersion interaction energy.

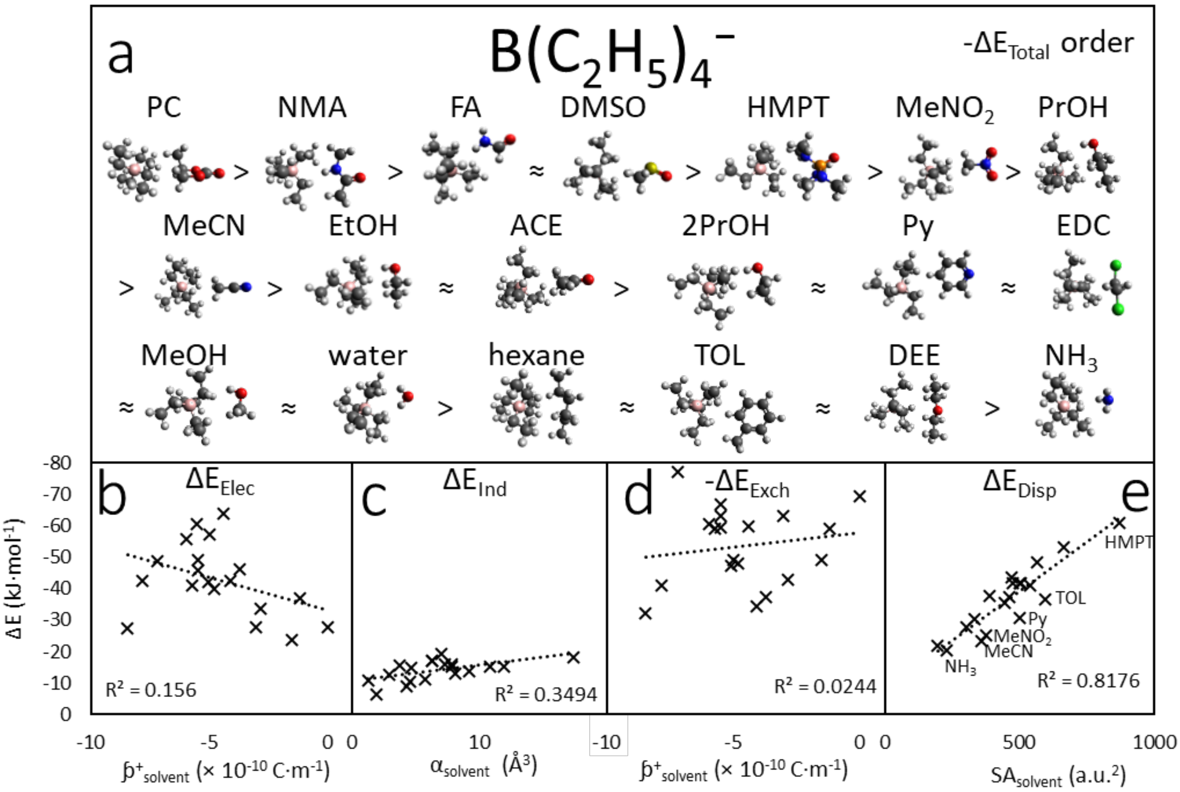

Figure S38: Specific 1:1 $B(C_2H_5)_4^-$-solvent complexes in the gas phase and their interaction energy components. $B(C_2H_5)_4^-$ here serves as a model polyatomic charge diffuse anion to more fully understand the effects of changing the solvent for such anions. (a) M06-2X/aug-cc-pVDZ optimised $B(C_2H_5)_4^-$-solvent structures are ordered in terms of their overall interaction energy, with the polarisable PC having the strongest interaction and the small ammonia molecule the weakest. As for the $B(C_2H_5)_4^-$-solvent interactions, for these $B(C_2H_5)_4^-$-solvent interactions, the solvents' radial charge densities ($\text{þ}^{+}_{\text{solvent}}$) at its positive dipole atom are compared to the SAPT2+3/aug-cc-pVDZ (b) electrostatic and (d) exchange energy contributions, (c) the solvent's polarisability with the SAPT2+3/aug-cc-pVDZ induction contribution and the (e) solvent's surface area is compared to the SAPT2+3/aug-cc-pVDZ dispersion interaction energy.

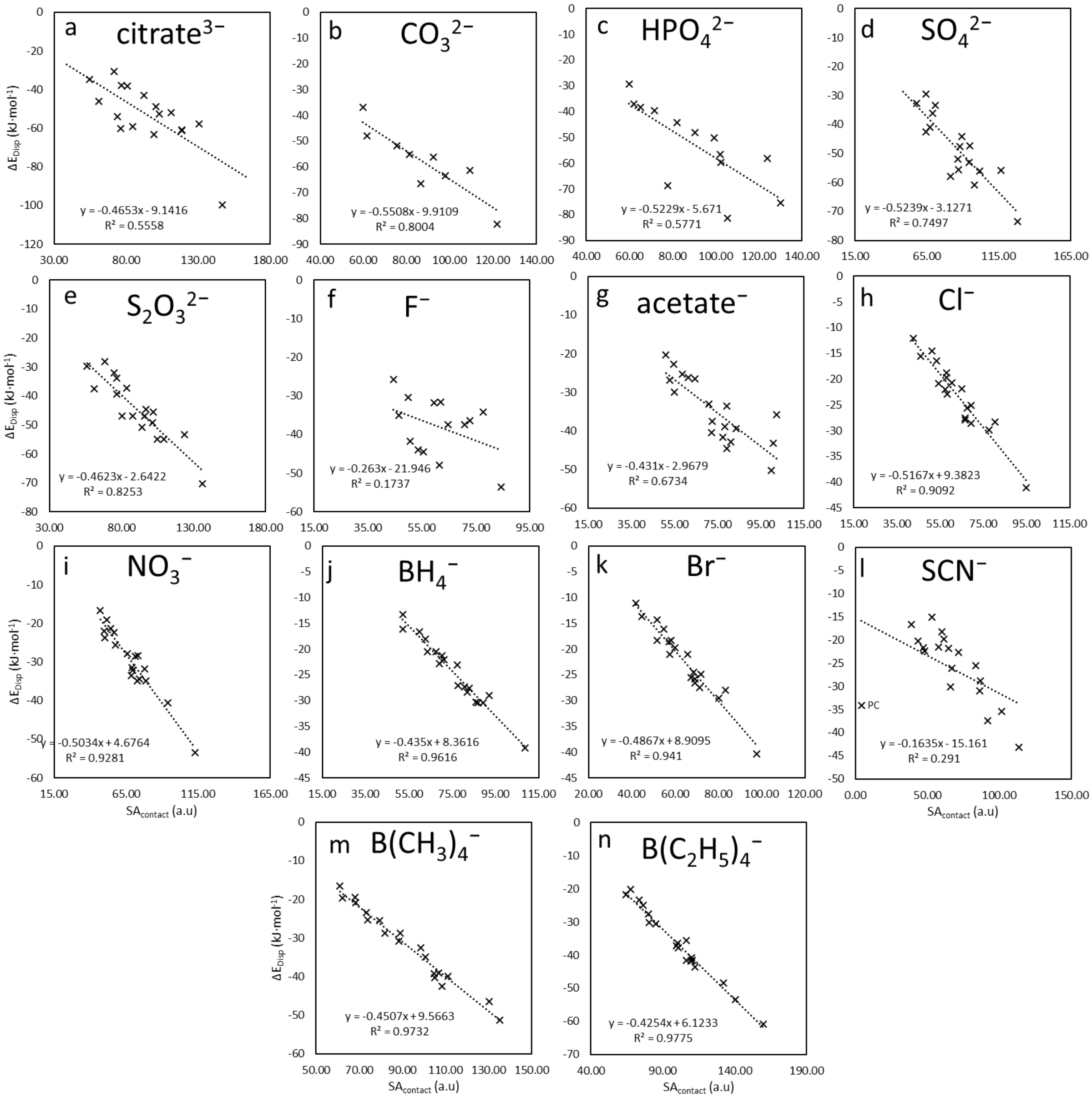

Figure S39: Comparison of the dispersion energy contribution (M06-2X/aug-cc-pVDZ//SAPT2+3/aug-cc-pVDZ) from anion-solvent pairwise interactions with the contact surface area for (a) citrate^{3-}, (b) CO_3^{2-}, (c) HPO_4^{2-}, (d) SO_4^{2-}, (e) $S_2O_3^{2-}$, (f) F^-, (g) acetate$^-$, (h) Cl^-, (i) NO_3^-, (j) BH_4^-, (k) Br^-, (l) SCN^-, (m) $B(CH_3)_4^-$ and (n) $B(C_2H_5)_4^-$. These correlations, generally appear to be better for larger more charge diffuse anions.

S7. Propylene carbonate – multiple binding sites

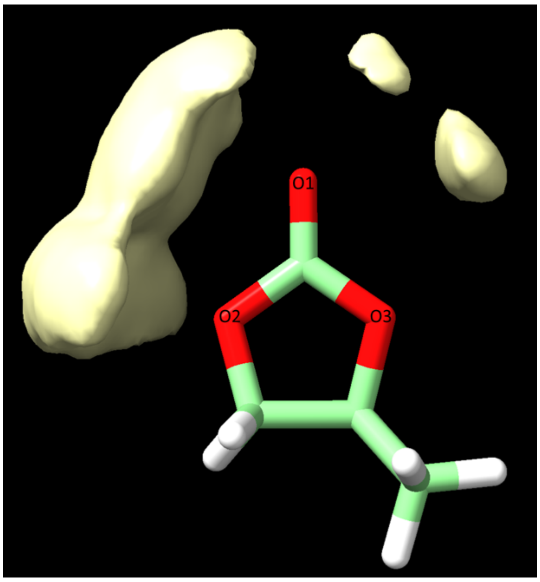

Figure S40: The Na^{+}-PC spatial distribution function from a DFTB/3ob-3-1 MD trajectory of a single pair of Na^{+} and Cl^{-} ions in a periodic box of 32 PC solvent molecules under NVT conditions using the experimental density of the bulk PC solvent at 298.15K. þ$^{-}_{\mathrm{solvent}}$(O1), þ$^{-}_{\mathrm{solvent}}$(O2) and þ$^{-}_{\mathrm{solvent}}$(O3), are -5.35, -3.65 and -3.33 × 10^{-10} C·m^{-1} respectively. Since the majority of the binding occurs through O1 and O2, or O1 and O3 simultaneously, the average of averages of the O1 and O2 and the O1 and O3 þ$^{-}_{\mathrm{solvent}}$ values is used in Figure 3 (*i.e.*, $\frac{-5.35 + -3.65 + -5.35 + -3.33}{4} \times 10^{-10}$ C·m^{-1} = -4.42×10^{-10} C·m^{-1}). While possible an average may not be the most general mathematical approach to these mixed þ values, it appears valid in systems tested thus far (potentially through a convenient cancellation of errors).

S8. Solvent-solvent interactions and their component energies

Cohesive solvent-solvent self-interactions are an important consideration in the establishment of generalisable solvent interaction parameters. The differences (or similarities) between self-interactions and inter-species interactions underlie the premise of like-dissolves-like (*i.e.*, miscibility and solubility). Furthermore, a solvent-solvent self-interaction represents a system which requires both the positive and negative dipole contributions to be considered and hence unified onto the same scale (of which AN and DN are not). While electrostatic interactions appear to be the dominant contribution in ion-solvent (or charge-dipole) interactions, the extension to solvent-solvent interactions – which are more likely to be dominated by dipole-dipole interactions - may be less certain. Investigating if $\text{þ}^{-}_{\text{solvent}}$ and $\text{þ}^{+}_{\text{solvent}}$ are able to represent bulk solvent properties in the absence of ions presents a final challenge of these fundamental parameters, and inherently tests their general utility. §S8.1-S8.3show that the electrostatic trends in the ion-solvent interactions also exist for ion-free solvent-solvent interactions (Figure S41).

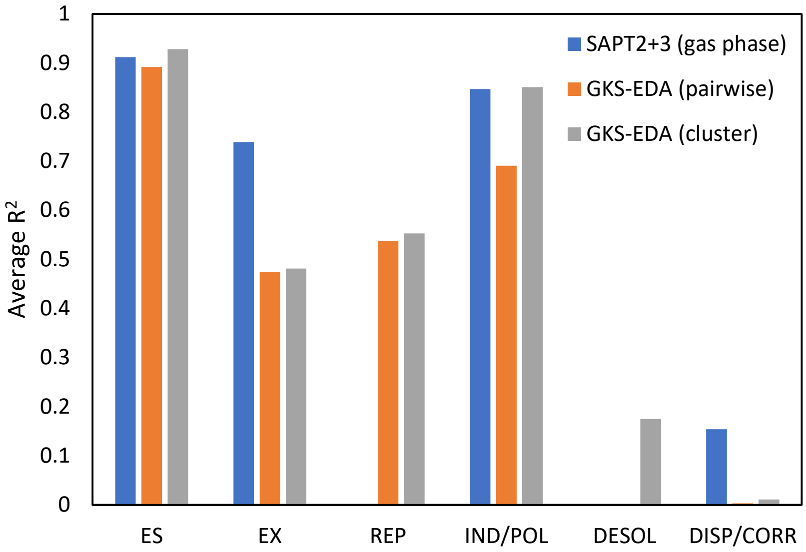

Figure S41: The average of all coefficients of determination (R^2) for each of the solvent-solvent energetic contributions (electrostatics – ES, exchange – EX, repulsion - REP, induction or polarisation – IND/POL, desolvation – DESOL and dispersion or correlation – DISP/CORR) with the total energy in the three different solvent models. Note that in SAPT2+3 exchange and repulsion is combined into the exchange term, induction is used, rather than GKS-EDA's polarisability term and SAPT2+3 does not have the desolvation term as there is no implicit solvation present. These values relate to the data presented in Figure S42, Figure S45 and Figure S46.

S8.1 Gas phase solvent-solvent interactions and their component energies

Figure S42 shows that even in these isolated solvent-solvent interactions, which are expected to be dominated by interactions between the respective molecular dipoles, there is a strong linear relationship between the electrostatic interaction energy and the total interaction energy (Figure S42(a)). Notably, for both cation and anion interactions with the solvent molecules, the electrostatic interaction energy was of a similar magnitude to the total interaction energy, whereas for these solvent-solvent interaction energies, the electrostatic contribution exceeds the total interaction energy in most cases (from 98% for toluene to 187% ammonia). The induction contribution (Figure S42(b)) also has a strong correlation, however, it is roughly half the magnitude of the electrostatic contribution for these solvents. The electrostatic component energy being of a larger magnitude than the total energy requires a large repulsive exchange energy contribution (from -131% for MeCN to -331% for DEE) for this to be possible (Figure S42(c)). This is especially true for some solvents such as DEE and HMPT, where even the dispersion contribution is also much larger than the total energy (238% and 217% respectively).

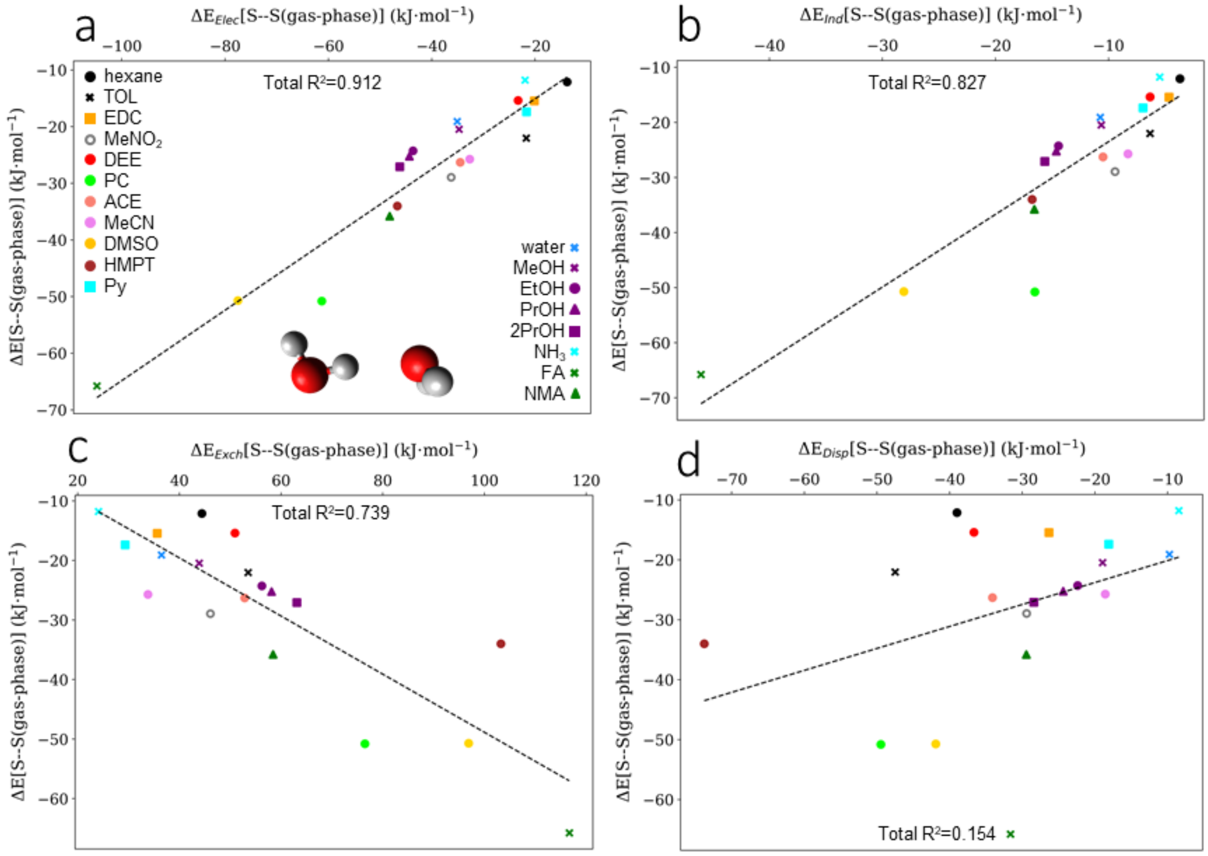

Figure S42: Comparison of the total M06-2X/aug-cc-pVDZ//SAPT2+3/aug-cc-pVDZ interaction energy for solvent-solvent pairwise gas phase interactions with the (a) electrostatic, (b) induction, (c) exchange and (d) dispersion component energies. Here we can see that for any protic or polar solvent (with few exceptions) there is a strong trend between the (a) electrostatic contribution and the total energy. It appears that this trend persists for the (b) induction contribution. For the (c) exchange contribution this is weakened however and the (d) dispersion contribution has an even weaker correlation, however can be the dominant contribution for large solvents such as HMPT and TOL.

Indeed, the electrostatic correlations for these solvent-solvent interactions, indicates this ion-free system provides a useful testcase for the generalisation of the hypotheses and first principles parameters developed in Figure 3. In this circumstance however, using both the positive and negative dipole parameters simultaneously, given the interaction geometries of these solvents generally occur between these dipolar atoms (Figure S43(a)). Using an adaptation of Eq. S7 from §S10.1 (which is defined for cations), reveals the electrostatic interaction may still be quantified via U_E, yet here, between two solvent molecules where there are no ionic species present (Figure S43(b)). For these solvent-solvent interactions, the induction contribution (Figure S43(c)) also correlates well with U_E. This is in contrast with the cation-solvent interactions, where the solvent polarisability appeared to be the governing factor (Figure S26(c) and Figure S27(c)), whereas the solvent polarisability appears to have no correlation with its self-induction energy (Figure S44(a)). Similarly, anion-solvent induction interactions appeared to have no reliance on the solvent's average polarisability (Figure S37(c) and Figure S38(c)), indicating that polarisability is primarily significant for species interacting with cations (or perhaps strong Lewis acids more generally). The exchange contribution is, in general, the largest in magnitude for these solvents (Figure S43(d)) and also has some correlation with U_E. Finally, the dispersion contribution has a moderate correlation with the solvent surface area (Figure S43(e)). This correlation is slightly improved further by directly investigating the solvent-solvent contact surface area (Figure S44(b)).

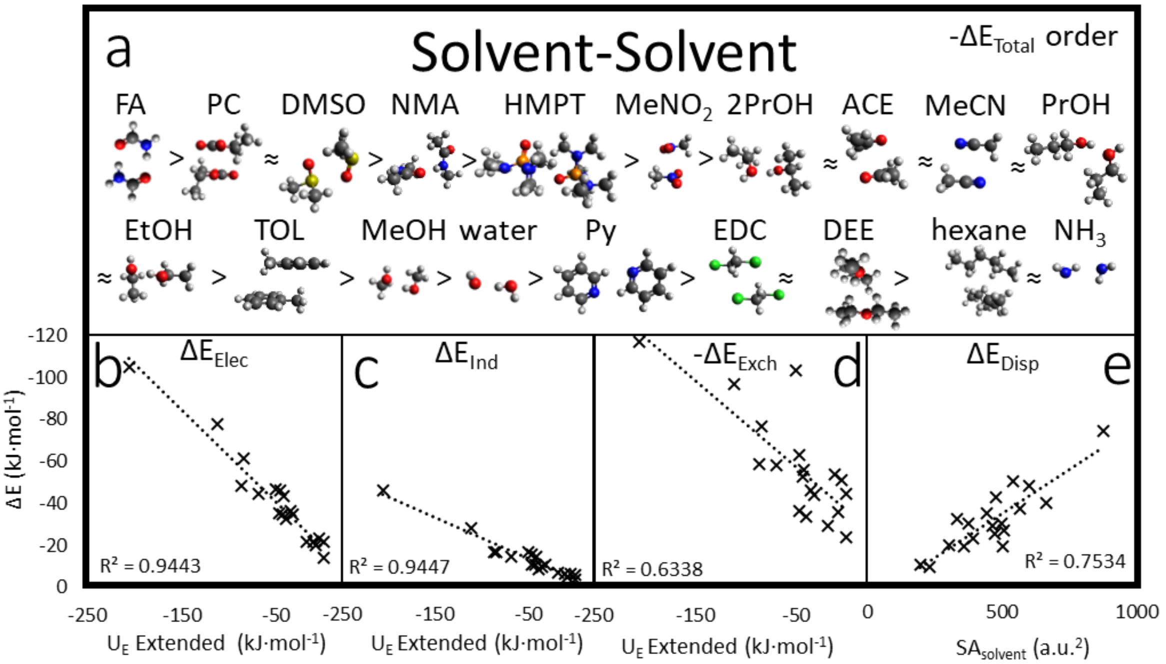

Figure S43: Specific 1:1 solvent-solvent gas phase interaction geometries ordered by their overall interaction strength. (a) M06-2X/aug-cc-pVDZ optimised solvent-solvent structures are ordered in terms of their overall interaction energy, with the protic dipolar FA having the strongest interaction and the large apolar hexane and small protic NH_3 solvents the weakest. For these solvent-solvent interactions the electrostatic potential energy (U_E) are used to investigate the SAPT2+3/aug-cc-pVDZ (b) electrostatic, (c) induction and (d) exchange energy contributions and (e) the solvent's surface area is compared to the solvent-solvent SAPT2+3/aug-cc-pVDZ dispersion interaction energy.

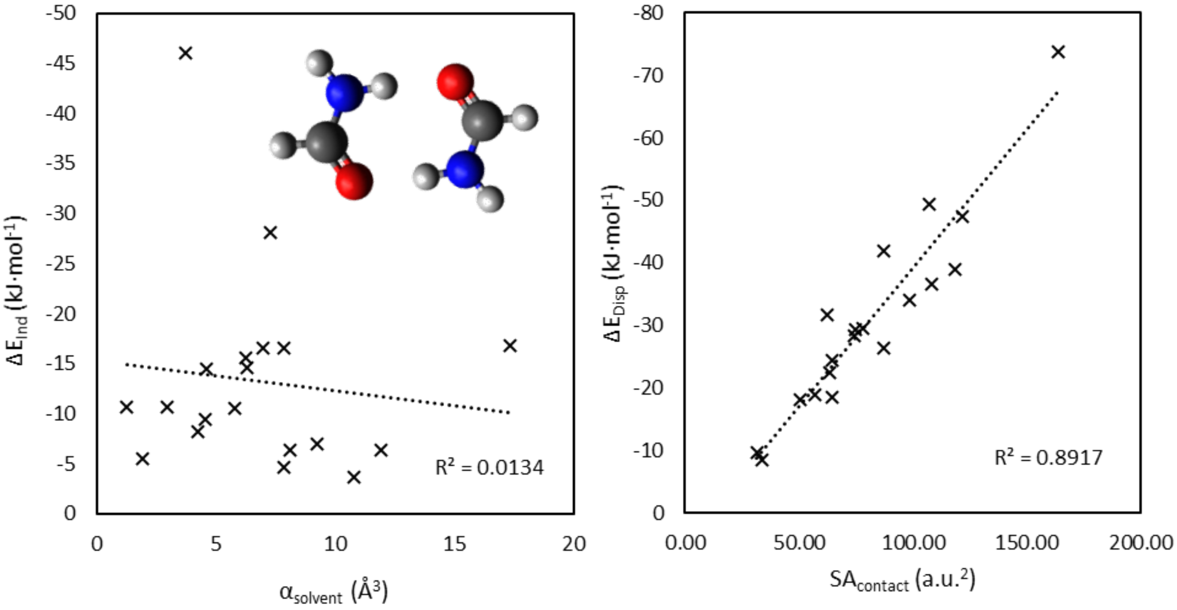

Figure S44: (a) The solvent-solvent M06-2X/aug-cc-pVDZ//SAPT2+3/aug-cc-pVDZ induction energy contribution compared to the solvent's MP2/aug-cc-pVTZ average polarisability. (b) The solvent-solvent M06-2X/aug-cc-pVDZ//SAPT2+3/aug-cc-pVDZ dispersion energy contribution compared to the M06-2X/aug-cc-pVDZ contact surface area between the two solvent molecules.

S8.2 Pairwise Solvent-Solvent Interactions (Solvent Cluster)

The pairwise solvent-solvent interaction in a solvent cluster is consistent with the cation and anion solvent pairwise solvent cluster interactions, as well as the gas-phase solvent-solvent interactions. More specifically, the electrostatic contribution correlates well with the total interaction energy, irrespective of the solvent (Figure S45(a)). The exchange (Figure S45(b)), repulsion (Figure S45(c)) and polarisation (Figure S45(d)) contributions each only show moderate correlations, while both the desolvation (Figure S45(e)) and correlation (Figure S45(f)) contributions show no correlation what-so-ever.

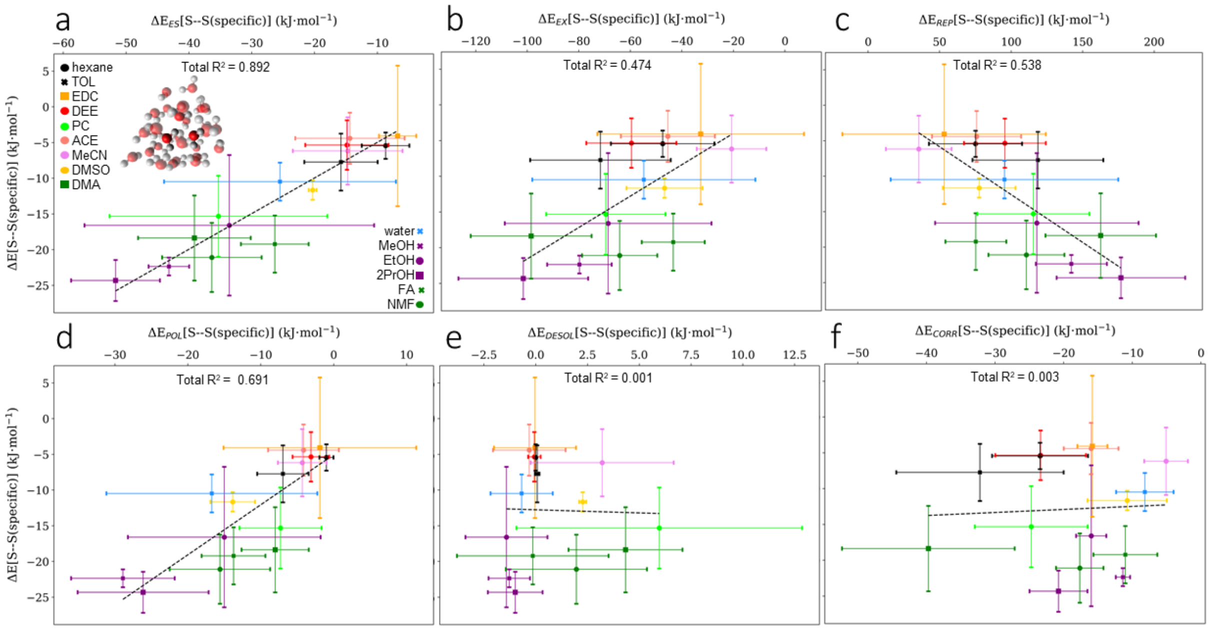

Figure S45: Comparison of the GKS-EDA (DFTB3(D3-BJ)/3-ob-3-1//M06-2X/cc-pVDZ) total *solvent-solvent pairwise interactions in the cluster model* interaction energy with the (a) electrostatic, (b) exchange, (c) repulsion, (d) polarisation, (e) desolvation and (f) correlation component energies. All data is averaged across multiple independent configurations; error bars denote 1 standard deviation.

S8.3 Solvent-Solvent Cluster Interactions

When considering a solvent molecule interacting with its entire solvation shell (Figure S46), the contribution trends observed in the pairwise-interactions of the same geometries persist, or get even stronger. However, there is a notable change in which solvents are exhibiting the strongest interactions. For the pairwise cluster interactions this was 2PrOH and MeOH (Figure S45), yet here in the solvation shell model it is now FA and water (Figure S46). This is likely due to the smaller solvent molecules being able to pack more solvent molecules into a single solvation shell, and therefore are greater increase in interaction strength from the pairwise to solvation shell EDA partitions. There is a similar difference that occurs from the gas-phase to cluster-phase pairwise interactions, where FA is the (significantly) strongest interaction in the gas phase (Figure S43), whereas it is only the fourth strongest interaction in the cluster model (Figure S45). FA's interaction decreases from -65.8 kJ·mol^{-1} to -19.2 kJ·mol^{-1}, as it deviates from a strong antiparallel dual-binding interaction to single C=O---H-N interaction with many coexisting interactions in the cluster. Then finally for the solvation shell energy, the interaction strength of the single FA molecule with its FA solvation shell is -125.4 kJ·mol^{-1}, or roughly 6.5 times as much. On the other hand, 2PrOH which has an interaction strength of only -27.1 kJ·mol^{-1} in the gas-phase, retains an 1:1 interaction strength of -24.3 kJ·mol^{-1} in the cluster model. In this circumstance the pairwise interaction geometry is unchanged in the cluster model for the molecules actually interacting through their charged dipoles. The single 2PrOH molecule has an interaction strength of -83.1 kJ·mol^{-1} with its solvation shell, roughly 3.5 times as much. For both FA and 2PrOH here, the magnitude change from pairwise to shell interactions is slightly higher than the number of directional dipole-dipole interactions for these specific geometries (~5 and 2 respectively from the optimised geometries). However, in both circumstances there are many additional weaker interactions that are side or via the non-polar component of the molecule.

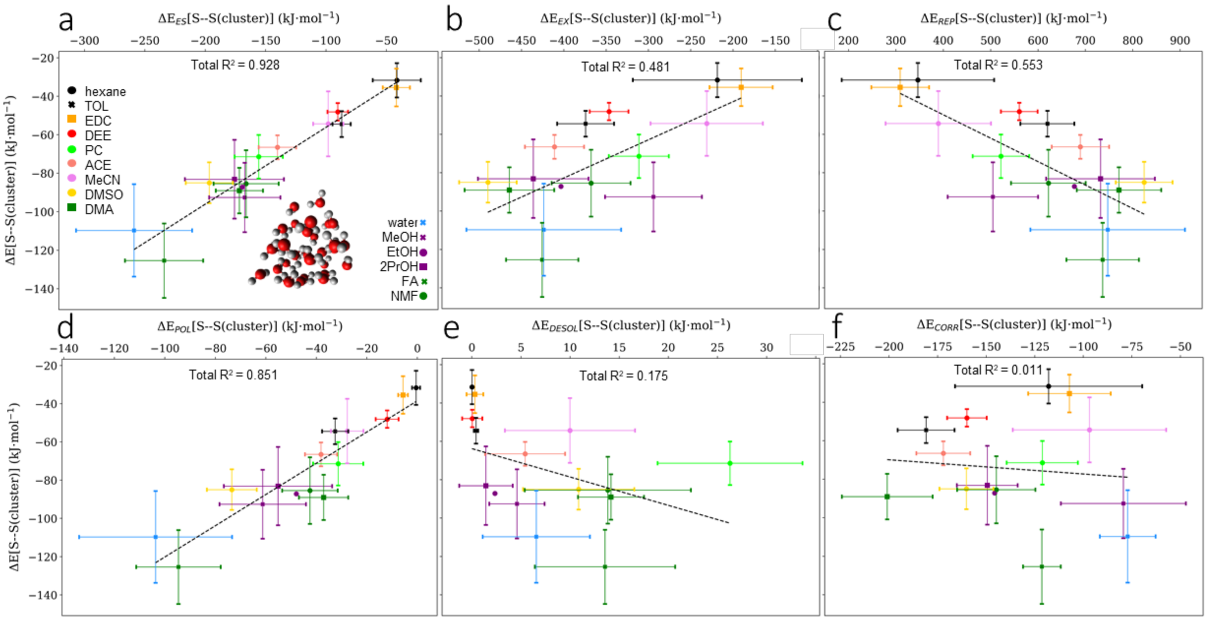

Figure S46: Comparison of the GKS-EDA (DFTB3(D3-BJ)/3-ob-3-1//M06-2X/cc-pVDZ) total *solvent and its solvating shell in the cluster model (including a PCM solvent environment)* interaction energy with the (a) electrostatic, (b) exchange, (c) repulsion, (d) polarisation, (e) desolvation and (f) correlation component energies. All data is averaged across multiple independent configurations; error bars denote 1 standard deviation.

S9. Direct relationship between the electrostatic interaction energy and the Gutmann Donor and Acceptor number with different solvation models

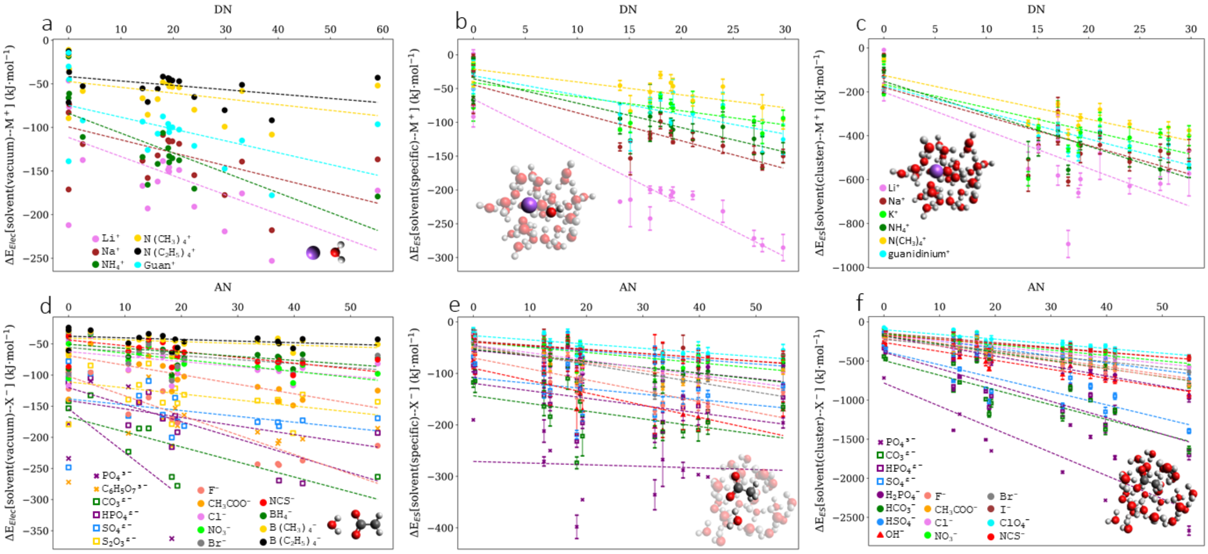

Figure S47. Correlation between the solvent basicity as measured via Gutmann donor and the *electrostatic contribution* to (a) the 1:1 cation-solvent interactions in the gas-phase calculated via M06-2X/aug-cc-pVDZ//SAPT2+3/aug-cc-pVDZ and (b) 1:1 cation-solvent and (c) cation-solvent shell interactions in a local solvent environment calculated with DFTB3-D3(BJ)/3-ob-3-1//GKS-EDA/M06-2X/cc-pVDZ. Correlation between the solvent acidity as measured via Gutmann-Mayer acceptor number and the *electrostatic contribution* to the (d) the 1:1 anion-solvent interactions in the gas-phase calculated via M06-2X/aug-cc-pVDZ//SAPT2+3/aug-cc-pVDZ and (e) 1:1 anion-solvent and (f) anion-solvent shell interactions in a local solvent environment calculated with DFTB3-D3(BJ)/3-ob-3-1//GKS-EDA/M06-2X/cc-pVDZ. R^2 values for each energetic component with the donor numbers presented in Table S2 and with the acceptor numbers in Table S3. This differs from Figure S7 which showed the total interaction comparison, rather than just the electrostatic contribution to that energy presented here.

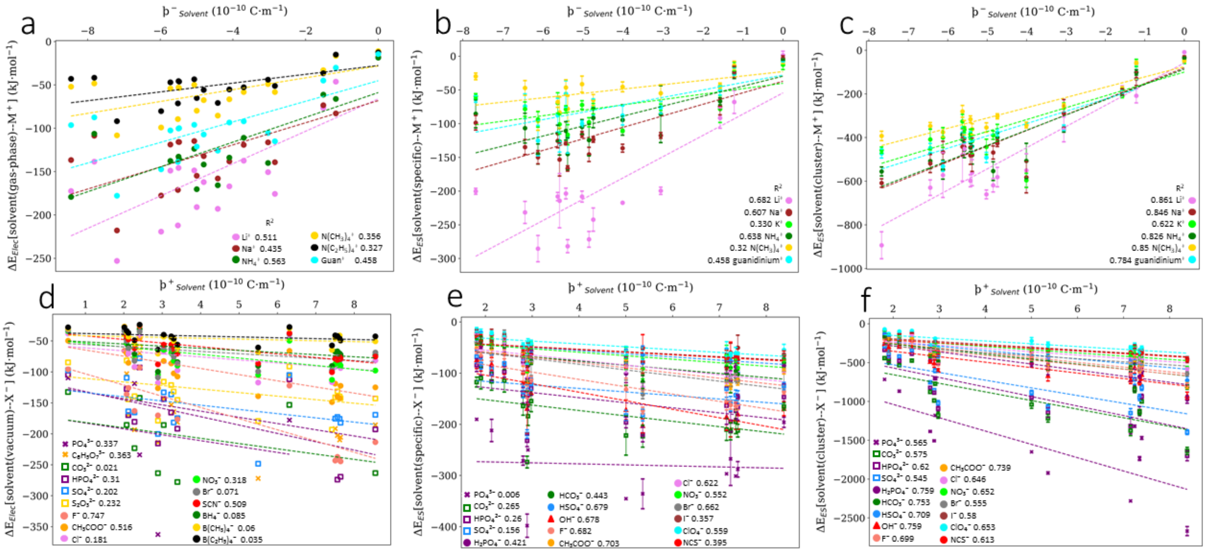

Figure S48: Correlation between the solvent $þ^{-}$ and the *electrostatic contribution* to (a) the 1:1 cation-solvent interactions in the gas-phase calculated via M06-2X/aug-cc-pVDZ//SAPT2+3/aug-cc-pVDZ and (b) 1:1 cation-solvent and (c) cation-solvent shell interactions in a local solvent environment calculated with DFTB3-D3(BJ)/3-ob-3-1//GKS-EDA/M06-2X/cc-pVDZ. Correlation between the solvent $þ^{+}$ and the *electrostatic contribution* to (d) the 1:1 anion-solvent interactions in the gas-phase calculated via M06-2X/aug-cc-pVDZ//SAPT2+3/aug-cc-pVDZ and (e) 1:1 anion-solvent and (f) anion-solvent shell interactions in a local solvent environment calculated with DFTB3-D3(BJ)/3-ob-3-1//GKS-EDA/M06-2X/cc-pVDZ.

S10. Caveats in the ion-solvent electrostatic interactions

S10.1 Discussion on outliers in the SAPT2+3 1:1 cation-solvent electrostatic interactions

Despite the non-electrostatic energy contributions varying quite substantially between cation families, the electrostatic contribution still approximates the total energy (Figure S12-Figure S13(a)) in most circumstances. For recent work,[4] where a similar dominant electrostatic contribution was observed for ion-water interactions, Coulomb's Law of electrostatic potential energy was useful for calculating ion-water properties (such as the ion's enthalpy of hydration and it's viscosity B coefficients),

$$U_E = k_e \frac{q_{solvent}^{-/+} \cdot q_{ion}^{+/-}}{r} \tag{S5}$$

where the solvent-ion distance can be approximated simply via the sum of the interacting atom's cubed root of the r-cubed moments, *i.e.*, $r \approx \sqrt[3]{\langle r_{solvent}^{-/+\;3} \rangle} + \sqrt[3]{\langle r_{ion}^{+/-\;3} \rangle}$, and the electrostatic interaction is the result of partial atomic charges $q_{solvent}^{-/+}$ and $q_{ion}^{+/-}$. It is hypothesised here that this can apply more generally for ion-solvent interactions in all solvents. A molecular nonaqueous solvent will most likely interact with the cation via the most (negatively) charge dense accessible atom (*e.g.*, the oxygen in water, alcohols, formamide and DMSO, the nitrogen in ammonia (NH_3) or the chlorine in 1,1-, and 1,2-dichloroethane).

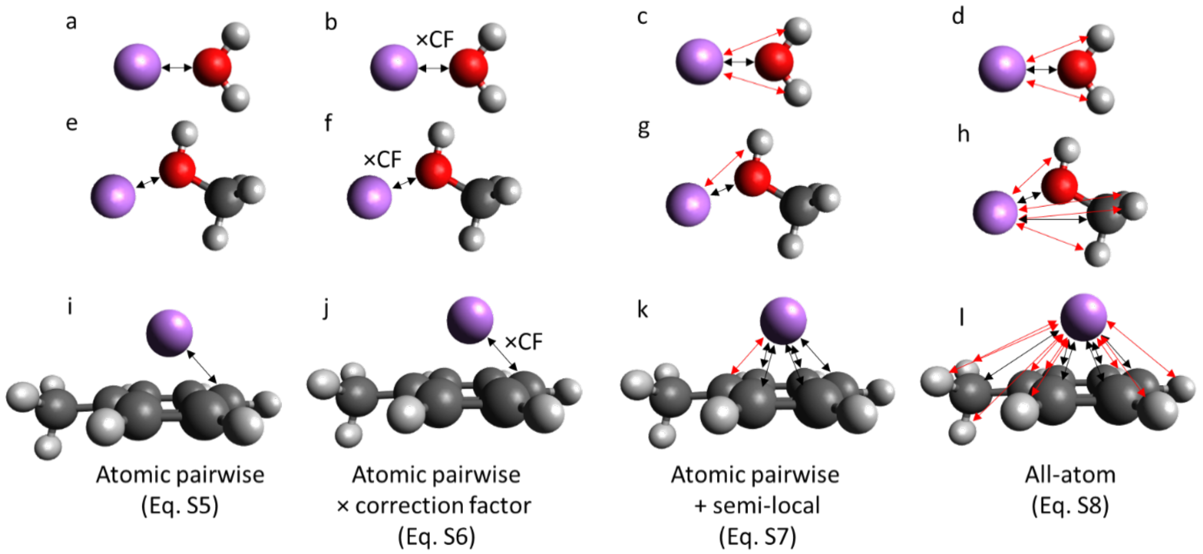

Atomic pairwise (Eq. S5)

Atomic pairwise × correction factor (Eq. S6)

Atomic pairwise + semi-local (Eq. S7)

All-atom (Eq. S8)

Figure S49: Locality to consider when approximating the electrostatic potential energy using (a-d) Li^+-water, (e-h) Li^+-MeOH and (i-j) Li^+-TOL as representative examples. (a, e, i) Pairwise-atomic electrostatic potential energy, (b, f, j) pairwise-atomic electrostatic potential energy with a solvent-dependent correction factor, (c, g, k) pairwise-atomic electrostatic energy including adjacent repulsive atoms (red arrows) and (d, h, l) all-atom electrostatic energy. As the complexity of the interaction increases (d → h → l) the simplicity of the all-atom approach diminishes, and requires an accurate description of the interaction geometry in lieu of radial moments.

An overall trend between the theoretical electrostatic potential energy (U_E) and the electrostatic contribution of the total energy is observed for these pairwise interactions, however water and NH_3 appear to consistently overestimate the electrostatic energy contribution (Figure S50(a)) by a factor of ~2.25 (*i.e.*, U_E is roughly 2.25 the value that would place these points on the line of best fit). Similarly, the U_E values for MeOH, EtOH, PrOH and 2PrOH interactions overestimate the electrostatic energy by a factor of ~1.35-1.5. Conversely, the U_E value for Py, TOL and DEE underestimates the electrostatic energy by a factor of ~1.5, ~1.4 and ~1.25 respectively. Similarly, the protic cations (NH_4^+ and guanidinium$^+$) have consistently underestimated electrostatic energies (Figure S51(c)), likely due to partial proton transfer discussed previously. Using the consistent deviation amounts as solvent dependent correction factors (CF) numerically correlates the data for non-protic cations and the entire solvent dataset (Figure S50(b), Figure S52),[†]

$$U_E = k_e \frac{q^-_{solvent} \cdot q^+_{cation}}{r^-_{solv} + r^+_{cation}} \cdot CF_{solvent} \tag{S6}$$

Considering this fact, as well as the consistent trends that appear when separating the data by the solvent (Figure S50(a, b), Figure S53), indicates that there is something physical missing from the calculated U_E values that is required to account for these deviations. In the "anomalous" cases that overestimate the electrostatic energy, the atom where the negative solvent dipole resides has neighbouring atom(s) with a strong positive dipole. For example, there are two neighbouring protons for water (Figure S49(a-d)), but only one for the alcohols (Figure S49(e-h)). Conversely, Py and DEE are the only two solvents present here that have two carbon atoms adjacent to the negative dipole atom and TOL is unique within this dataset as the only aromatic solvent with no single donor atom, so is interacting through 6 atoms,[‡] not just the carbon with the highest charge density (Figure S29(a), Figure S49(i-l)).

[†] For simplicity of notation here, $r_i = \sqrt[3]{\langle r_i^3 \rangle}$

[‡] For toluene, each interaction distance derived from the radial moments has been multiplied by $\sqrt{2}$ to approximate the increased length of interaction from the cation sitting centrally above the π-ring rather than a single atom.

If the pairwise U_E calculations are expanded to include multiple (n^-) attractive interactions in conjunction with multiple (n^+) repulsive electrostatic interactions on adjacent atoms, we obtain the equation,

$$U_E \sim k_e\left(\frac{q^-_{solv}\cdot q^+_{cation}}{r^-_{solv}+r^+_{cation}}\times n^- + \frac{q^+_{solv}\cdot q^+_{cation}}{\left(r^-_{solv}+r^+_{solv}\right)+\left(r^-_{solv}+r^+_{cation}\right)}\times n^+\right) \tag{S7}$$

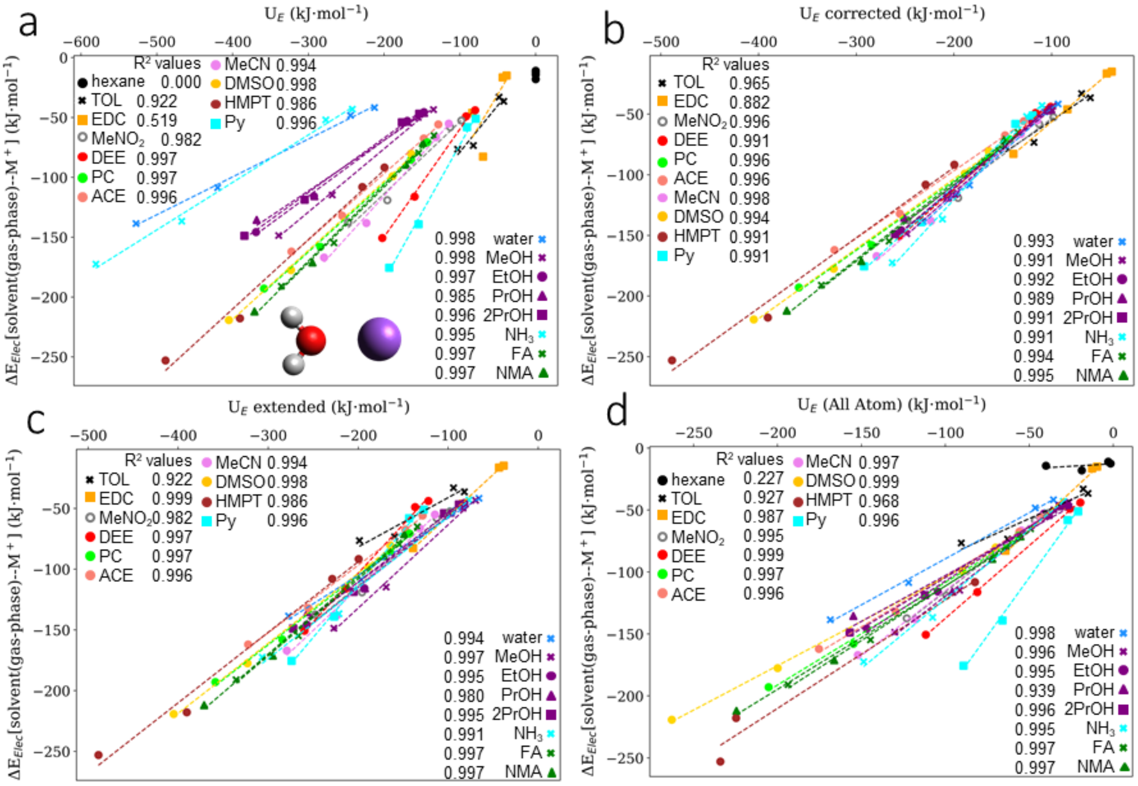

Figure S50: The theoretical electrostatic interactions between cations and solvents as calculated via (a) Eq. S5, (b) Eq. S6, (c) Eq. S7 and (d) Eq. S7 compared to the SAPT2+3 electrostatic interaction energies. DDEC6 partial charges and radial moments are used in (a-c). The DDEC6 partial charges are used in conjunction with M06-2X/aug-cc-pVDZ optimised geometries in (d). This data excludes the protic cations to avoid introducing charge transfer effects.

This provides a physical basis for the correction factors, given the strong correlations presented in Figure S50(c) and the clustering of each solvent onto a single trend as opposed to distinct solvent dependent trends (Figure S50(a)). This indicates that when comparing solvents for specific cation effects, the entire local region is required to adequately account for the cation-solvent electrostatic interactions, not just the immediate interacting atoms. If we completely consider the electrostatic interactions of all atoms in the entire pairwise interaction,

$$U_E = k_e \sum_{i\in solv}\sum_{j\in ion}\frac{q_i\cdot q_j}{R_{ij}} \tag{S8}$$

Where R_{ij} is the internuclear distance between ion atom i and solvent atom j from the M06-2X/aug-cc-pvdz optimised geometry, we obtain further insight (Figure S50(c)). In this circumstance, no further improvement is made with respect to the correlations between U_E (all atom) and ΔE_{Elec}. This indicates that the local region calculated by Eq. S7 is sufficient for approximating the electrostatic contribution to the interaction energy. For example, for the Li^+-HMPT interaction the longrange interaction with atoms on a methyl group results in U_E(Li$^+$-C) of -56 kJ·mol^{-1} and U_E(Li$^+$-H) of 27, 25 and 21 kJ·mol^{-1} for each of the hydrogen atoms for a total U_E(Li$^+$-CH$_3$) of -56 kJ·mol^{-1} for a total repulsive interaction of 17 kJ·mol^{-1}. This is negligible in comparison to the local U_E(Li$^+$-O) of -606 kJ·mol^{-1}, so would require a significant number of these for non-local effects to become significant.

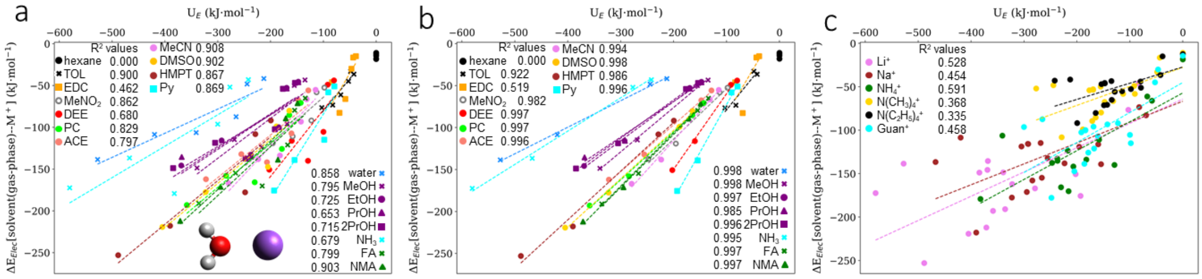

Figure S51: The correlation between the theoretically electrostatic potential energy (U_E) calculated via Eq. S5 and the electrostatic contribution of the cation-solvent energy as calculated by SAPT2+3/aug-cc-pVDZ, sorted (a) by solvent, (b) by solvent excluding the protic cations and (c) by cation.

It should be noted however, that the magnitude of U_E adjusts from roughly two times ΔE_{Elec} via Eq. S7 to be of similar magnitude via Eq. S8. The primary reason for this is that R_{ij} obtained directly from the interaction geometry, is shorter than $r_i + r_j$, and significantly shorter for $(r_i^- + r_i^+) + (r_i^- + r_j^+)$. While this increases the magnitude of the immediate attractive U_E, the repulsive U_E values are more significantly increased to compensate for this. Using the Li$^+$-water interaction as the simplest example (where only the interaction distance changes between Eq. S7 and Eq. S8), U_E(Li$^+$-O) is -528 kJ·mol^{-1} via Eq. S7 and -608 kJ·mol^{-1} via Eq. S8, whereas U_E(Li$^+$-H) is 125 kJ·mol^{-1} via Eq. S7 and 220 kJ·mol^{-1} via Eq. S8. Therefore, U_E(Li$^+$-water) is -277 kJ·mol^{-1} via Eq. S7 and -169 kJ·mol^{-1} via Eq. S8. The geometric considerations for the local interactions are discussed further in §S10.2.

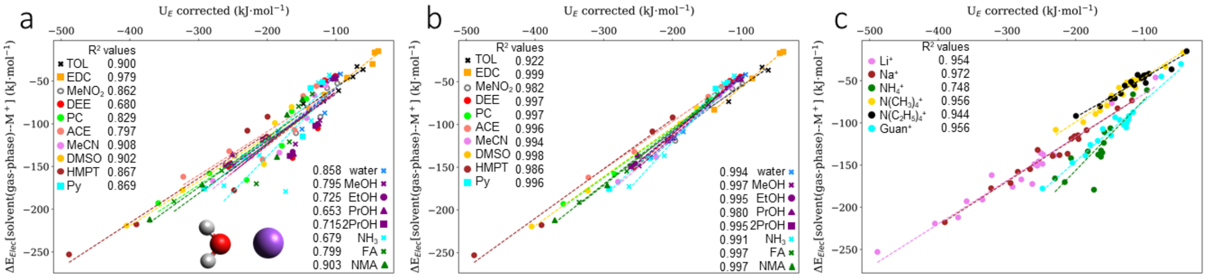

Figure S52: The correlation between the electrostatic potential energy with solvent-correction factors (U_E corrected) calculate via Eq. S6 and the electrostatic contribution of the cation-solvent energy as calculated by SAPT2+3/aug-cc-pVDZ, sorted (a) by solvent, (b) by solvent excluding the protic cations and (c) by cation.

Pyridine has ΔE_{Elec} values of larger magnitudes than the other solvents when compared to U_E calculated via Eq. S8. Py has a π-enhanced interaction, serving as the only solvent here that is interacting through a single donor atom located in an aromatic ring, making it unique amongst this dataset. In fact, for Li$^+$-solvent interactions, the DDEC6 calculated partial charge on the interacting nitrogen atom of Py almost doubles from its isolated structure, increasing by 85%. This indicates that a larger charge accumulates on the nitrogen atom in the presence of the ion. This is indeed the largest percent increase of all the solvent molecules (Table S6). If the DDEC6 charges calculated used in Eq. S8 are obtained from a DDEC6 analysis on the interacting complex as opposed to their isolated fragments the calculated interaction does indeed increase significantly. For the Li$^+$-Py interaction this increases from -89 kJ·mol^{-1} to -149 kJ·mol^{-1} when calculating via Eq. S8. Unfortunately, the evolution of the electrostatic analysis from Eq. S5-8 complicates *a priori* predictions of such systems, and so presents a limitation of this current model.

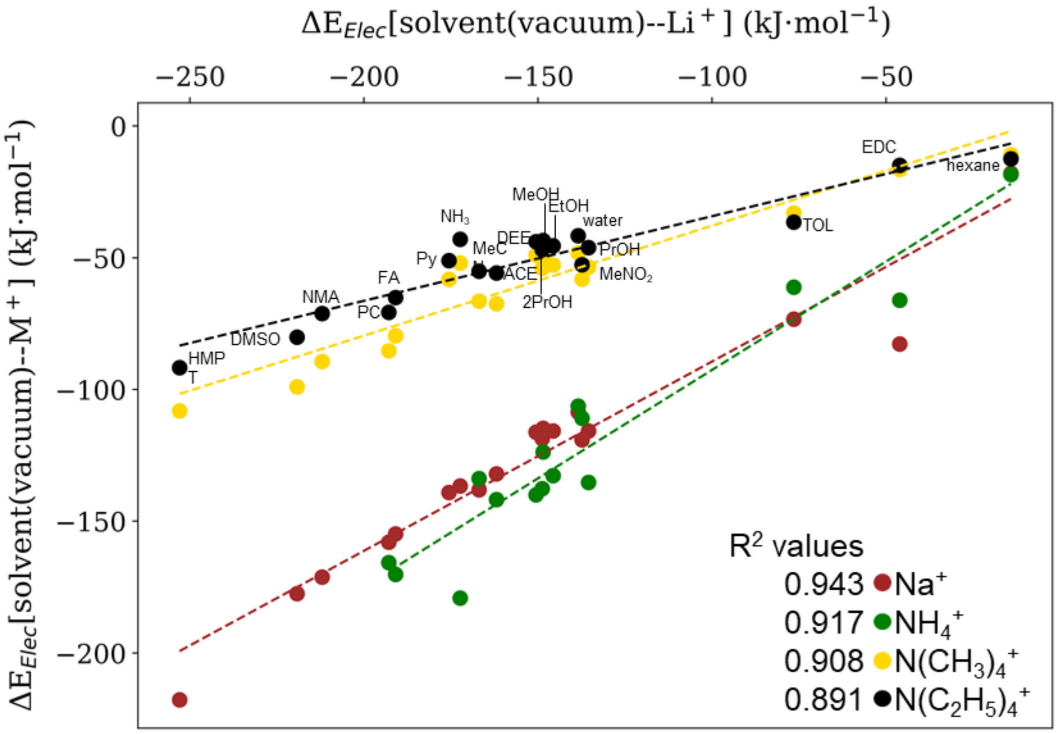

Figure S53: Comparison of the Li$^+$-solvent electrostatic interaction energy with the other cation-solvent electrostatic interaction energies. This reveals the solvents to have consistent trends in their interaction strengths for each of these cations.

S10.2 Geometric Considerations for the Pairwise Electrostatic Potential Energy

To approximate the interaction distance between interacting atoms on species j and atoms covalently bonded to the interacting atom on i requires some geometric considerations about the bond angles, and a further assumption that $R_{i_1 i_2} \approx r_{i_1} + r_{i_2}$. Using the cation interactions as an example results in the following equation,

$$U_E = k_e \frac{q_{solv}^- \cdot q_{cation}^+}{r_{solv}^- + r_{cation}^+} + k_e \sum_{i \in solv} \sum_{j \in cation} \frac{q_i^{+/-} \cdot q_j^+}{\sqrt{\left(r_i^- + r_i^{+/-}\right)^2 + \left(r_i^- + r_j^+\right)^2 - \left(2\left(\left(r_i^- + r_i^{+/-}\right) + \left(r_i^- + r_j^+\right)\right) cos\theta\right)}} \tag{S9}$$

where θ is the angle between the cation, the atom of the negative dipole and the adjacent atom of the positive dipole, and n is the number of adjacent (protic) “dipoles”. Given the chemical nature of such cation-solvent interactions, an angle (between the cation, solvent negative dipole and adjacent atoms) of 90-180 degrees could be expected such that, in general, assuming molecular symmetry and orthogonal cation binding,

$$k_e \left| \frac{q_{solv}^- \cdot q_{cation}^+}{r_{solv}^- + r_{cation}^+} + \frac{q_{solv}^+ \cdot q_{cation}^+}{\left(r_{solv}^- + r_{solv}^+\right) + \left(r_{solv}^- + r_{cation}^+\right)} \times n^+ \right| < |U_E| < k_e \left| \frac{q_{solv}^- \cdot q_{cation}^+}{r_{solv}^- + r_{cation}^+} + \frac{q_{solv}^+ \cdot q_{cation}^+}{\sqrt{\left(r_{solv}^- + r_{solv}^+\right)^2 + \left(r_{solv}^- + r_{cation}^+\right)^2}} \times n^+ \right| \tag{S10}$$

This could be simplified into five main categories; linear, trigonal planar, tetrahedral, trigonal pyramidal and octahedral, however, in the cases explored, the approximation using θ of 180° (*i.e.*, linear, Eq. S7) appears to largely linearise these electrostatic correlations (even though the cation-O-H angle in water is clearly non-linear) for simple cations with a variety of molecular solvents (Figure S50(c)). It is likely that the errors introduced by approximating the interaction distances in this manner outweigh any benefit that might be obtained from this increased complexity.

Unfortunately, this doesn't easily account for the underestimations observed in TOL, Py and DEE. Initial U_E calculations were only considering the attractive interaction with the most charge dense atom within the π-ring according to the DDEC6 calculations. For a complete electrostatic calculation of π-interactions in toluene, considerations of the whole ring should be required, since the whole ring is involved in the interaction (Figure S29(a)), *i.e.*,

$$U_E = \sum_{i \in solv} \sum_{j \in cation} \frac{q_i^- \cdot q_j^+}{r_i^- + r_j^+} + \sum_{i \in solv} \sum_{j \in cation} \frac{q_i^{+/-} \cdot q_j^+}{\sqrt{\left(r_i^- + r_i^{+/-}\right)^2 + \left(r_i^- + r_j^+\right)^2 - \left(2\left(\left(r_i^- + r_i^{+/-}\right) + \left(r_i^- + r_j^+\right)\right) cos\theta\right)}} \qquad \text{(S11)}$$

In conjunction to these geometric considerations for pairwise electrostatic approximations, conformation considerations should also be considered.

S10.3 Conformational Considerations for the Pairwise Electrostatic Potential Energy

In these gas-phase bimolecular interactions, the conformation of the molecular solvent must be considered, as the optimal energy minimum ion-solvent structure might vary from a cluster model or bulk solvent, where crowding effects and multiple solvent binding interactions might be favoured over a bidentate style binding interaction (*e.g.*, 1,2-dichloroethane might adopt a cis form to interact with the cation via both chlorine atoms simultaneously). For different ions, when a solvent-ion interaction occurs in the same manner, the deviation of the electrostatic energy from the U_E trend is consistent (Figure S54). These electrostatic contributions appear to be near additive, such that for the Na^+-EDC interaction doubling the theoretical U_E put this on trend with cation-EDC interactions interacting with a single chlorine atom.[§] More generally, the ΔE_{Elec} changes from -46.1, -37.8 and -33.0 kJ·mol^{-1} for interactions with one chlorine atom, to -94.3, -82.8 and -66.1 kJ·mol^{-1} for interactions with two chlorine atoms for Li^+, Na^+ and NH_4^+ respectively.

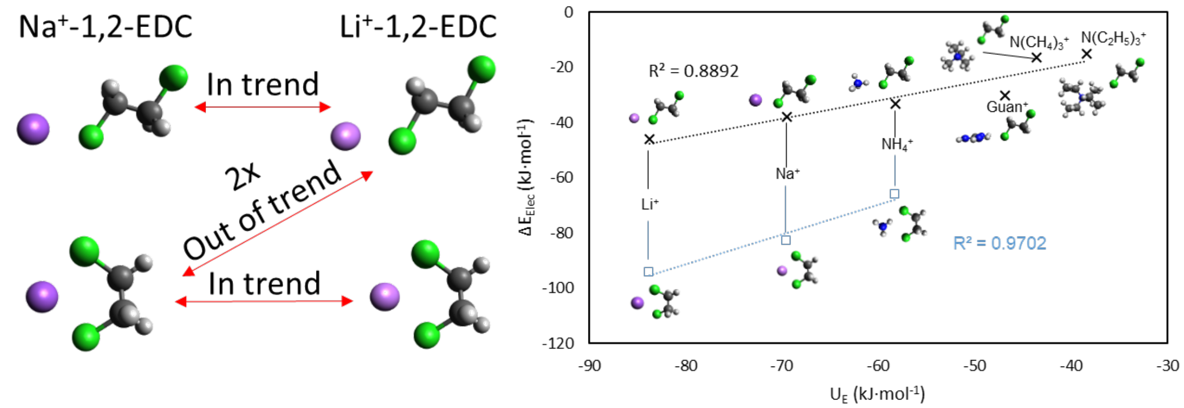

Figure S54: EDC example of how the solvent geometry and conformation can affect the energetic trends or deviations from trends.

S10.4 Anion further analysis on outliers

Given the similarity to the trends observed in cations and anions and the fact that anions appeared to be more consistent regarding specific ion effect trends,[4] the solvent contributions to the anion-solvent interactions too might be predictable via their electrostatic potential energy. Furthermore, for each solvent's the anion-solvent interaction energy (Figure S55) and electrostatic contribution (Figure S56) correlates well with $Þ^-_{anion}$ addressing the point that the applicability of $Þ^-_{anion}$ extends beyond water to nonaqueous solvents. However, regarding solvents and the versatility of AN as a solvent property, this is not the case for these 1:1 interaction energies (Figure S57). Unlike the relationship identified in ref 4 for Gibbs energies of transfer, there is a poor correlation between AN and the solvent-dependent

---

[§] The interaction with two chloride atoms of 1,2-dichloroethane didn't naturally arise in the dataset for Li^+, and only occurred only once each for Na^+ and NH_4^+ in the 10 geometry optimisations.

gradient of each ion's þ$^{-}_{\text{anion}}$-energy relationship (Figure S57(a)). This relationship is similarly poor for the Cl^{-}-solvent interaction energies themselves (Figure S57(b)). Therefore, it appears that both AN and þ$^{+}_{\text{solvent}}$ are poor solvent parameters for a direct approximation of the 1:1 anion-solvent interaction energies. In fact, it appears that the solvent parameters that had strong correlations (Figure S26-Figure S27) with cation-solvent intermolecular energy contributions don't retain the same correlation for anion-solvent interactions (Figure S37-Figure S38). This might suggest that positive charges (*i.e.*, cations) and positive dipoles in general are more challenging to utilise for electrostatic approximations via radial charge densities. This is not entirely surprising since r^{+} is generally much smaller than r^{-}, and therefore r^{-} exclusion from the definition of þ$^{+}$ is prone to error.

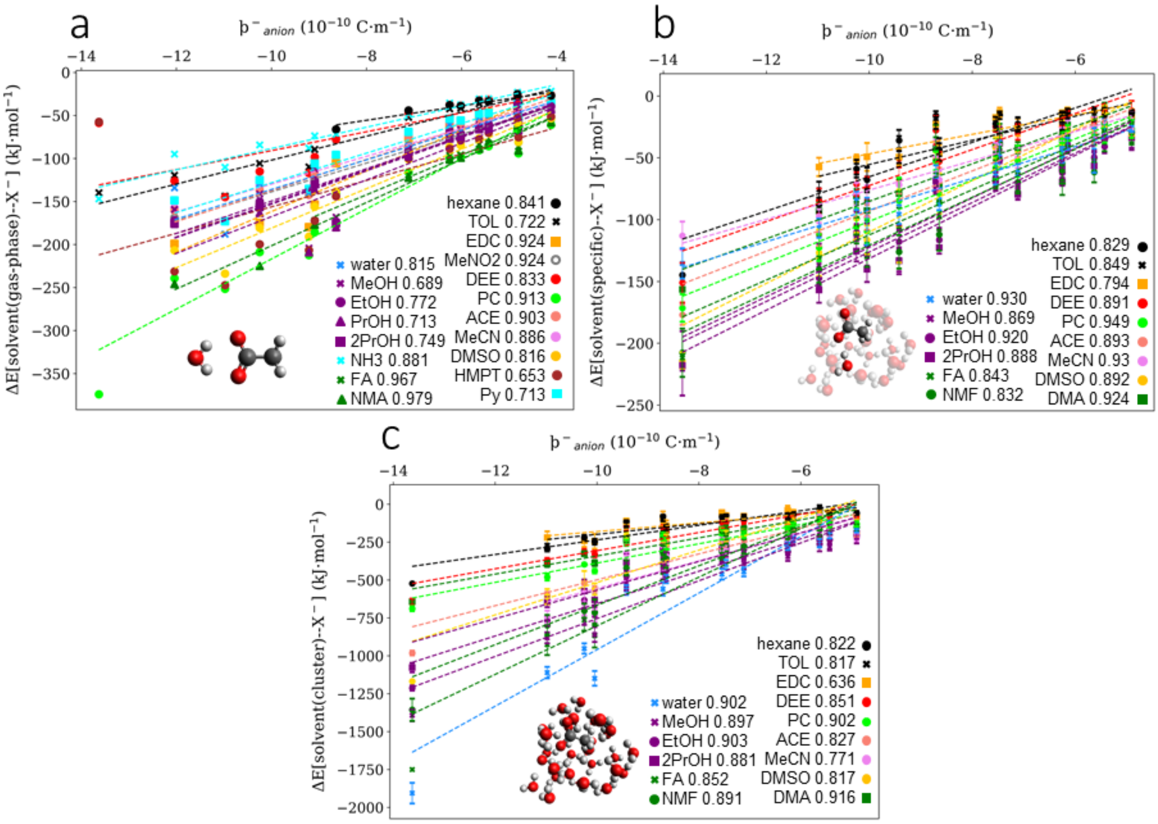

Figure S55: A comparison of þ$^{-}_{\text{anion}}$ with the total anion-solvent interaction energies. þ$^{-}_{\text{anion}}$ consistently correlates with the (a) M06-2X/aug-cc-pVDZ//SAPT2+3/aug-cc-pVDZ gas-phase anion-solvent interaction energies, as well as the (b) specific 1:1 and (c) whole cluster interactions in a solvent cluster calculated with GKS-EDA (DFTB3(D3-BJ)/3-ob-3-1//M06-2X/cc-pVDZ).

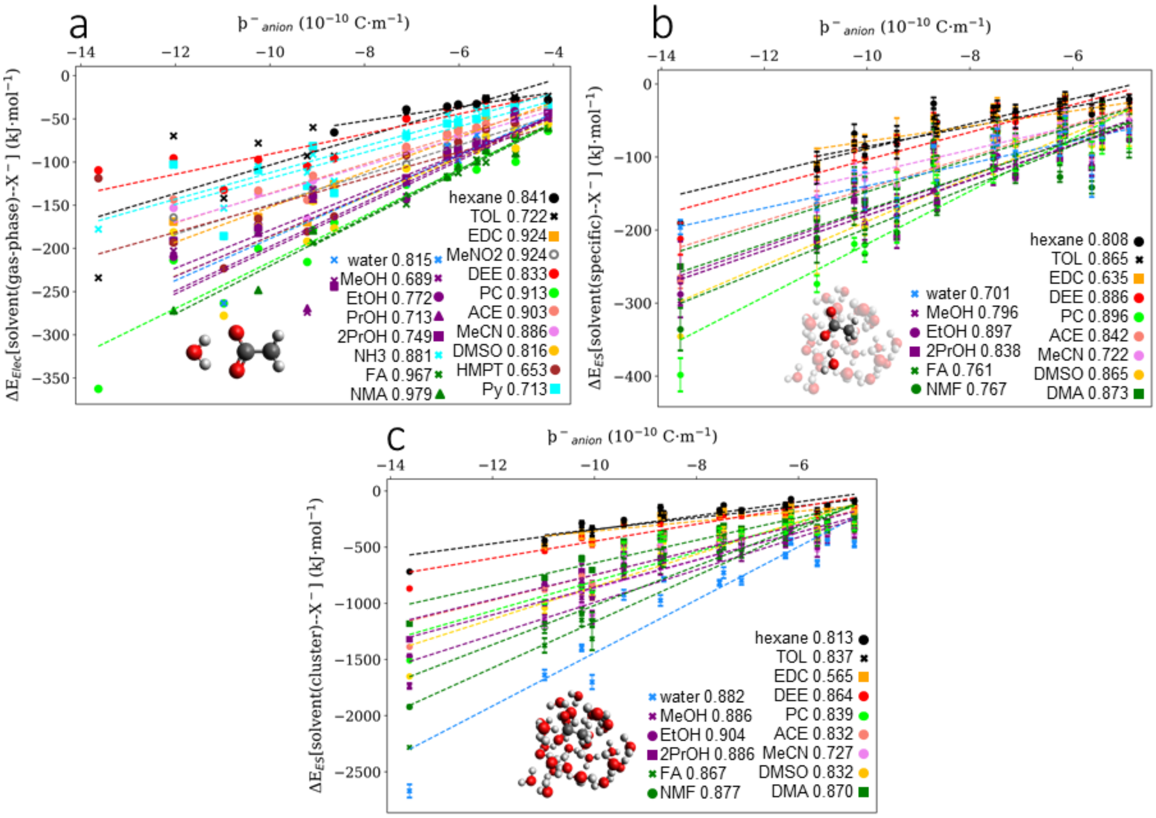

Figure S56: A comparison of þ$^{-}_{\text{anion}}$ with the electrostatic anion-solvent interaction energies. þ$^{-}_{\text{anion}}$ consistently correlates with the (a) M06-2X/aug-cc-pVDZ//SAPT2+3/aug-cc-pVDZ gas-phase anion-solvent interaction energies, as well as the (b) specific 1:1 and (c) whole cluster interactions in a solvent cluster calculated with GKS-EDA (DFTB3(D3-BJ)/3-ob-3-1//M06-2X/cc-pVDZ).

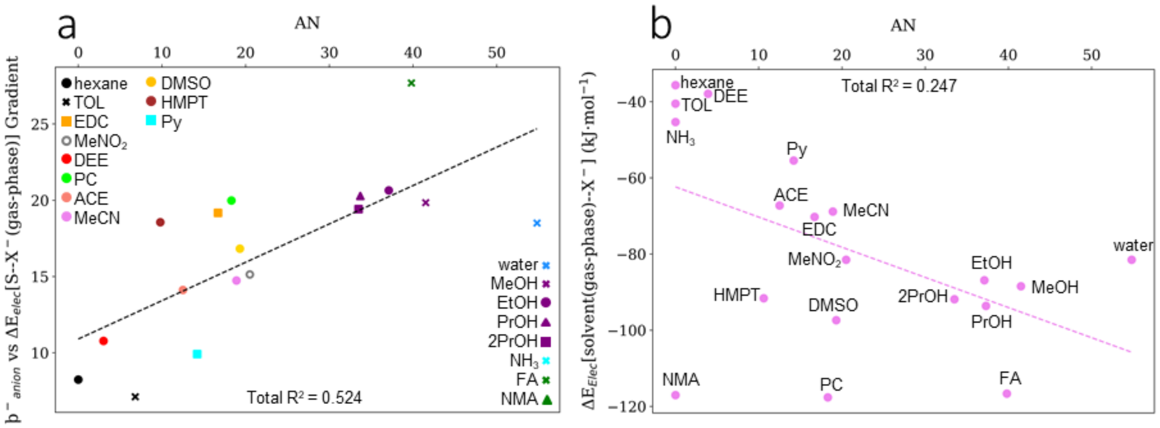

Figure S57: (a) The gradient of each solvent's þ$^{-}_{\text{anion}}$- electrostatic energy relationship gradient (from Figure S55 (a)) correlated with the Gutmann-Mayer acceptor number. (b) The M06-2X/aug-cc-pVDZ//SAPT2+3/aug-cc-pVDZ Cl^{-}-solvent gas phase energy compared to each solvents Gutmann-Mayer acceptor number.

S10.5 Extended Electrostatic Analyses (Anions)

When using a theoretical U_E calculation via Eq. S5 to account for the missing r^- term in $þ^+$ for pairwise interactions (discussed at the end of §S10.1, though U_E for solvent-solvent interactions seems well approximated by $þ^+ \cdot þ^-$, see Figure S61), there are still general anion trends (Figure S58), however for a constant Cl^- there seems to be very little correlation between differing solvents between U_E and the electrostatic component of the anion-solvent interaction energy (Figure S60(a)). However, if the electrostatic contribution of the Cl^--solvent interaction is compared with the other anion-solvent interactions there are consistent trends for electrostatic contribution to the total energy indicating that there is some constant unaccounted-for factor at play for each solvent (Figure S59). This implies that while only considering the pairwise electrostatic potential energy (U_E) of the two nearest (intermolecular) neighbours is still insufficient, there is some physical factor that can approximate pairwise intermolecular electrostatic energies for anion-solvent interactions. Indeed, if the interaction geometries are considered, it would be surprising if a single U_E or $þ^+_{\text{solvent}}$ value could approximate the solvents electrostatic contribution to the interaction energy, given these often occur through multiple hydrogen atoms (Figure S60(b)). If a correction factor (C.F.) accounting for this is applied to U_E the correlation improves significantly (Figure S60(c)). However, this is skewed by the choice of interacting hydrogens, as well as interactions where the charge densities on each interacting hydrogen vary. A complete electrostatic analysis of the Cl^--solvent interactions using Eq. S8 can account for this and improves the correlation further still (Figure S60(d)). However, this compromises the simplicity of the initial models, and still doesn't obtain the correlations for cation-solvent interactions via a similar analysis (Figure S50(d)).

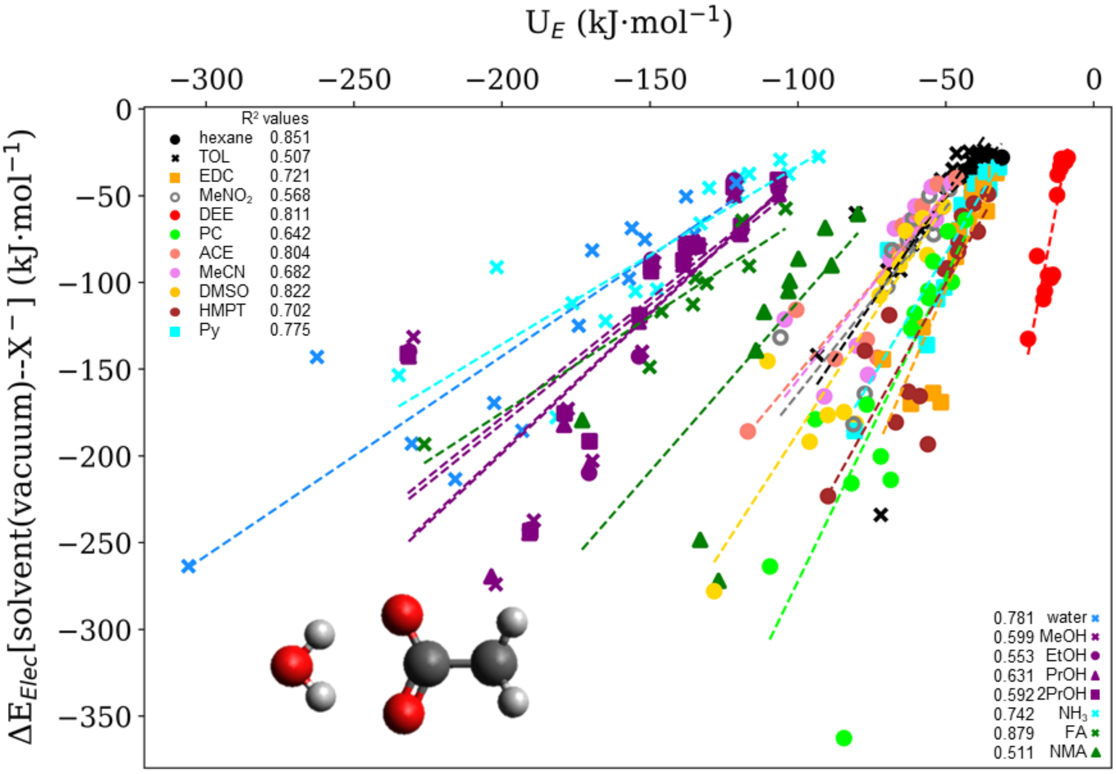

Figure S58: The theoretical electrostatic interactions between anions and solvents as calculated via Eq. S5 compared to the M06-2X/aug-cc-pVDZ//SAPT2+3/aug-cc-pVDZ electrostatic interaction energies.

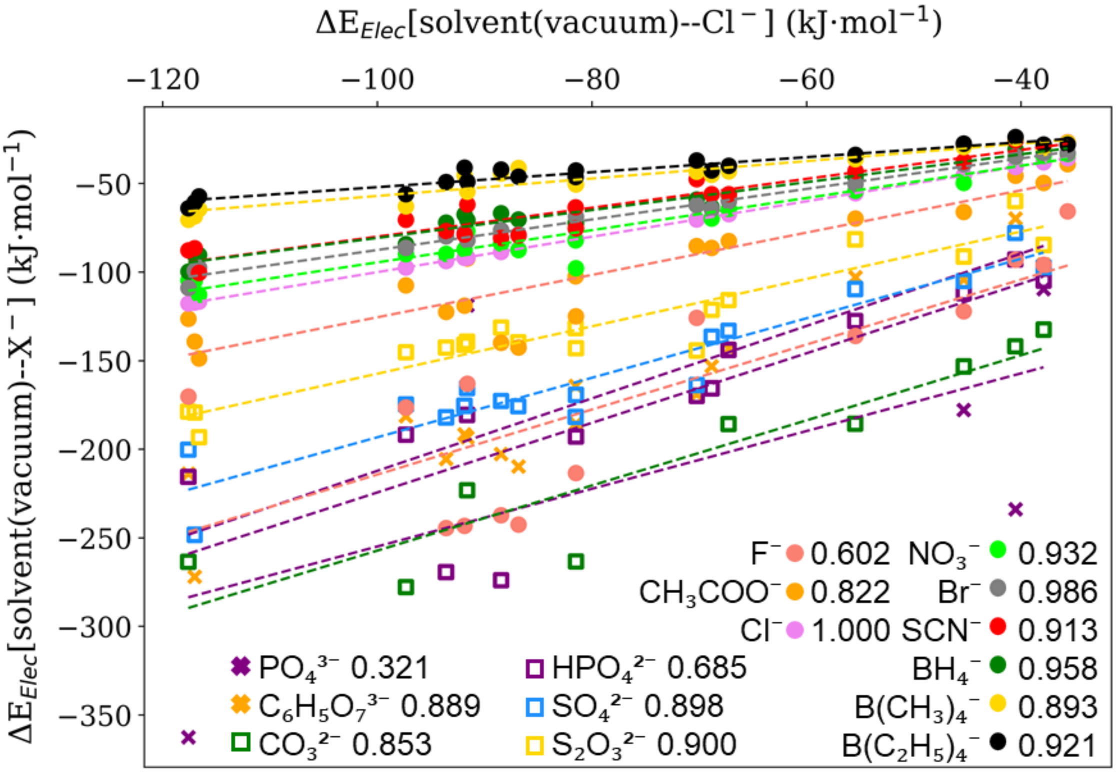

Figure S59: Comparison of the Cl⁻-solvent M06-2X/aug-cc-pVDZ//SAPT2+3/aug-cc-pVDZ electrostatic interaction energy with other anion-solvent M06-2X/aug-cc-pVDZ//SAPT2+3/aug-cc-pVDZ electrostatic interaction energies. This reveals the solvents to have consistent trends in their interaction strengths for each of these anions, with the worse correlations occurring for the phosphates and fluoride.

Two key considerations arise here:

a) The number (and type) of interacting atoms between the anion and solvent should be accounted for in anion-solvent interactions.

b) Given AN are experimentally useful, yet didn't correlate well with these gas-phase anion-solvent ΔE_{Elec}, what is missing from the model that might account for this?

The empirical Gutmann-Mayer acceptor number has many practical uses for experimental behaviour as displayed in ref 4. However, since AN is insufficient to describe solvent effects on these gas-phase 1:1 interactions (Figure S57), and AN isn't based on 1:1 interactions by design like the cation, the molecular origins may require the solvent cluster model to properly replicate these (for instance, accounting for the coordination number of the solvent).

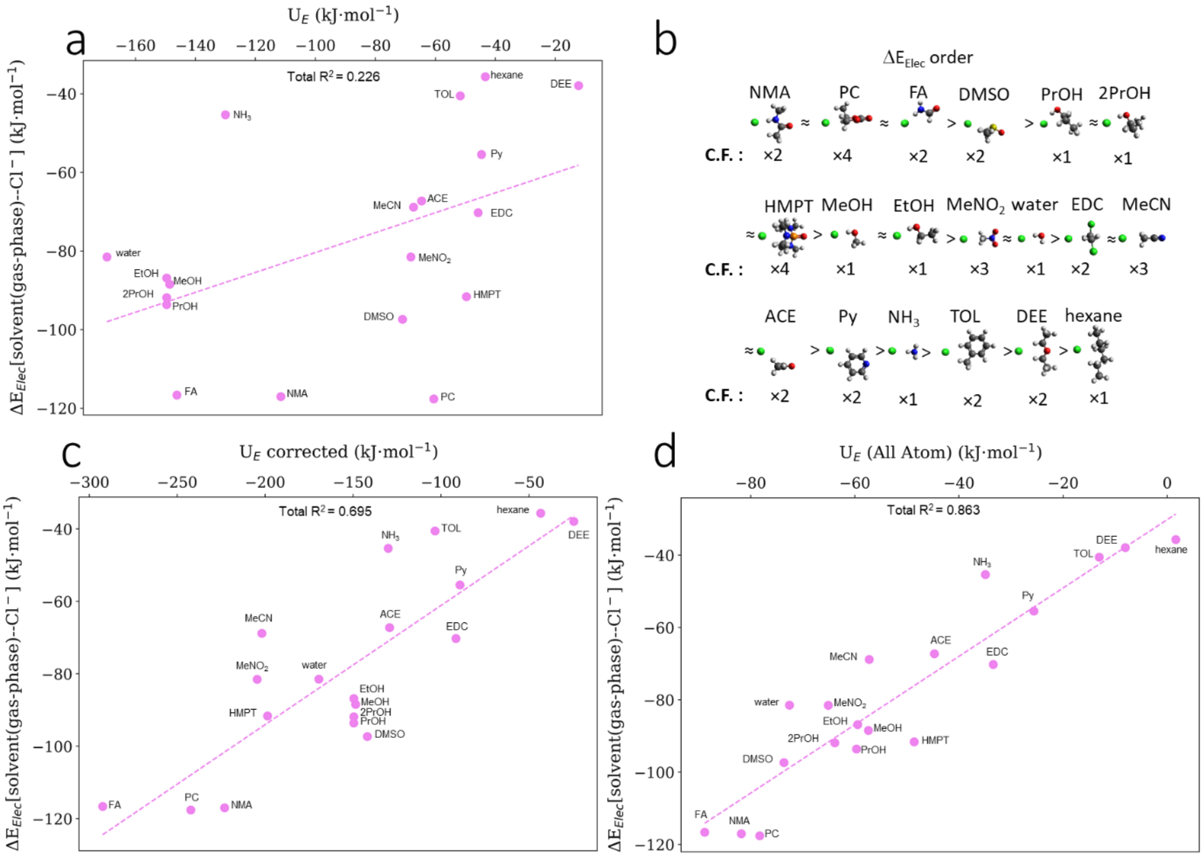

Figure S60: (a)The theoretical electrostatic interactions between chloride and solvents as calculated via Eq. S5 compared to the M06-2X/aug-cc-pVDZ//SAPT2+3/aug-cc-pVDZ electrostatic interaction energies. (b) When adjusting U_E by some correction factor (C.F.) which is the perceived number of interactions (except of hexane), (c) the correlation between the electrostatic contribution and the "corrected" theoretical electrostatic potential energy improves. This is rather primitive, as the U_E values of all the alcohols are identical here, however the ΔE_{Elec} would likely increase here with increasing numbers of weak interactions with increasing the aliphatic tail length. (d) The electrostatic component of the M06-2X/aug-cc-pVDZ//SAPT2+3/aug-cc-pVDZ Cl$^-$-solvent interaction compared to the theoretical U_E using Eq. S8. R_{ij} is obtained from the same optimised geometry accounting for all atoms using charges of the Cl$^-$ and solvents from DDEC6/aug-cc-pVTZ calculations.

S11. Additional considerations

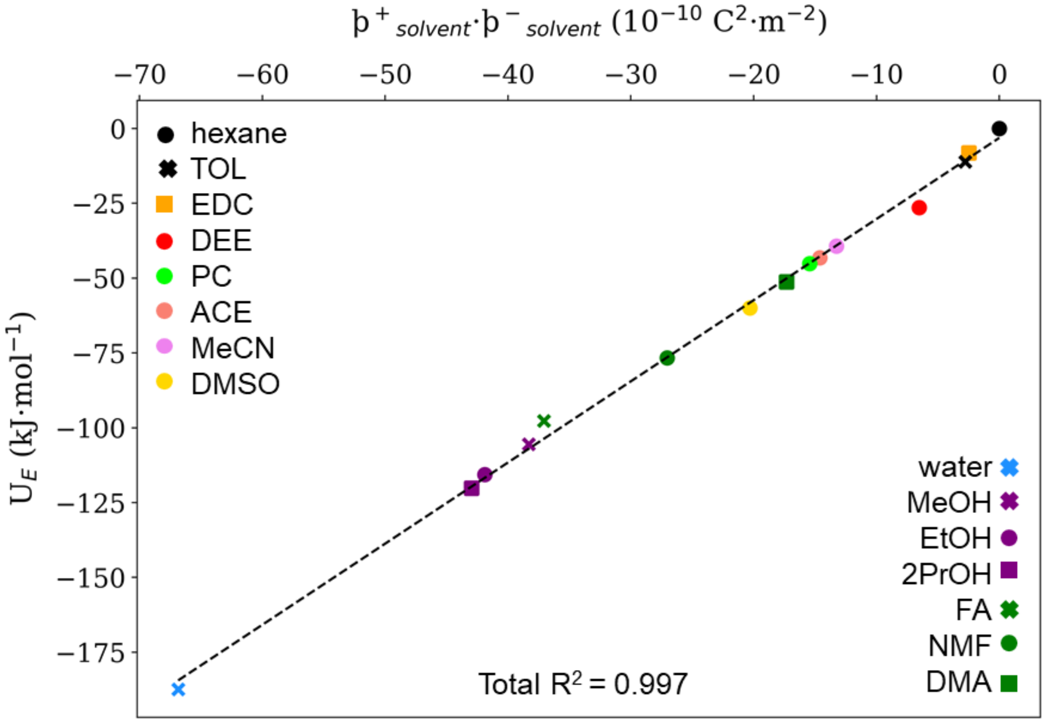

Figure S61: $\text{þ}^+\cdot\text{þ}^-$ is effectively a measure of the electrostatic potential energy U_E for these solvents. They only differ in the denominator term that accounts for the radii, as this is multiplicative ($r^+\cdot r^-$) in $\text{þ}^+\cdot\text{þ}^-$, but additive ($r^+ + r^-$) in U_E. Since r^+ is a measure of a hydrogen radius for all the solvents investigated here, it is effectively constant and small, therefore having very little effect on the trends observed, albeit it does have an effect on the magnitude.

Table S5: The MP2/aug-cc-pVTZ calculated delocalisation index (DI) for the atoms at the negative and positive dipolar atoms. The sum of the pairwise DI calculated with for the negative and positive dipolar atoms every other atom in the molecule. The HOMO and LUMO energies in Hartree.

Solvent	**DI on δ^-**	**DI on δ^+**	**Pairwise DI on δ^-**	**Pairwise DI on δ^+**	**HOMO (a.u.)**	**LUMO (a.u.)**
Py	1.29	0.48	2.57	0.95	-0.34592	0.02612
EDC	0.57	0.47	1.13	0.95	-0.44139	0.03287
DEE	0.98	0.49	1.97	0.97	-0.41884	0.03123
MeCN	1.01	0.47	2.03	0.94	-0.45426	0.02154
ACE	0.76	0.48	1.52	0.96	-0.41358	0.02595
FA	0.73	0.37	1.47	0.74	-0.42223	0.02065
PC	0.72	0.48	1.44	0.96	-0.46641	0.01951
NMA	0.76	0.38	1.52	0.77	-0.39164	0.02224
DMSO	0.70	0.48	1.40	0.95	-0.37154	0.02375
MeOH	0.77	0.30	1.55	0.60	-0.45231	0.02848
2PrOH	0.81	0.31	1.61	0.61	-0.43844	0.02967
EtOH	0.79	0.30	1.58	0.60	-0.44332	0.02919
PrOH	0.79	0.30	1.58	0.60	-0.44255	0.02989
TOL	1.73	0.48	3.45	0.97	-0.32203	0.03011
water	0.58	0.29	1.16	0.59	-0.50984	0.02929
NH_3	1.16	0.40	2.33	0.81	-0.43015	0.02943
HMPT*	0.63	0.49	1.33	0.98	-0.35664	0.03110
$MeNO_2$	0.87	0.47	1.75	0.94	-0.45724	0.02180
hexane	1.77	0.49	3.35	0.97	-0.44196	0.03186

*HMPT was calculated with MP2/aug-cc-pVDZ.

Table S6: The change in the charge (q) of the atom at the negative dipole from the lone solvent molecule, to the solvent molecule interacting with a Li$^+$ cation. These values are all calculated using DDEC6, with M06-2X/aug-cc-pVDZ and are order by the percentage change (Δq (%)).

Solvent	q$^-$ (w/o Li$^+$)	q$^-$ (w. Li$^+$)	Δq (absolute)	Δq (%)
Py	-0.302	-0.557	-0.255	84
EDC	-0.159	-0.284	-0.126	79
DEE	-0.284	-0.501	-0.217	76
MeCN	-0.435	-0.691	-0.256	59
ACE	-0.485	-0.731	-0.245	51
FA	-0.509	-0.762	-0.253	50
PC	-0.545	-0.816	-0.270	50
NMA	-0.563	-0.836	-0.273	48
DMSO	-0.644	-0.904	-0.260	40
MeOH	-0.488	-0.682	-0.194	40
2PrOH	-0.556	-0.752	-0.197	35
EtOH	-0.536	-0.717	-0.181	34
PrOH	-0.534	-0.703	-0.169	32
TOL	-0.166	-0.213	-0.046	28
water	-0.786	-0.955	-0.169	21
NH_3	-0.901	-1.076	-0.175	19
HMPT	-0.764	-0.890	-0.125	16
$MeNO_2$	-0.386	-0.448	-0.061	16
hexane	-0.342	-0.352	-0.009	3

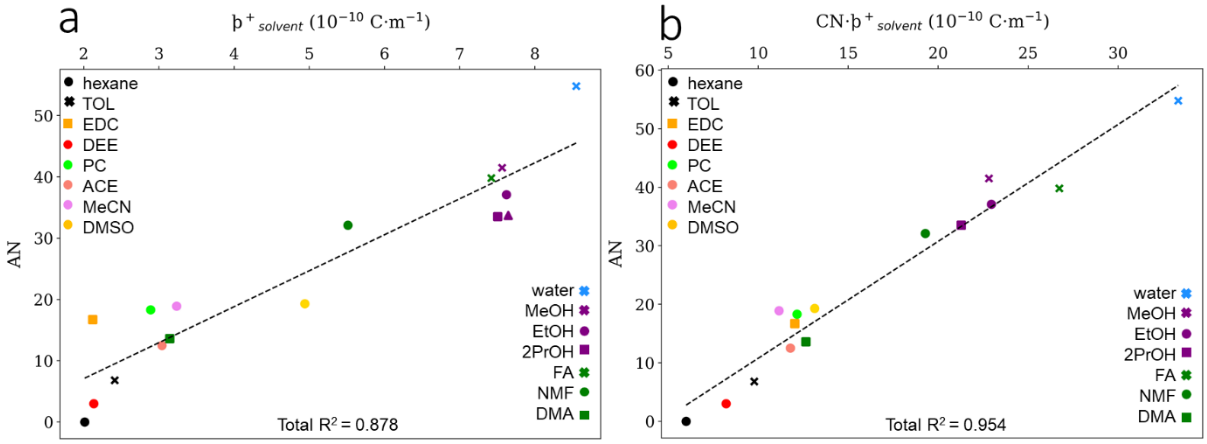

Figure S62: The “protic” radial charge density relationship, þ$^+_{\text{solvent}}$ with the Gutmann-Mayer Acceptor number AN (a) without and (b) with accounting for the coordination number of Et_3PO. Coordination numbers determined from DFTB-MD simulations (values in Table S7).

Table S7: The coordination number of Et_3PO in each solvent, calculated from the RDF between the oxygen on Et_3PO and the hydrogen atoms on the solvent from DFTB-MD simulations of Et_3PO in a solvent box with 64 solvent molecules.

Solvent	**CN (solvent)H-O(Et_3PO))**
EDC	5.7
PC	4.2
TOL	4.1
DMA	4.0
water	3.9
DEE	3.8
ACE	3.9
DMSO	3.9
FA	3.6
NMF	3.5
MeCN	3.45
MeOH	3.0
EtOH	3.0
hexane*	3.0
2PrOH	2.8

*hexane was run with 32 solvent molecules due to simulation issues with the 64 solvent molecule box.

S12. First Principles Solvent Properties

S12.1 The relative permittivity

Electrostatics maintains strong correlations with the total interaction energy (Figure S41) for the gas-phase pairwise (§S8.1), solvated pairwise (§S8.2) and cluster (§S8.3) interactions. This is consistent with cation-solvent §S4 and anion-solvent §S5 analyses. §S4 and §S5, showed that Lewis basicity (represented by DN) and acidity (represented by AN) respectively, could be approximated from first principles electronic properties of each molecular solvent. Since both appear to have their origins in electrostatics, quantified by $\text{þ}^{-}{}_{\text{solvent}}$ and $\text{þ}^{+}{}_{\text{solvent}}$ respectively, it is conceivable that $\text{þ}^{+/-}{}_{\text{solvent}}$ may be utilised in a new form of simplified LSER. It follows that some bulk solvent properties should be calculable from first principles, if the property is fundamentally dependent on the solvent-solvent self-interactions. One property that fits this criterion is the relative permittivity (or dielectric constant), which (experimentally) is a measure of a solvent's ability to stabilise a parallel plate capacitor. Therefore, conditions conducive to a high relative permittivity are:

i) A strong positive dipole that can pack densely on the negative plate (this becomes negative due to a supplied electric current) and stabilise it such that more charge can accumulate on its surface.

ii) A strong negative dipole that can pack densely on the positive plate (this becomes positive due to the nearby negative partial charge of the solvent).

iii) A large separation of the positive and negative partial charges/dipoles (*i.e.*, large dipole moment) of the solvent such that they aren't shielding their own electrostatic stabilisation of either parallel plate. Alternatively, a small separation may instead allow for greater charge density accumulation due to that very shielding.

iv) Adequate solvent structure to propagate the partial charges (and therefore charge stabilising "power") through the solution.

Assuming that solvent structure (iv) will be partially encompassed by accounting for the other three terms (i-iii), the relative permittivity (ε_r) might be approximated via a mix of pre-existing and new solvent parameters. In this instance, the first and second points may be encompassed by $\text{þ}^{+}{}_{\text{solvent}}$ and $\text{þ}^{-}{}_{\text{solvent}}$ respectively. The third term might be approximated via the solvent's dipole moment, μ_{solvent}. $\text{þ}^{\pm}{}_{\text{solvent}}$ and μ_{solvent} represent the first (monopole) and second (dipole) terms respectively of a (truncated) Taylor series expansion of the electrostatic energy.[16] The natural logarithm is taken here to account for exponential damped oscillatory decay of the Debye length, as noted by Kjellander.[17] Given the $\text{þ}^{\pm}$ and μ values are on the molecular scale, they are not subject to this macroscopic exponential decay as there is no charge screening. Indeed, an *ab initio* LSER (fit via regression models) of these three terms correlates with the natural logarithm of measured empirical relative permittivities (Figure S63).

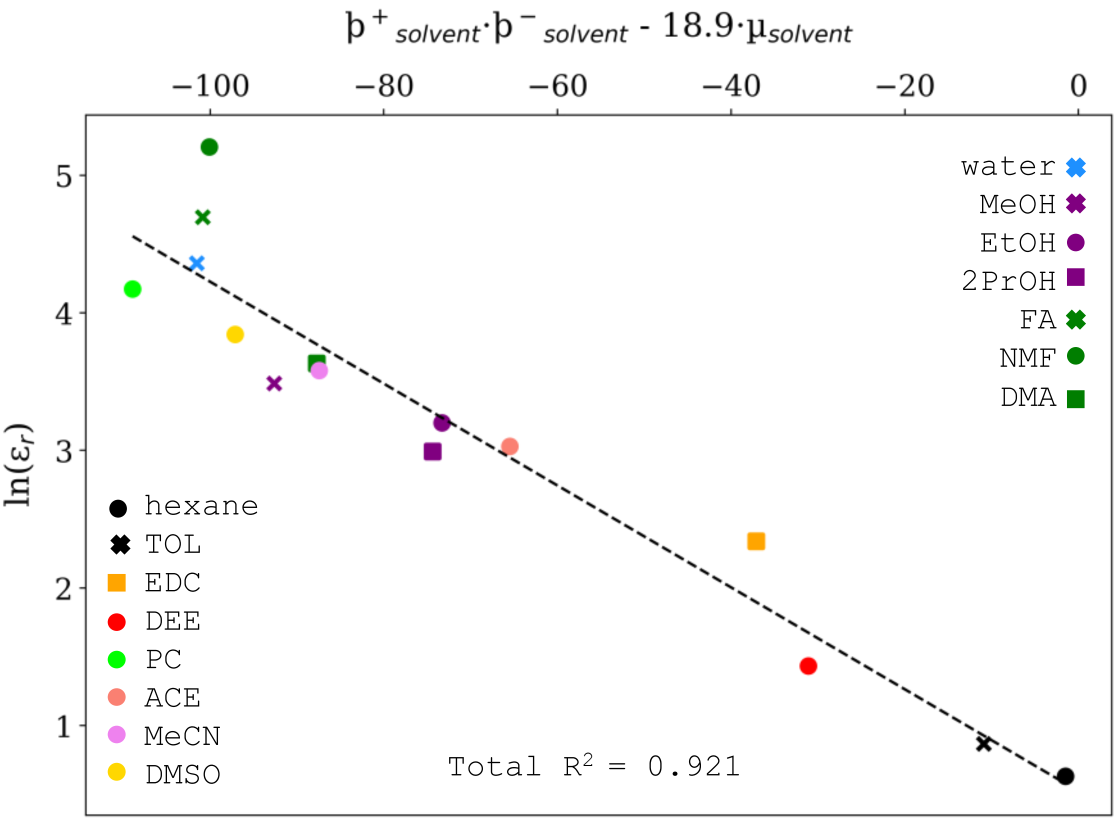

Figure S63: The natural logarithm of the solvent’s relative permittivity (ε_r) may be approximated from first principles charge analyses using multiplicative þ values in conjunction with the solvent’s dipole moment (µ$_{solvent}$).

In Figure S63, the þ$^{+}_{solvent}$ and þ$^{-}_{solvent}$ values are multiplied together. This effectively measures the intermolecular electrostatic potential energy U_E between the positive and negative dipole of the solvent (Figure S61). The solvent’s dipole moment (µ$_{solvent}$) is then used to account for how well the positive and negative charges can pack, where a smaller dipole moment implies a higher charge density may accumulate as these are stabilised by the covalent bonds within the solvent. The 18.9 coefficient was determined by a linear regression analysis as a correction factor given the different units between these parameters. Further work to unify these terms is still required, and other combinations of these parameters may better represent the underlying physical basis for these correlations.

þ$^{+}_{solvent}$·þ$^{-}_{solvent}$ by itself does not correlate as well with ln(ε_r) (Figure S64 (a)), nor does þ$^{+}_{solvent}$ (Figure S64 (b)), or þ$^{-}_{solvent}$ (Figure S64 (c)) or µ$_{solvent}$ (Figure S64 (d)) separately. Evidently, ln(ε_r) is dependent on the higher-order terms of the Taylor series.

In summary, þ$^{+}_{solvent,}$ þ$^{-}_{solvent}$ and µ$_{solvent}$ form the basis of a new form of *ab initio* LSER capable of quantifying and predicting macroscopic solvent properties, tested here for ε_r. Although each set of solvent parameters will require a different set of considerations, it would seem that if they have a basis in the strength of their solvent-solvent interaction, these parameters will be of use.

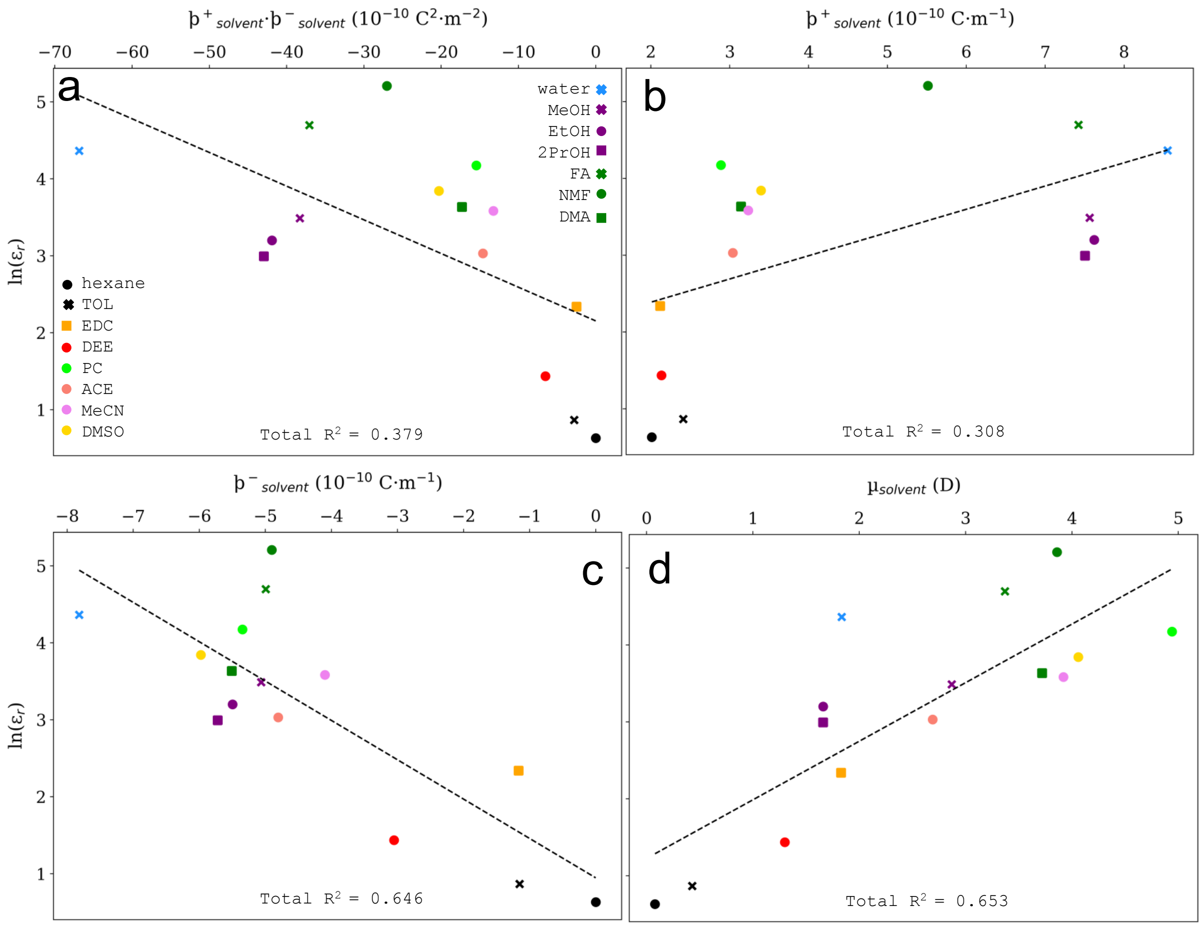

Figure S64: The natural logarithm of the solvents relative permittivity correlated with its (a) positive and negative radial charge densities multiplied together, as well as separately in (v) and (c) respectively, and the solvent's (d) dipole moment. Trends can be observed; however, outliers are common.

S12.2 The Gibbs Free Energy of transfer of ions

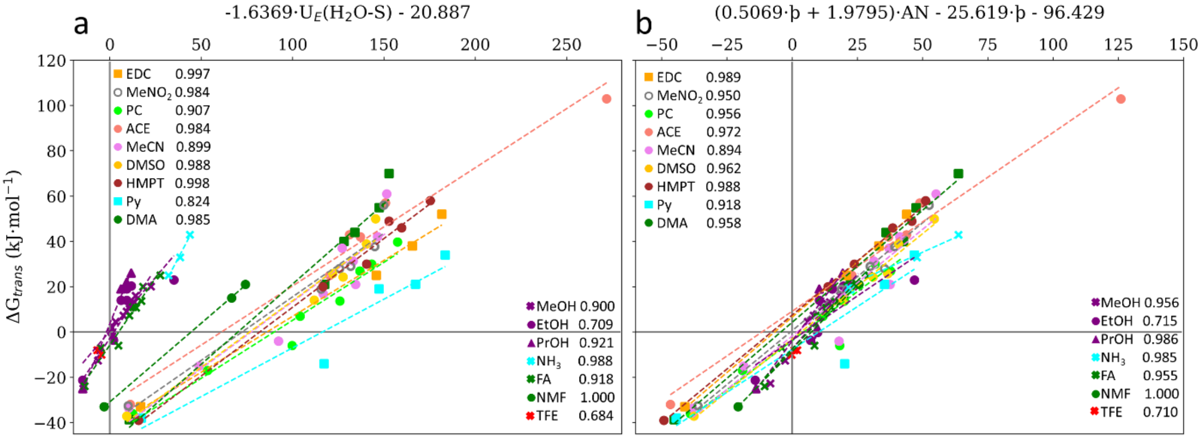

Figure S65: The Gibbs energy of transfer from water to nonaqueous solvents for an array of anions compared to (a) predicted values based solely on the difference in the theoretical electrostatic potential energy between the ion and water and the ion and nonaqueous solvent (Figure S66). This overestimates the Gibbs free energy of transfer for aprotic solvents. (b) predicted values based on the anion's þ value and solvent's AN (Figure S67). Since AN correlates well with $þ^{+}_{solvent}$ if corrected for by its coordination number, this would present a fully electrostatic predictive capability for Gibbs energies of transfer for ions. However, these correlations utilised fitting calibrations so further work is required for an entirely first principles analysis.

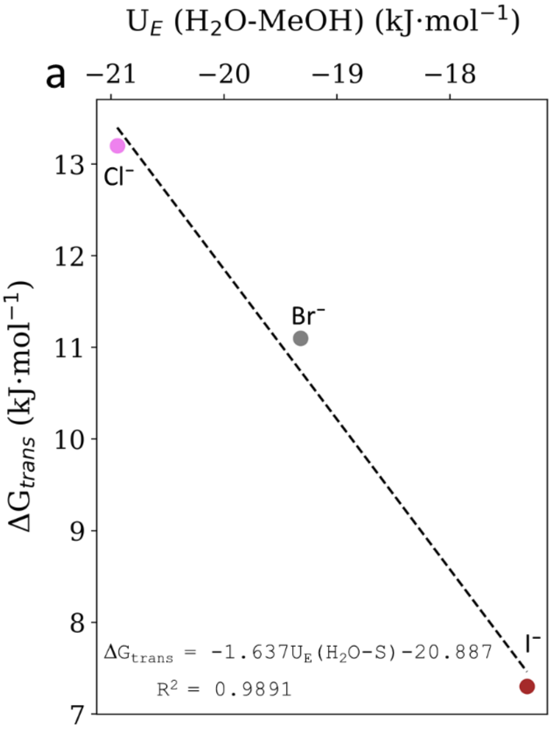

Figure S66: Gibbs energy of transfer from water to methanol compared to the theoretical electrostatic energy of transfer from water to methanol. This serves as a calibration for the remainder of the solvents and anions presented in Figure S65 (a).

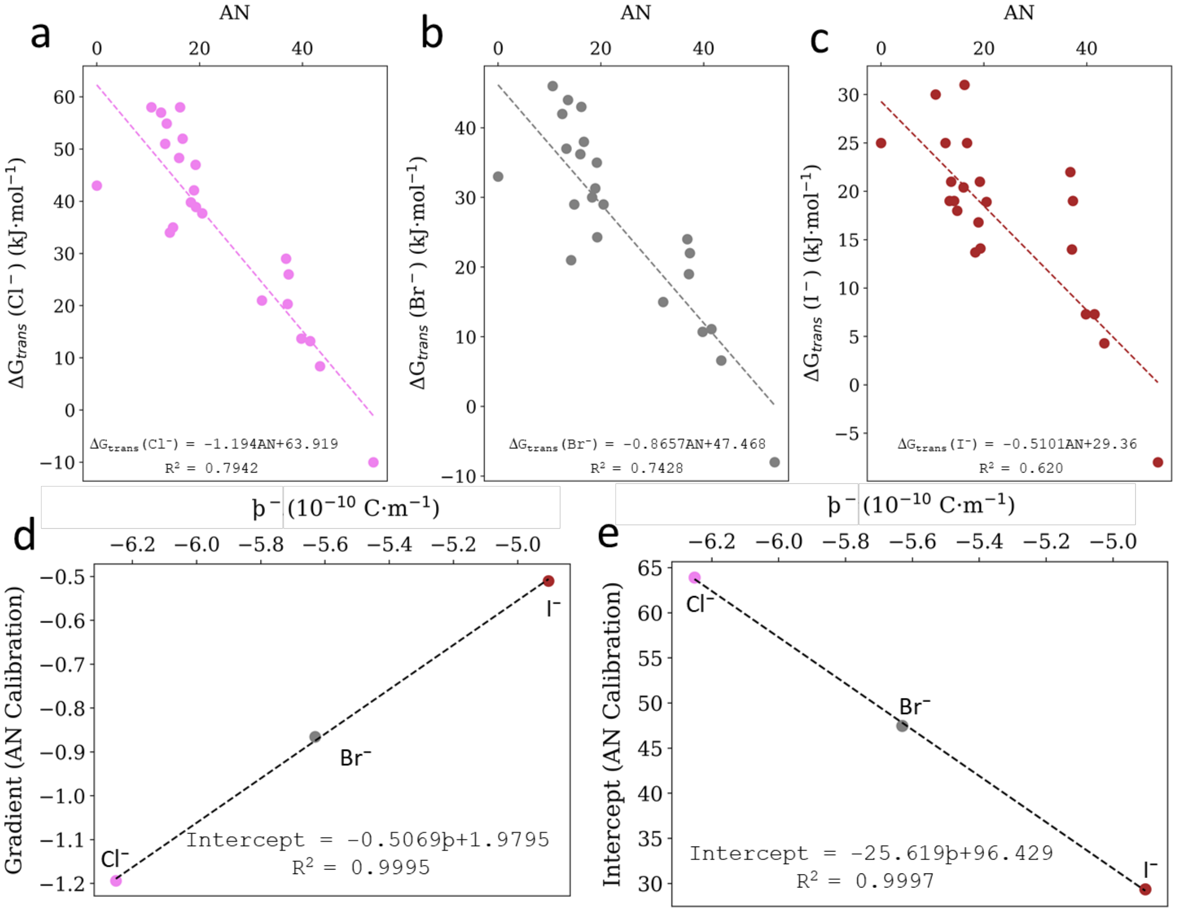

Figure S67: The dependence of the Gibbs energy of transfer on the solvent's acceptor number for (a) Cl^-, (b) Br^- and (c) I^-. The (d) gradient and (e) y-intercept of these halide-AN dependences are compared to the halide þ$^-$ values and used for the fits in Figure S65 (b).

S13. Funcational and basis set dependence

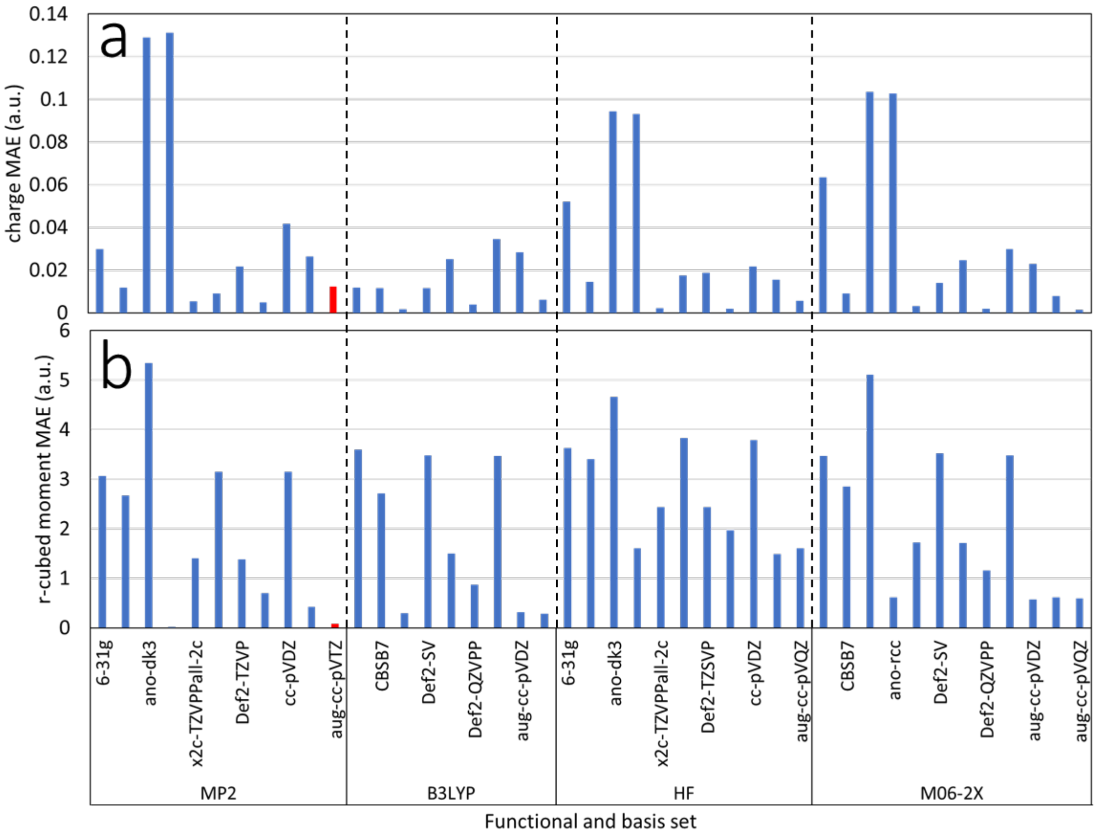

Figure S68: The mean absolute errors for every atom in an acetate ion of the (a) partial charge and (b) atomic r-cubed moment calculated with DDEC6 for various functionals and basis sets compared to MP2/aug-cc-pVQZ values.

SI References

1. Kamlet, M. J., Abboud, J. L. M., Abraham, M. H. & Taft, R. W. Linear solvation energy relationships. 23. A comprehensive collection of the solvatochromic parameters,. π*,. alpha., and. beta., and some methods for simplifying the generalized solvatochromic equation. *J. Org. Chem.* **48**, 2877–2887 (1983).
2. Kamlet, M. J., Doherty, R. M., Abraham, M. H., Marcus, Y. & Taft, R. W. Linear solvation energy relationship. 46. An improved equation for correlation and prediction of octanol/water partition coefficients of organic nonelectrolytes (including strong hydrogen bond donor solutes). *J. Phys. Chem.* **92**, 5244–5255 (1988).
3. and, M. H. A. & Platts, J. A. Hydrogen Bond Structural Group Constants. *J. Org. Chem.* **66**, 3484–3491 (2001).
4. Gregory, K. P., Wanless, E. J., Webber, G. B., Craig, V. S. J. & Page, A. J. The electrostatic origins of specific ion effects: quantifying the Hofmeister series for anions. *Chem. Sci.* **12**, 15007–15015 (2021).
5. Gutmann, V. Empirical parameters for donor and acceptor properties of solvents. *Electrochim. Acta* **21**, 661–670 (1976).
6. Soteras, I., Orozco, M. & Luque, F. J. Induction effects in metal cation–benzene complexes. *Phys. Chem. Chem. Phys.* **10**, 2616–2624 (2008).
7. Israelachvili, J. N. *Intermolecular and surface forces*. (Academic press, 2015).
8. Smaga, A. & Sadlej, J. Computational study on interaction energy changes during double proton transfer process. *Comput. Theor. Chem.* **998**, 120–128 (2012).
9. Gregory, K. P., Webber, G. B., Wanless, E. J. & Page, A. J. Lewis Strength Determines Specific-Ion Effects in Aqueous and Nonaqueous Solvents. *J. Phys. Chem. A* **123**, 6420–6429 (2019).
10. Gutmann, V. & Wychera, E. Coordination reactions in non aqueous solutions - The role of the donor strength. *Inorg. Nucl. Chem. Lett.* **2**, 257–260 (1966).
11. Gutmann, V. *The Donor-Acceptor Approach to Molecular Interactions*. (Springer US, 1978).
12. T. Duignan, T., F. Parsons, D. & W. Ninham, B. A Continuum Solvent Model of the Multipolar Dispersion Solvation Energy. *J. Phys. Chem. B* **117**, 9412–9420 (2013).
13. Stone, A. *The theory of intermolecular forces*. (OUP Oxford, 2013).
14. Okur, A. & Simmerling, C. Chapter 6 Hybrid Explicit/Implicit Solvation Methods. in (ed. Spellmeyer, D. C. B. T.-A. R. in C. C.) vol. 2 97–109 (Elsevier, 2006).
15. Keith, T. A. & AIMAll, V. 19.10. 12, TK Gristmill Software. *Overl. Park KS, USA* (2019).
16. Volkov, A. & Coppens, P. Calculation of electrostatic interaction energies in molecular dimers from atomic multipole moments obtained by different methods of electron density partitioning. *J. Comput. Chem.* **25**, 921–934 (2004).
17. Kjellander, R. A multiple decay-length extension of the Debye-Hückel theory: To achieve high accuracy also for concentrated solutions and explain under-screening in dilute symmetric electrolytes. *Phys. Chem. Chem. Phys.* **22**, 23952–23985 (2020).